DEVELOPING A PROCESS ANALYTICAL TECHNOLOGY FOR MONITORING THE PARTICLE SIZE DISTRIBUTION IN TWIN SCREW GRANULATION

DEVELOPING A PROCESS ANALYTICAL TECHNOLOGY FOR MONITORING THE PARTICLE SIZE DISTRIBUTION IN TWIN SCREW GRANULATION

BY HASSAN ABDULHUSSAIN, B.Eng

A Thesis Submitted to the School of Graduate Studies in Partial Fulfilment of the Requirements of the Degree of Doctor of Philosophy

McMaster University

Doctor of Philosophy (2024) McMaster University

Chemical Engineering Hamilton, Ontario

TITLE: DEVELOPING A PROCESS ANALYTICAL TECHNOLOGY FOR MONITORING THE PARTICLE SIZE DISTRIBUTION IN TWIN SCREW GRANULATION

AUTHOR: Hassan Abdulhussain

B.Eng (McMaster University)

SUPERVISOR: Dr. Michael R. Thompson

PAGES: xvi, 169

Lay Abstract

Granulation is a size enlargement process used in tablet manufacturing that converts fine powders into larger agglomerates that we refer to as granules (similar structure/size to instant coffee). Traditionally, granulation of drugs is done in batches and suffers from quality control issues but there have been efforts over the past two decades to convert this process to granulate powder continuously. This thesis focuses on developing an inexpensive, robust ultrasound sensor for monitoring the size distribution of the granules in real time exiting from a twin screw granulator. The technique itself uses a newly created filtering technique based on particle mechanics along with use of artificial intelligence to collect sound waves and convert its frequency spectrum into a distribution. The technology was tested on multiple formulations used by the pharmaceutical industry and has shown an overall accuracy of 97% when estimating the size distribution. This development of technology is a big step towards the idea of integrated quality testing in continuous pharmaceutical drug production.

Abstract

Twin screw wet granulation (TSG) has been studied as a continuous manufacturing alternative to batch granulation for nearly twenty years. One of the main differences between batch granulation and TSG lies in the exiting granules being presented as a bimodal particle size distribution (PSD) in the latter case. Current process analytical technologies (PAT) can monitor a monomodal distribution well but there have been no techniques disclosed in the public domain so far that can accurately monitor this unusually shaped PSD. Acoustic emissions (AE) has been identified as a PAT of interest due to its ease of use (lack of calibration), low cost, and non-invasive design relative to other PATs used for monitoring PSDs. Hence the goal of this thesis was to develop AE as a process analytical technology (PAT) capable of estimating the full distribution of produced granules by TSG in real time.

The first research study of this thesis focused on the development of the new technology. The AE PAT consisted of an acoustic sensor, an impact plate, and software to convert the time-domain signal of particle collisions into a time-averaged frequency-domain spectrum to be subsequently used to estimate a weight-averaged particle size distribution. A novel and much required addition to the PAT was inclusion of a digital filter based on particle mechanics parameters to overcome auditory masking which hindered accurately converting the cumulative sounds of impact into a PSD. The PAT was tested in this study with granulated lactose monohydrate and with the new digital filter, obtaining a maximum error of 1 wt% across all particle sizes tested. In the second research study, as

more formulations commonly used in the industry were tested, the filter proved unable by itself to account for the differences in impact mechanics and therefore needed to be modified to incorporate the more inelastic behaviour now being seen. Two micromechanical models were explored, and the Walton-and-Braun model was found to be the most suitable for the AE PAT – reducing its error from 8 wt% down to 2.75 wt% across four formulations producing coefficients of restitution from 0.79 to 0.24.

In the last research study in this thesis, the now-functional inline PAT was used to reveal mechanistic details related to the transition state in granulation as a TSG starts up, to improve the field's understanding of the granulation mechanism. The technique was able to estimate the PSD over much shorter periods of material collection compared to sieving, allowing the evolution of the PSD as a function of time to be examined for varying degrees of fill (DF) and liquid-to-solids ratios. It was determined that the time to steady state, at both DF tested, occurred at approximately 5 times the mean residence time of the process by both PAT and sieving analyses. Particle sizes between 102-2230 μm were then tracked as a function of time below 120 s and variations of granule growth were seen for each degree of fill which added to the understanding of the granulation mechanism. This PAT shows great promise as a monitoring tool to implement quality by design principles for TSG in pharmaceutical manufacturing.

Acknowledgments

I would like to express my sincere gratitude for everyone who helped me develop this thesis. First, I thank God for the opportunity and privilege of being able to focus all my time to complete this degree in the last 4 years and for surrounding me with a good group of people to make this a memorable journey.

I'd like to thank my supervisor Dr. Michael Thompson, for his support and guidance throughout my PhD. In our meetings his advice and critiques (and his patience with my struggles) have completely changed my approach to research, critical thinking, project management, and problem solving which has made me a better engineer and researcher. I have immensely benefited from his mentorship which I am endlessly grateful for.

I am also grateful to have been in the CAPPA-D group and would like to thank all its members, past and present, for their support in the lab, collaborative spirit, and overall being a great group of people to work with and meet. This includes Heera, Felipe, Ahmed, Tomi, Ubani, and Varsha for their support at the start of my graduate studies, and for making the lab a welcoming environment. Special shoutouts to the rest of the CAPPA-D group who I have been able to work with either on different projects or have helped me as an extra pair of hands with my experiments including (but certainly not limited to): Ariel, Cecilia, Sumon, Nikol, Mukesh, Samuel, and Kavitha. This thesis would not have been completed without their support.

My extracurriculars have greatly shaped my graduate journey so I would also like to thank all the people I have met and worked with throughout the years (including faculty and staff) in the Chemical Engineering Graduate Student Society and Engineering Graduate Society as well as all the faculty who have supported my studies in the Chemical Engineering Department. This especially includes Dr. Shelir Ebrahimi, Dr. Jake Nease, and Dr. Carlos Filipe, and again Dr. Michael Thompson who have supported my interest in academia which enabled me to become a sessional instructor at McMaster.

Lastly, I'd like to thank my family, starting with my parents, Ali and Amal, for their support throughout my life and especially in the last four years. They have constantly pushed me to pursue higher education and were a crucial factor in making this PhD possible. I am also thankful to have my siblings, Mohammad and Mustafa, in my life. I have learned a lot from your patience and dedication and hope to support your endeavors like you supported mine. I am eternally grateful for all the people I have met the past 4-5 years and look forward to starting a new chapter in my professional career.

Table of Contents

List of Figures

List of Tables

Chapter 1: Introduction

1.1. Background and Motivation

Research in manufacturing since the early 2000's has focused on utilizing existing data from processes to develop and integrate smart sensors with the ultimate goal of producing more integrated and flexible manufacturing lines [1]. The demand for mass product personalization, faster delivery times, and higher quality products is driving companies towards the fourth industrial revolution, also termed "Industry 4.0" [1, 2].

In the context of the pharmaceutical industry, the current manufacturing steps for drug tablets, operate predominantly via batch processes [3]. Batch processing was initially advantageous for its quality assurance as it allowed for batches to be recalled if they were improperly prepared, mitigating serious consequences. However, these processes were also found to be relatively less efficient when compared to the rest of the chemical process industries [4]. The lack of flexibility in process operations and high potential for drug wastage within pharmaceutical manufacturing poses serious public health concern related to drug shortages [4]. The United States Food and Drug Administration recognized these concerns at the end of the 20^{th} century and is now encouraging improvements to the manufacturing process with a vision to "promote a maximally efficient, agile, flexible pharmaceuticals sector that reliably provides high quality drugs without extensive regulatory oversight" [5].

Continuous manufacturing is one such solution that has the potential to improve the pharmaceutical sector due to its ability to produce drugs of consistent quality, ease of scale up, and incorporate in-line monitoring of quality parameters through process analytical technologies (PAT) [6]. Quality in this case refers to the strength and dissolution profile of the finished tablet, to which the manufacturing step of granulation plays a critical role [7].

Granulation is an enlargement process that turns fine powders into larger particles called granules, most commonly through the addition of a liquid or molten binder. This process improves plant air quality as well as the flowability, bulk density, and content uniformity of the formulation with applications within[8-10] and outside the pharmaceutical industry[11, 12]. The type of binder used signals the mode of operation of the process. It is called wet granulation when a liquid binder is used or melt granulation when a molten binder is employed, with the former being the most common mode studied in the literature [13]. The critical quality attributes of the granulation process such as particle shape, size distribution, porosity, moisture content, and mechanical properties (i.e. inelasticity, fracture strength) drive the performance of both intermediate unit operations (milling, tableting) and the final tablet [14]. The focus of this thesis will be on continuous wet granulation and how a PAT can be developed for monitoring one of its critical quality attributes, namely the particle size distribution (PSD).

Twin screw extrusion is a popular process technology used in the food and polymer industries [15] and has been extensively studied as a tool for continuous granulation for the past two decades[16]. This specific continuous granulation method is called twin screw granulation (TSG). TSG has multiple advantages over its batch counterpart (i.e. high shear wet granulation), including its superior dispersive & distributive mixing which reduces the amount of granulation liquid needed[17], high throughput due to its low residence time[18], along with the potential for advanced process control through implementation of PAT[19]. One of the main differences of TSG compared to a batch granulation process, is the PSD produced from the process. Batch granulation processes typically output a narrow Gaussian (or unimodal) PSD, whereas TSG typically outputs a bimodal PSD[19-22]. The uniqueness of this PSD makes single descriptors like d_{50} inadequate. The PSD from granulation is an important quality attribute as it both influences downstream units such as drying and milling along with the properties of the final product, including tablet strength and dissolution[23, 24]. A major hurdle slowing adoption of TSG as a widely adopted manufacturing technique is the few PAT available for monitoring PSD. An inexpensive, robust, and accurate PAT for continuous monitoring of PSD would be highly desirable, especially if suited to Quality by Design principles where the end goal is developing an intelligent control system capable of rapidly correcting deviations in quality descriptors in a manner that can be explained to regulators.

1.2. Thesis Objectives

The goals of this thesis are to address some of the knowledge gaps identified above by exploring the tools and techniques available in determining PSD in a continuous and non-destructive manner. The challenge undertaken in this work involved developing an accurate monitoring tool and applying it to multiple model (placebo) formulations representative of ingredients used by the pharmaceutical industry. The work shown is broken down into these major objectives:

1- To develop acoustic emission as a PAT for monitoring bimodal PSDs by creating a novel digital filter based on particle mechanics parameters and coupling it with artificial intelligence techniques to properly count particles of different sizes typical of TSG [25]
2- To expand the utility of this new PAT for broad range of formulations that are representative of pharmaceutics. This involves adjusting the novel digital filter to account for varying levels of elasticity and adhesion [26]
3- To showcase how the PAT can be used both as a process monitoring tool as well as to gain insights into the TSG mechanism by observing steady state and transient behaviour

1.3. Thesis Outline

The thesis is composed of two published papers and 1 manuscript yet to be submitted to a peer reviewed journal. The papers have been written by the author of this thesis and have the approval of all co-authors, and the journal to be used in this thesis. The author has conducted the experiments and have analysed all the resulting data.

- Chapter 1 introduces the motivation and major objectives of the thesis;

- Chapter 2 is a review of all PAT tools relevant to predicting particle size, an overview of the TSG process, artificial intelligence techniques used, and the granulation mechanism within TSG;
- Chapter 3 is the seminal paper of this project, published in *Powder Technology*. This paper investigates how acoustic emissions was used to determine a bimodal PSD, and showcases the development of an auditory masking filter to significantly improve the estimation accuracy;
- Chapter 4 is a paper by H. Abdulhussain and M.R. Thompson published in the *International Journal of Pharmaceutics*. This paper investigates how the PAT developed in Chapter 3 was expanded to handle formulations with varying properties of cohesion and inelasticity, so it could be useful for a broad range of pharmaceutics produced by TSG. This involved incorporating tunable micromechanical parameters into the auditory masking filter from viscoelastic and elastoplastic equations to compare the differences in accuracy and stability of the technique;
- Chapter 5 is a prepared manuscript yet to be submitted where the acoustic PAT is used as a process monitoring tool to study steady state and transient behaviours in the TSG process to investigate the mechanism of how granules grow at various degrees of fill;
- Chapter 6 summarizes the conclusions and recommendations for future work.

1.4. References

[1] C.G. Machado, M.P. Winroth, E.H.D. Ribeiro da Silva, Sustainable manufacturing in Industry 4.0: an emerging research agenda, International Journal of Production Research, 58 (2020) 1462-1484.

[2] T. Zheng, M. Ardolino, A. Bacchetti, M. Perona, The applications of Industry 4.0 technologies in manufacturing context: a systematic literature review, International Journal of Production Research, 59 (2021) 1922-1954.

[3] Q. Su, S. Ganesh, M. Moreno, Y. Bommireddy, M. Gonzalez, G.V. Reklaitis, Z.K. Nagy, A perspective on Quality-by-Control (QbC) in pharmaceutical continuous manufacturing, Comput Chem Eng, 125 (2019) 216-231.

[4] S.L. Lee, T.F. O'Connor, X. Yang, C.N. Cruz, S. Chatterjee, R.D. Madurawe, C.M.V. Moore, L.X. Yu, J. Woodcock, Modernizing Pharmaceutical Manufacturing: from Batch to Continuous Production, Journal of Pharmaceutical Innovation, 10 (2015) 191-199.

[5] PHARMACEUTICAL CGMP'S FOR THE 21ST CENTURY — A RISK-BASED APPROACH, U.S. Food and Drug Adminisitration, https://www.fda.gov/media/77391/download, 2004.

[6] A.S. Myerson, M. Krumme, M. Nasr, H. Thomas, R.D. Braatz, Control Systems Engineering in Continuous Pharmaceutical Manufacturing May 20–21, 2014 Continuous Manufacturing Symposium, Journal of Pharmaceutical Sciences, 104 (2015) 832-839.

[7] H.B. Grangeia, C. Silva, S.P. Simoes, M.S. Reis, Quality by design in pharmaceutical manufacturing: A systematic review of current status, challenges and future perspectives, Eur J Pharm Biopharm, 147 (2020) 19-37.

[8] P. Suresh, I. Sreedhar, R. Vaidhiswaran, A. Venugopal, A comprehensive review on process and engineering aspects of pharmaceutical wet granulation, Chemical Engineering Journal, 328 (2017) 785-815.

[9] J. Litster, B. Ennis, The science and engineering of granulation processes, Springer Science & Business Media2004.

[10] R.M. Dhenge, J.J. Cartwright, M.J. Hounslow, A.D. Salman, Twin screw granulation: Steps in granule growth, International Journal of Pharmaceutics, 438 (2012) 20-32.

[11] H. Ghafarifarsani, S.H. Hoseinifar, M. Aftabgard, H. Van Doan, The improving role of savory (Satureja hortensis) essential oil for Caspian roach (Rutilus caspicus) fry: Growth, haematological, immunological, and antioxidant parameters and resistance to salinity stress, Aquaculture, 548 (2022) 737653.

[12] H. Gong, R. Pishgar, J. Tay, Artificial neural network modelling for organic and total nitrogen removal of aerobic granulation under steady-state condition, Environmental technology, (2018).

[13] L.S.C. Wan, P.W.S. Heng, G. Muhuri, Incorporation and distribution of a low dose drug in granules, International Journal of Pharmaceutics, 88 (1992) 159-163.

[14] M. Singh, S. Shirazian, V. Ranade, G.M. Walker, A. Kumar, Challenges and opportunities in modelling wet granulation in pharmaceutical industry – A critical review, Powder Technology, 403 (2022) 117380.

[15] C. Martin, Twin Screw Extrusion for Pharmaceutical Processes, in: M.A. Repka, N. Langley, J. DiNunzio (Eds.) Melt Extrusion, Springer New York, New York, NY, 2013, pp. 47-79.

[16] S. Bandari, D. Nyavanandi, V.R. Kallakunta, K.Y. Janga, S. Sarabu, A. Butreddy, M.A. Repka, Continuous twin screw granulation - An advanced alternative granulation technology for use in the pharmaceutical industry, Int J Pharm, 580 (2020) 119215.

[17] Y. Zhang, T. Liu, S. Kashani-Rahimi, F. Zhang, A review of twin screw wet granulation mechanisms in relation to granule attributes, Drug Development and Industrial Pharmacy, 47 (2021) 349-360.

[18] P. Chen, M.J. Ansari, D. Bokov, W. Suksatan, M.L. Rahman, M.S. Sarjadi, A review on key aspects of wet granulation process for continuous pharmaceutical manufacturing of solid dosage oral formulations, Arabian Journal of Chemistry, 15 (2022) 103598.

[19] C. Portier, C. Vervaet, V. Vanhoorne, Continuous Twin Screw Granulation: A Review of Recent Progress and Opportunities in Formulation and Equipment Design, Pharmaceutics, 2021.

[20] M. Verstraeten, D. Van Hauwermeiren, K. Lee, N. Turnbull, D. Wilsdon, M. am Ende, P. Doshi, C. Vervaet, D. Brouckaert, S.T.F.C. Mortier, I. Nopens, T.D. Beer, In-depth experimental analysis of pharmaceutical twin-screw wet granulation in view of detailed process understanding, International Journal of Pharmaceutics, 529 (2017) 678-693.

[21] J. Vercruysse, M. Toiviainen, M. Fonteyne, N. Helkimo, J. Ketolainen, M. Juuti, U. Delaet, I. Van Assche, J.P. Remon, C. Vervaet, T. De Beer, Visualization and

understanding of the granulation liquid mixing and distribution during continuous twin screw granulation using NIR chemical imaging, European Journal of Pharmaceutics and Biopharmaceutics, 86 (2014) 383-392.

[22] R.M. Dhenge, R.S. Fyles, J.J. Cartwright, D.G. Doughty, M.J. Hounslow, A.D. Salman, Twin screw wet granulation: Granule properties, Chemical Engineering Journal, 164 (2010) 322-329.

[23] N. Millen, A. Kovačević, J. Djuriš, S. Ibrić, Machine Learning Modeling of Wet Granulation Scale-up Using Particle Size Distribution Characterization Parameters, Journal of Pharmaceutical Innovation, 15 (2020) 535-546.

[24] V. Pauli, Y. Roggo, P. Kleinebudde, M. Krumme, Real-time monitoring of particle size distribution in a continuous granulation and drying process by near infrared spectroscopy, European Journal of Pharmaceutics and Biopharmaceutics, 141 (2019) 90-99.

[25] H.A. Abdulhussain, M.R. Thompson, Predicting the particle size distribution in twin screw granulation through acoustic emissions, Powder Technology, 394 (2021) 757-766.

[26] H.A. Abdulhussain, M.R. Thompson, Considering inelasticity in the real-time monitoring of particle size for twin-screw granulation via acoustic emissions, International Journal of Pharmaceutics, 639 (2023) 122949.

Chapter 2: Literature Review

This chapter aims to cover the major concepts in this thesis including a review of process analytical technologies available for monitoring particle size distributions (PSD) covering laser based, optical, and the acoustic emission method. As particle processing is the main application, the basics of impact mechanics as well as the granulation mechanism will be covered along with a review of how artificial neural networks are used for process monitoring/prediction.

2.1: Twin Screw Granulation Mechanism

The wet granulation mechanism in general can be separated into three rate processes: nucleation, consolidation and growth, along with attrition and breakage [1]. Nucleation in TSG occurs at the injection site where the liquid binder makes contact and is distributed throughout the powder bed – a schematic is shown in Figure 2-1 (a) [2]. The regime map for nucleation by Hapgood et al. shows that nucleation is separated into drop controlled, intermediate, and mechanical dispersion zones, and is shown in Figure 2-1 (b) [3]. The nucleation regime is based on the dimensionless drop penetration time and spray flux (τ_p & Ψ_a) and although it was originally developed for batch granulation systems, the authors mention that it also applies to TSG [3]. Due to the confined space in TSG and its high shear, mechanical dispersion is the only nucleation regime applicable as there is no time for the liquid to equilibrate with the powder bed on its own – meaning the nucleation is only partially completed at the injection site, which leads to uneven wetting[4]. Wetting kinetics are formulation dependent and are not fully understood in TSG. However, in general drop penetration time is affected by binder viscosity, powder bed porosity, surface tension, and work of adhesion which affect nucleation kinetics [3, 5].

(a) (b)

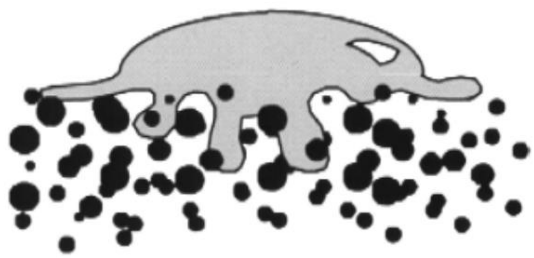

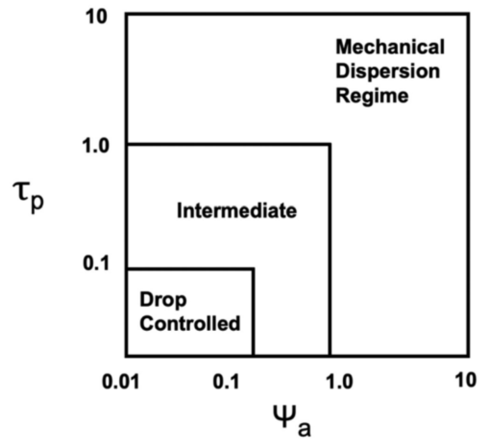

Figure 2-1. (a) Initial nucleation of liquid binder with the powder bed and (b) nucleation regime in granulation as a function of dimensionless drop penetration time and spray flux [2, 3].

After nucleation, granule growth occurs in the upstream conveying zone through layering of powder onto the wetted granules [4]. The wetted granules may also clump together to coalesce, depending on the state of saturation. Multiple saturation states can exist for granules depending on the physiochemical properties of the granules themselves and the amount of liquid binder available. Conway-Jones et al. [6] divided granule saturation states into: pendular, capillary, funicular, droplet, and pseudo droplet – a schematic is shown in Figure 2-2. The pendular state refers to the particles in the powder bed connected with each other through liquid bridges after initial contact with the binder. Funicular is a transition state between capillary and pendular where the voids in the granules are not fully saturated with liquid. The droplet state is when all particles are completely held in or at the surface of a liquid drop whereas the pseudo-droplet occurs in poor wetting systems where unfilled voids are trapped in the liquid droplet [2].

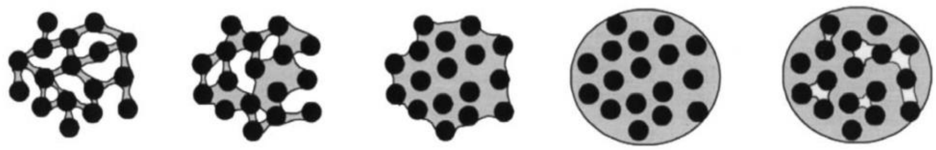

Figure 2-2. Granule saturation states described by Conway-Jones et al [6].

As the granules approach the kneading zone of TSG, granule growth and breakage occur simultaneously at the kneading block [4]. The compaction caused in the kneading zone forces the granules to contact each other and coalesce increasing granule growth. Granule growth in the kneading zone is affected by both process parameters and formulation properties. One of the most widely known growth regime map developed by Iveson et al. [7] originally developed for drum granulation divided granule growth into seven sections depending on the extent of granule deformation and pore saturation: dry powder, crumb, slurry, nucleation, induction, steady growth, and rapid growth [7]. The authors described pore saturation and granule deformation in terms of granule porosity, liquid/solid density, liquid to solids (L/S) ratio, granule yield strength, and collision velocity [4, 7]. Despite it being widespread, the parameters do not fully translate to TSG due to the differences in the mechanism, operation, and process parameters. Kotamarthy et al. [8] developed a granule growth regime specific to twin screw granulation through the use of existing data. They gathered 132 experiments from multiple studies which varied

L/S ratio, RPM, flowrate, temperature, binder viscosity, formulation, extruder size, and screw design to develop this regime map [8]. They had separated the granule growth regime into the following: under-wetted, crumb, nucleation dominated, breakage dominated, aggregation dominated, layering dominated, slurry. The two growth regimes are plotted in Figure 2-3 for comparison.

(a) (b)

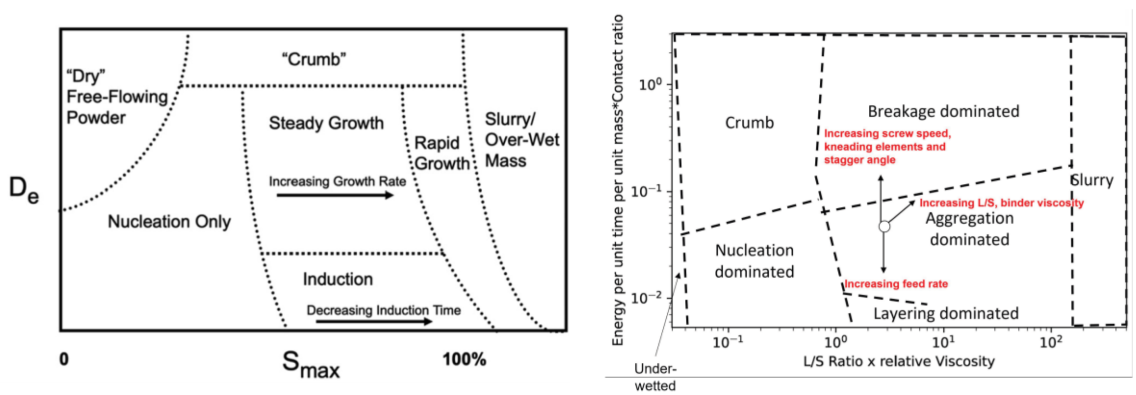

Figure 2-3. Granulation growth regime map by (a) Iveson et al. [7] and (b) Kotamarthy et al. [8]

Both regime maps use the same principles of surface wetness and deformation to quantify granule growth regimes. Iveson et al. [7] used S_{max} which quantifies liquid content for the x-axis and Stokes deformation number in the y-axis. Kotamarthy et al. [8] utilized the L/S ratio multiplied by the relative viscosity of the binder relative to water as the parameter for surface wetness. The y-axis for granule deformation utilized the specific mechanical energy normalized with the mean residence time (MRT) and ratio of free volume to the maximum available volume in the extruder and combined it to one variable (E_s). This variable was then multiplied by the contact ratio, which is defined as the ratio between the maximum post-impact radius to the original radius of a granule [9]. The contact ratio was regressed to be a function of L/S ratio, impact velocity, particle size, and binder viscosity with an R^2 value of 0.98. The parameters E_s and the contact ratio regression equation are shown in Equations 2-1 and 2-2.

$$E_s = \frac{\tau\omega}{FR \times MRT \times \frac{V_{free}}{V_{max}}} \tag{2-1}$$

$$Contact\ Ratio = 0.0735 D_p \times 0.03486\ \sigma_{binder} \times L/S + 0.1352\ v_s \times L/S \tag{2-2}$$

where τ is the impeller torque, ω is impeller speed, FR is the mass flow rate, MRT is the mean residence time, V_{free} is the free volume in the extruder, V_{max} is the maximum volume without the screws, D_p is the primary particle diameter, σ_{binder} is the viscosity of the binder, and L/S is the liquid to solids ratio.

Increasing the screw speed decreases the MRT due to increased velocity of the powder bed. Increasing screw speed has also been shown reduce the degree of fill in the extruder to an extent, which reduces the impeller torque. Vercruysse et al. [10] and Mendez et al. [11] showed that the effect of screw speed on torque drastically decreases at high screw speeds. As the axial velocity in the extruder increases, it will likely also increase the impact velocity of particles in the machine, generating an overall positive effect for both E_s and the contact ratio [8]. The increase in screw speed to moderate amounts will allow more granules to coalesce with each other, thereby driving more granular growth. Once the screw speed becomes extremely high, granule breakage will increase to increased particle collisions as well as shear being applied on the granules.

The L/S ratio is another important parameter affecting particle growth and has a direct positive impact on the x & y-axis of Kotamarthy's regime map [8]. An increase in the L/S ratio directly increases the amount liquid available in the system, which increases pore saturation as well as the rate of granule coalescence, driving up granule growth [7]. Increasing the L/S ratio also impacts the MRT and torque in the system which impact the contact ratio. Dhenge et al. [12] reported that increasing the L/S ratio increases the powder resistance due to increased viscous forces, increasing the MRT and torque. Kumar et al. [13] also reported the effects of L/S ratio on torque and MRT with respect to degree of fill and found that at very high degrees of fill, the L/S ratio decreases impeller torque and the MRT. The opposite effect was reported for lower degrees of fill. At high degrees of fill where the powder bed moves in an almost plug-like manner, the torque is already high due to the amount of material in the barrel and this increases the amount of binder to act like a lubricant. This improves powder flowability which reduces the impeller torque and the MRT. For lower degrees of fill, it was reported increasing the L/S ratio increases powder resistance due to an increase in viscous forces, matching the behaviour reported by Dhenge et al. [12].

The last major variable which affects granule growth is the solids feed rate which produces an overall negative effect on the y-axis of the regime map. Increasing the solids flowrate reduces the MRT at low to moderate degrees of fill due to the increased throughput speed of the powder bed [14, 15]. This reduces the amount of time the granules have to coalesce due to uneven wetting. At high degrees of fill when the powder moves in a plug-like manner, the MRT increases due to increased friction of the granules with the barrel – ultimately increasing the torque in the system. The increased compression force at a high degree of fill allows for improved coalescence granules as well as wetting time which improves granule growth overall.

2.2. Process Analytical Technologies for Monitoring Particle Size

The above section describes granule growth as a complex function of formulation properties and process parameters, with the final output PSD being typically bimodal for twin screw granulation. To accurately monitor this distribution in real time, the use of process analytical technologies (PAT) is required. PAT is defined as a tool or system that can utilize and analyze real time measurements from the process during manufacturing to ensure ideal processing conditions are utilized to produce a final product that conforms to desired quality metrics [16]. The goal of PAT is to enhance process understanding and control of the manufacturing process, embedding the idea of quality testing as a real time goal rather than after production. The benefits of PAT include reduced cycle times and human error, as well as improved efficiency[17]. The PAT implementation cycle shown in Figure 2-4 consists of the following [18, 19]:

1) Understanding relevant process parameters in relation to critical quality attributes;

2) Designing a measurement system that can collect process data (image, spectroscopic, etc.) in real time;

3) Developing a mathematical relationship (statistical or first principles) between product quality and collected data;

4) Integrating process control strategies with the PAT to optimize for product quality.

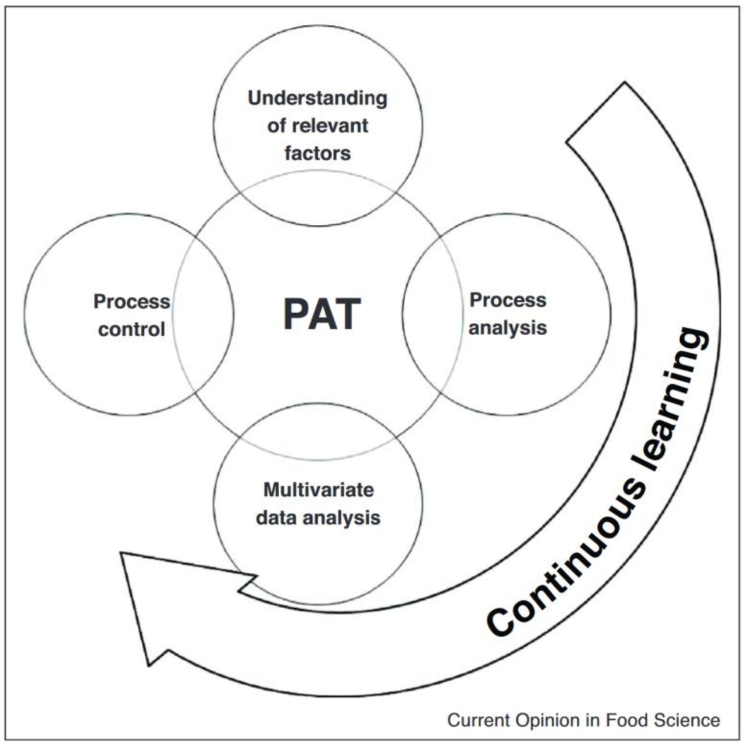

Figure 2-4. Process analytical technology implementation cycle starting with understanding relevant factors to process control[18].

Figure 2-4 highlights that developing a robust PAT is dependent on a strong understanding of the process as well as the data collection technique itself, and so this section will examine the principles of common PAT used for monitoring particle size or PSDs and their suitability for monitoring a bimodal distribution.

2.2.1. Near Infrared Spectroscopy

Spectroscopic sensors such as near infrared spectroscopy (NIR or NIRS) are one of the more common techniques for real time quality testing in manufacturing processes due to being rapid, non-invasive, and an inexpensive technique[18]. NIRS is an in-line vibrational spectroscopy tool that emits energy in the range of 750 to 2500 nm [20]. These wavelengths correspond to an object's lowest vibrational state with the end goal of gaining qualitative (physical or chemical) information from the absorption and scattering effects after interacting with the particle [20, 21]. This makes the NIRS technique sensitive to particle properties, including size, morphology, shape, and surface texture [21]. In the pharmaceutical industry, NIRS has been successfully used to monitor product and process attributes such as moisture and API content along with particle size. Some examples include Févotte et al. [22] applying NIRS to monitor the polymorphic transitions in the crystallization of an active pharmaceutical ingredient (API). Liew et al. [23] also applied NIRS for identifying formulation composition in a blending process. Bär et al. [24] applied NIRS for monitoring both particle size and moisture content in fluidized bed granulation. Meng et al and Pauli et al both have applied NIRS to monitor the PSD in twin screw granulation (TSG), although in both cases only singular descriptors including d_{10}, d_{50}, and d_{90} were predicted [25, 26]. Finally, Colón et al applied NIRS to monitor the API content in a tabletting process [27]. Despite the wide spread applicability of NIRS, Troup et al. [28] and others [29, 30] report that NIRS suffers from the fouling of the probe or the window, along with the large amount of data needed to calibrate the sensor before it can be actively used [31], making the technique unsuitable given the focus of this work – to find a robust, inexpensive, and accurate PAT for monitoring a bimodal distribution.

2.2.2. Optical Tools

Optical based methods are one of the most known for measuring PSDs, and can be split into a static tool like the Flashsizer ® 3D[32] or a dynamic tool like the Eyecon ® camera [32]. For the purposes of process monitoring, this review will only be focused on techniques potential for in-line monitoring. Image based techniques involve using custom camera systems with integrated with edge detection algorithms either with or without artificial intelligence models [33, 34] have shown great promise to predicting the PSD.

The Eyecon ® camera is a commercial tool that has been used to measure PSDs in real time [32, 35, 36]. The principle behind the operation of the camera is that it uses a flash imaging technique coupled with built in image analysis to estimate the diameter of the particle falling. A schematic of how the camera works is shown in Figure 2-5 [32]. During operation, the particles are illuminated with red, green, and blue light from different angles to build a color based image of the particle free falling[32, 35]. Using its built-in algorithm an ellipse is fitted on the particle edges to obtain its maximum and minimum diameters to calculate the average aspect ratio (AAR) using Equation (2-1) below.

$$AAR = \frac{D_{max}}{D_{min}} \tag{2-1}$$

Where D_{max} and D_{min} represent the maximum and minimum diameter, respectively. The average diameter (d) is then computed by taking the average of D_{max} and D_{min}. The mass of the particle is then computed in Equation (2-2) and is modelled as a sphere.

$$m = \frac{\pi\, d^3}{6}\rho \tag{2-2}$$

Where d is the average diameter and ρ is the density of the particle. The camera assumes that all particles have the same density (and cannot be changed), so the mass outputted is a relative one. The distribution is then outputted by ordering particles based on their relative mass to output metrics like d_{10}, d_{50}, etc. [32, 35]. The measurement range of this camera is between 50 – 3000 μm and can capture granules moving up to 10 m/s [35, 36].

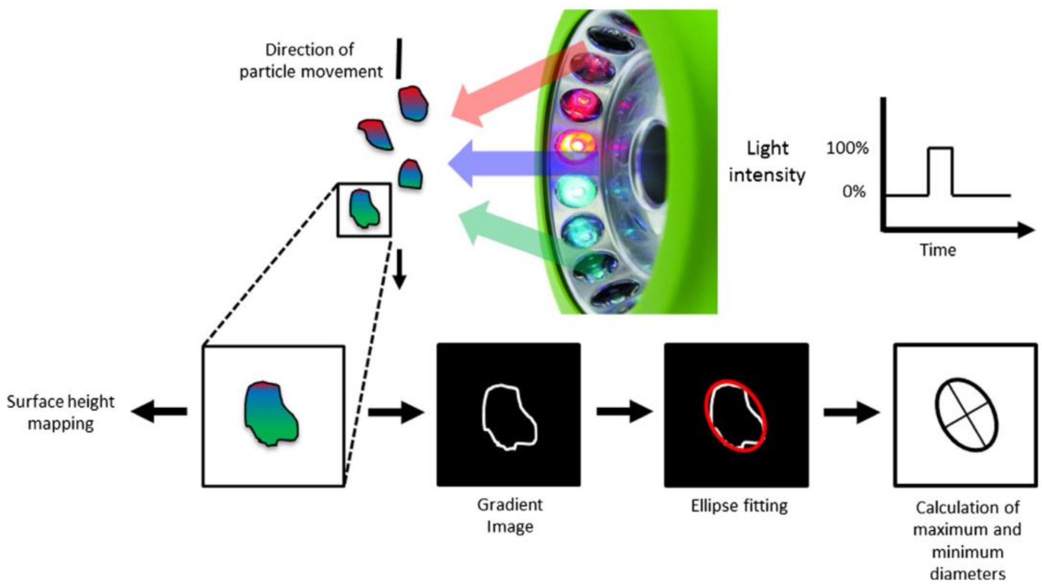

Figure 2-5. Operating principle of the Eyecon ® camera. Adapted from [32].

The advantages of this technique are that it is non-contact, non-destructive, and have successfully been implemented for in-line particle size monitoring for unit operations. Sayin et al and Kumar et al have used the Eyecon™ camera in TSG to monitor the PSD, but similar to NIRS only singular descriptors of the PSD were shown [37, 38]. McAuliffe et al also applied image processing to a roller compaction process to the monitor the PSD, with the distribution being monomodal in this case [39]. Disadvantages of camera-based systems like the Eyecon^{TM}, lie in fact that the optical surface is suspect to fouling. The Eyecon^{TM} in particular has been shown to have trouble estimating fines [36] and very elongated granules which are not uncommon in TSG [40].

2.2.3. Spatial Filtering Velocimetry

Spatial Filtering Velocimetry (SFV) is a laser-based technique that attempts to measure the cord length of a particle as a way to determine its size [41]. The cord length of a particle is defined as a geometric line on the surface of the particle reflected from the laser beam [32]. For a spherical particle, its diameter is defined as the largest cord length and is independent of the particle orientation, unlike an irregularly shaped particle where the orientation heavily influences the cord length measurement. A visualization of the cord length for spherical and elongated particles is shown in Figure 2-6 [32].

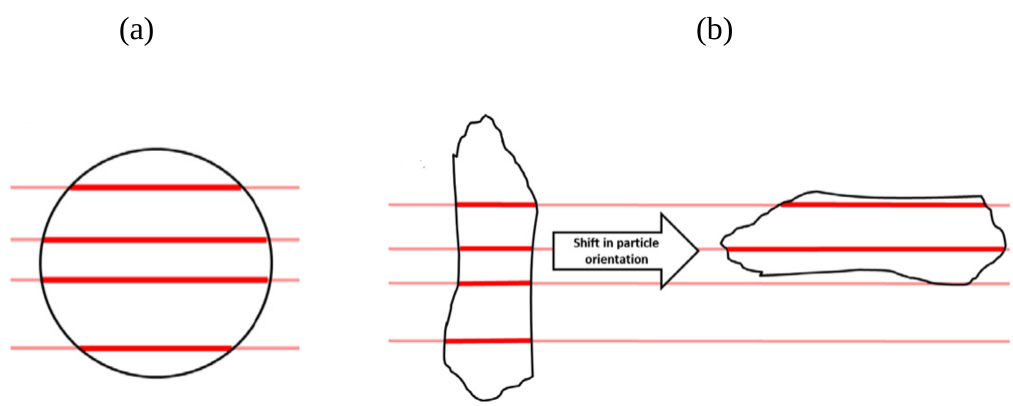

Figure 2-6. Cord length (bold lines) visualization of (a) spherical and (b) non spherical particles. Adapted from [32].

The number of times the cord length is measured takes the form of a probability density function and the location of the acquired cord length is random. From there the acquired cord length distribution can be related to the PSD, hence it not being a direct measurement of particle size. SFV relies on a set of optical fibers to detect the shadow of the particle after the laser beam hits the particles to compute the cord length. Two bursts (to be used by multiple optical fibers) and a pulse (for a single optical fiber) beam are sent out to compute the falling particle velocity, the velocity is then multiplied by the duration of the laser beam to compute the cord length [41, 42]. The SFV technique has been commercialized (i.e. Parsum ® IPP70 probe) and has been implemented to measure the PSD in multiple applications, including fluidized bed granulation, pellet coating, and twin screw granulation. Burggraeve et al. [43] installed a Parsum probe inside a fluidized bed granulator to monitor both particle size and particle growth as a function of time. Flottman et al. furthermore applied the probe to monitor the full PSD – with the process producing a monomodal one. For bimodal PSDs, Celokovic et al. [44] installed a parsum probe in an exit chute at the end of the twin screw granulator and successfully monitored the PSD – although they have reported detecting corrupted signals occasionally. The principle of operation for the Parsum ® probe is shown in Figure 2-7 [42]. To output the PSD, the Parsum probe has a built-in algorithm that convert the cord length distribution to a PSD.

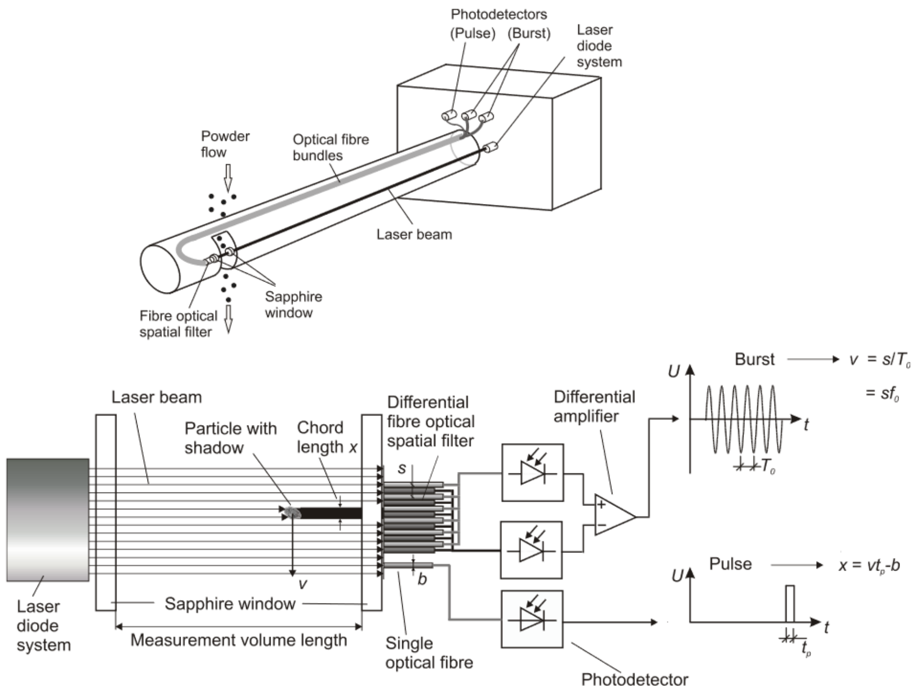

Figure 2-7. Working principle of the spatial filtering velocimetry technique in the Parsum ® probe [42].

Similar to optical techniques and NIRS, the Parsum ® probe has the advantage of being non-destructive, with the addition of being sensitive to particle shape, giving it more potential than optical techniques which rely of sphericity as part of its assumptions. It can measure particles between 50 to 6000 μm and can detect particles moving between 0.01 – 50 m/s. The disadvantage is similar to both techniques, in it being suspect to fouling of the probe despite an air cleaning system installed. Another disadvantage is the invasive nature of the probe on the process, needing to be in contact with the powder to detect the cord length distribution. This invasive nature has led some researchers to make direct modifications to process equipment [45].

2.2.4. Acoustic Emission

Acoustic emission (AE) is a non-destructive evaluation technique that measures the transient stress waves generated by localized changes in internal stresses within solid materials [46]. The stress waves are detected via piezoelectric sensor which then outputs a signal, a flow diagram of the technology is shown in Figure 2-8. This technology has been shown to be low cost, and portable [47]. In the context of the granulation process, stress waves can occur by either particle-particle or particle-surface interactions [48]. The shape of the measured signal or wave is highly dependent on the properties and kinetic energy of a moving particle. These properties include particle size, strength, porosity, and moisture content [49-51]. This makes AE suitable for monitoring, both process and product variables in real time.

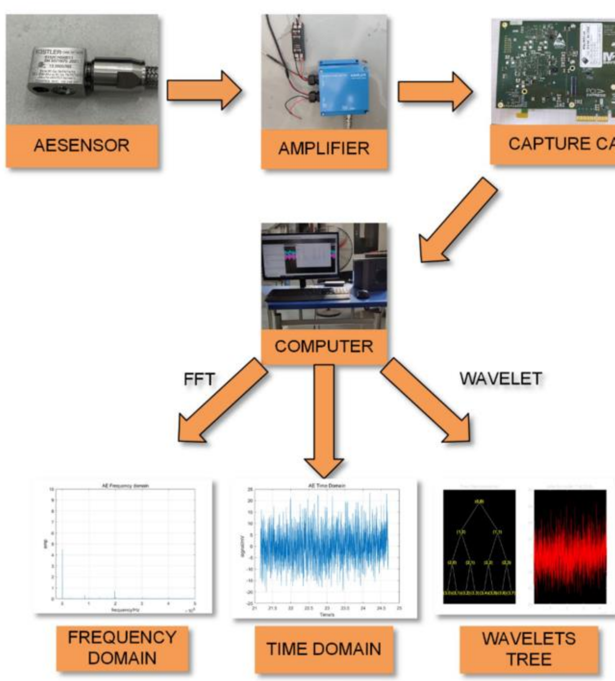

Figure 2-8. Flow diagram of the acoustic emission technology and analysis [47].

Unlike optical or laser-based technologies, the AE sensor does not need to be close to the process. The sensor can be placed on the surface of any process unit, but it can also be placed at a surface away from the process making it a relatively non-invasive technique. AE also has the advantage of needing no calibrations and is not limited to a particle size range or velocity. In theory so long as a signal can be detected, the particle size can be estimated. The sensor must detect a stress wave, from either particle-particle or particle wall impacts, which can be a disadvantage when attempting to analyze ultrasonic frequencies but as mentioned previously that can be mitigated by placing the sensor away from the process or on a separate platform near the process. Another disadvantage is if one is analyzing the audible range of the spectrum, the waveform can be convoluted with process and environmental noise, requiring extra filtering and potentially deconvolution before any analyses can be made. Lastly, AE is also susceptible to auditory masking, which is a phenomenon that occurs where sounds from multiple independent sources affect one another[52]. Auditory masking affects both the amplitude and frequency of the resulting spectrum with lower frequency impacts having a strong tendency of being masked by higher frequency impacts[52, 53].

There are multiple methods in the literature where AE has been used to predict both the average particle size and the PSD. Buttle et al. [54] deconvoluted particle impacts of spherical beads onto a metal plate using Green's functions to predict the PSD. Leach et al. [55] also analyzed parameters like the rise time, signal width, as well as the wavelength of the envelope and showed there was a linear relationship in the size range tested (50 μm – 3 cm) between those parameters and the diameter of particles colliding with each other.

Lastly, Uher et al. [56] applied Hertz Theory of Impact to predict the PSD by collecting particle impacts falling from a hopper, varying both the mass ratio of the mixture as well as the particle velocity. Outside the use of signal analysis, multivariate techniques such as latent variable methods and neural networks have also been used with AE data to predict particle distributions. Bastari et al. [57] workflow involved extracting signal features the signal through wavelet packet decomposition followed by principal component analysis to reduce the dimensionality of the feature vector. The resulting scores were then fed into a neural network model to predict the PSD for coal powder in a grinding process. Hansuld et al. [58] collected audible acoustic emissions from a high shear granulation process and utilized partial least squares to show that the total power spectral densities between 20 – 20,000 Hz can be used to predict individual particle sizes. In all cases, the studies were able to monitor or predict Gaussian distributions. Other applications which employed similar methods in the pharmaceutical industry have been applied to fluidized bed granulation [59, 60] along with high shear granulation [50, 61, 62].

As of the writing of this thesis, little literature exists with AE being applied to predict or estimate a bimodal distribution. The value that AE brings over other PAT is that it can potentially detect any particle size so long as a signal can be detected and that it can be placed away from the process. This makes AE far less susceptible to fouling thereby enhancing its practicality and will be the PAT of choice for this thesis. However, in TSG, concurrent small and large particle-wall or particle-particle collisions make it likely for auditory masking to occur, specifically in the amplitudes and frequencies of finer granule impacts in the recorded signal. The degree to which the granule impacts mask the resulting distribution in the acoustic spectrum is unknown but one potential solution that was undertaken in this work, is using digital filtering to minimize the masking behaviour. The details of the filtration technique are shown in Chapters 3 & 4. The waveform detected from an AE sensor is very dependent on the nature of impact occurring. To better understand how impact collisions affect AE signal, the basics of impact mechanics will be covered in next section.

2.3: Impact Mechanics

An impact is defined as a collision between two bodies at a specific instant in time. At each instant of the impact, the resulting pressure causes local deformation and an indentation of both bodies [63]. An impact is split into two phases, compression and restitution. During the compression phase, the kinetic energy is converted to internal energy through the contact force. Simultaneously, the work done by the contact force exerts an equal but opposite force on the two bodies causing deformation [63]. The compression phase ends when the relative velocity of both bodies is zero. During the restitution phase, the elastic energy stored from the compression phase is released and pushes both bodies away from each other until separation occurs at some relative velocity.

The type of impact analysis most relevant to AE data from TSG are rigid body impacts, which refer to the contact area being small relative to the overall dimensions of the two impacting bodies [64]. There are three types of collisions that can occur in solid impacts: elastic, viscoelastic, and elastoplastic collisions [65]. Figure 2-8 shows the contact force as a function of indentation for all three types of collisions [63]. If the impact is perfectly elastic, then no energy is dissipated during the collision, and the stress-strain relationship of the material can be modelled as a Hookean spring (i.e. independent of impact velocity). Energy dissipation (i.e. due to heat, friction) causes less energy to be released during restitution as kinetic energy, causing a hysteresis which can be modeled as the area under the curve of the restitution curve, as seen in Figure 2-9 (a) [63, 66]. The degree of elasticity (or how spring like) of a collision is quantified through a metric called the coefficient of restitution (COR). It has multiple definitions, which includes the area under the curve of the restitution plot (elastic energy released) divided by the area under the curve of the compression curve (kinetic energy converted to internal energy) [63]. Another more commonly used definition is the ratio of the rebounding velocity divided by the impact velocity [63, 65, 66]. The COR is vital for characterizing impact energy and is used in many particle discrete element method simulations and to characterize different types of materials.

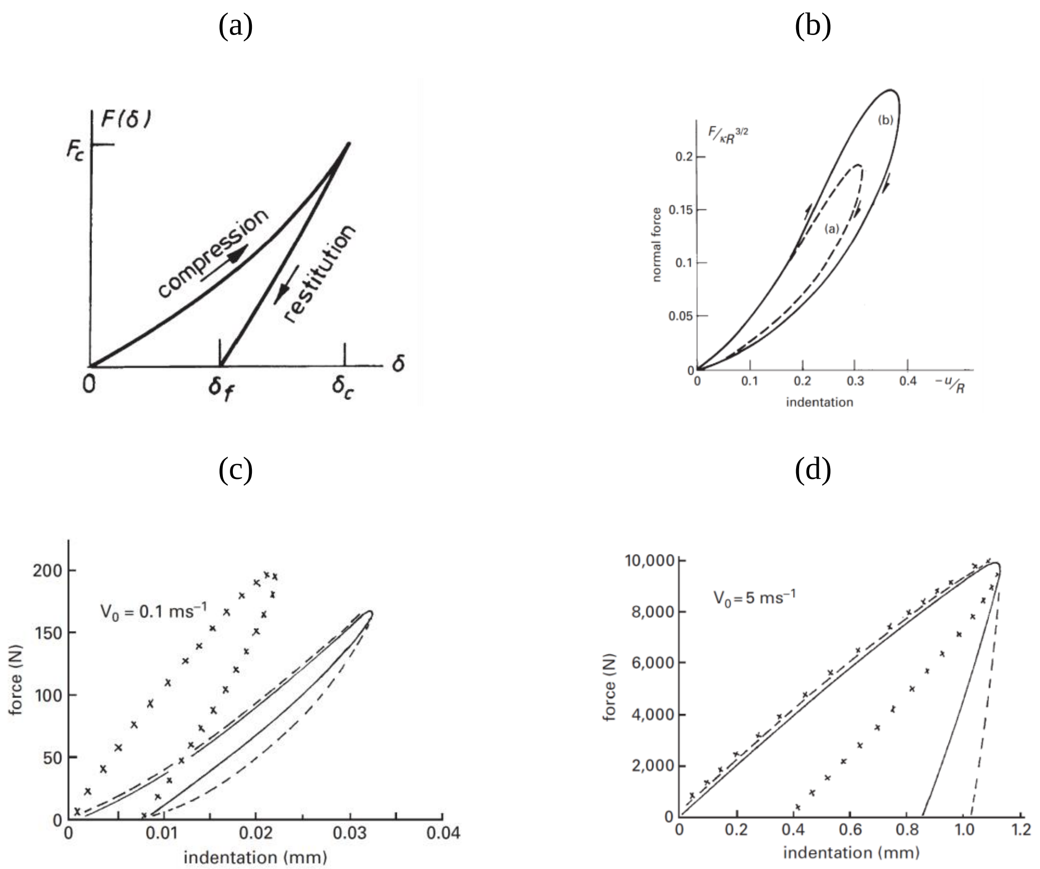

Figure 2-9. Contact force as a function of indentation for (a) elastic (b) viscoelastic and (c) & (d) elastoplastic collisions modeled with various micromechanical relations [63].

For viscoelastic collisions, Figure 2-9 (b) shows a hysteresis effect where the compression increases the impact force to some maximum which is dependent on the impact velocity, unlike perfectly elastic impacts [63, 67], followed by a decrease in the impact force back to the origin. Viscoelastic collisions are commonly modeled with a spring and dashpot which introduces dampening forces that increase as the impact velocity increases [67]. The increase in the dampening force increases the area of the hysteresis loop thereby decreasing the COR.

Elastoplastic impacts exhibit similarities to viscoelastic impacts in that it can be modeled with a spring and dashpot, but elastoplastic theory assumes that both the spring and the dashpot can undergo hysteresis. Figure 2-9 (c) and (d) shows an example of this behavior where the impact velocity changes the maximum contact force. The hysteresis in the restitution curve is a result of plasticity, wave propagation, and losses due to heat making it so that it does not return to the origin [63, 66, 68].

The type of impact occurring can have a strong effect on the AE waveform produced. As the COR decreases, the colliding force of a particle of specific size, density, and impact velocity upon impact with another object decreases due to a decrease in kinetic energy attributed to the particle's plasticity which is thereby affecting the AE waveform produced. The degree by which elasticity changes for an impact in the case of twin screw granulation is mainly dependent on formulation properties and liquid content. As the liquid content increases, the interstial fluid between individual particles in a granule will increase plasticity at the time of collision, making the impact more inelastic. For example, hydrogels have been shown to become increasingly inelastic once wet [69]. With simultaneous impacts of different particle sizes, the AE waveform increases in complexity requiring the use of multivariate techniques to correlate recorded emissions back to particle sizes. The

use of AE in this case can generate large datasets due to the high degree of particle collisions occurring, which makes AE very suited for artificial intelligence techniques covered in the next section.

2.4: Artificial Neural Networks

Artificial intelligence is a vast field that aims to develop computers to think or act similar to human beings [70]. Machine learning is a sub-branch of artificial intelligence that allows computer systems to learn and improve through statistical and optimization algorithms – with artificial neural networks (ANNs) being one of the more common tools used in materials science and engineering [70]. ANNs are computational algorithms used to model data and are typically used for pattern recognition or extracting trends [71]. Their advantages include the ability to learn and model highly non-linear relationships, work with very small or very large datasets, and the use of multiple types of data (image/text) to predict an output [71]. However, its main disadvantage is its black box nature. The convergence of the algorithm is not necessarily correlated to a scientific law, and it is often unclear how the input data influences its predictions, which is why it is often recommended to use a large amount of data for training so the model can learn any underlying behaviour in the process [71].

The structure of the ANN is divided into three layers: an input layer, hidden layer (s), and an output layer [70, 71]. The purpose of each layer is to compute the data received accordingly using a user set function (also called an "activation function") with the end goal of learning a weighting that maps the input data to the output [72]. Some common activation functions include the linear activation function ($y = x$), rectified linear activation function (ReLU), hyperbolic tangent function (tanh), and the sigmoid function[72]. A schematic of an ANN and the activation functions are shown in Figure 2-10 and Table 2-1 [72, 73].

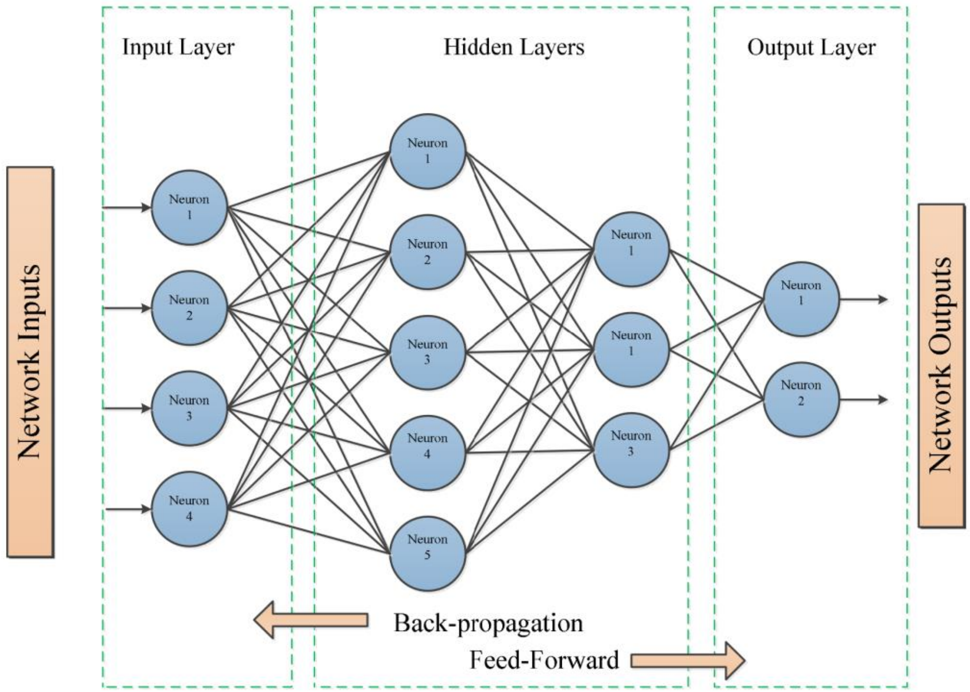

Figure 2-10. Schematic of ANN architecture with input, hidden, and output layers [73].

Table 2-1. Activation function equations used in ANNs.

Name	Equation	Output Range	Reference
Sigmoid	$\frac{1}{1+e^{-x}}$	$(0,1)$	[72]
Hyperbolic Tangent	$\frac{1}{1+e^{-2x}}-1$	$(-1,1)$	[72]
ReLU	$\max(0,x)$	$[0,\infty)$	[74]

Leakly ReLU	$\max(0,x)+\alpha\min(0,x)$	$(-\infty,+\infty)$	[74]
ReLU6	$\min(\max(0,x),6)$	$[0,6)$	[75]
ELU	$\max(0,x)+\min(0,\alpha(e^{x}-1))$	$(-\alpha,\infty)$	[76]
SELU	$\gamma(\max(0,x)+\min(0,\alpha(e^{x}-1))$	$(-\gamma\alpha,+\infty)$	[77]
Swish-1	$\frac{x}{1+e^{-x}}$	$(-1,+\infty)$	[78]
Mish	$x\tanh(\ln(1+e^{x}))$	$(0,+\infty)$	[79]

The design of the architecture (i.e. number of nodes or layers) for an ANN is very dependent on the application and in many cases, it is based on trial and error. However, there are some rules of thumb for activation functions that are common to regression-based problems. For instance, Goodfellow et al. [80] recommended that the default activation used in ANN's is the ReLU function – it is particularly useful for the hidden or input layers as it can introduce non-linearity to the training process. Other activation functions such as tanh or sigmoid are not used as much in deep neural networks as they are susceptible to the vanishing gradient problem [81, 82]. The gradients of the activation functions are used in the training process and since the output of the sigmoid/tanh is bounded between (0, 1) or (-1,1), this either slows down the training process or risks convergence to false local minima [80, 83]. The activation function of the output layer is partly dependent on the data itself. If the output data is between 0 and 1 and is non-negative the sigmoid function is better suited otherwise the linear activation function should be used as it is unbounded.

AE data has been used with ANNs for fault detection, process monitoring, or material property prediction (although this was less common). Kim et al. [84] used five AE data characteristics including the rise time, energy, event duration, and peak amplitude to predict the stress intensity factor arising from microcracks on tensile tests of structural steel. The architecture consists of an input, hidden, and output node – all with the sigmoid activation function. Taha et al. [85] employed the speed, load, and maximum amplitude for detection of bearing defects. Similar to Kim et al., Taha used one input, hidden, and output layers for the prediction. Laxman et al.[86] used 13 parameters from their AE spectra to monitor the vehicle load using a three layer network with one input, hidden, and output layer. The studies above show that using the characteristics of the AE waveform can be used to directly compute product quality metrics (regression) or detect faults/process monitoring (classification).

In TSG, the PSD is bimodal and is relatively complex, which in this thesis necessitated the use of a deep neural network with multiple hidden layers. AE parameters are generally well correlated with singular descriptors of the PSD such as d_{50} or d_{90} but as mentioned in Chapter 1, singular descriptors are not accurate indicators of this type of PSD itself, which demands the use of the entire spectrum for monitoring by an inline system.

2.5: References:

[1] R.M. Dhenge, J.J. Cartwright, M.J. Hounslow, A.D. Salman, Twin screw granulation: Steps in granule growth, International Journal of Pharmaceutics, 438 (2012) 20-32.

[2] S.M. Iveson, J.D. Litster, K. Hapgood, B.J. Ennis, Nucleation, growth and breakage phenomena in agitated wet granulation processes: a review, Powder Technology, 117 (2001) 3-39.

[3] K.P. Hapgood, J.D. Litster, R. Smith, Nucleation regime map for liquid bound granules, AIChE Journal, 49 (2003) 350-361.

[4] Y. Zhang, T. Liu, S. Kashani-Rahimi, F. Zhang, A review of twin screw wet granulation mechanisms in relation to granule attributes, Drug Development and Industrial Pharmacy, 47 (2021) 349-360.

[5] M. Denesuk, G.L. Smith, B.J.J. Zelinski, N.J. Kreidl, D.R. Uhlmann, Capillary Penetration of Liquid Droplets into Porous Materials, Journal of Colloid and Interface Science, 158 (1993) 114-120.

[6] D. Newitt, A contribution to the theory and practice of granulation, Trans. Instn. Chem. Engrs., 36 (1958) 422-442.

[7] S.M. Iveson, J.D. Litster, Growth regime map for liquid-bound granules, AIChE Journal, 44 (1998) 1510-1518.

[8] L. Kotamarthy, C. Sampat, R. Ramachandran, Development of a Granule Growth Regime Map for Twin Screw Wet Granulation Process via Data Imputation Techniques, Pharmaceutics, 2022.

[9] J. Fu, M.J. Adams, G.K. Reynolds, A.D. Salman, M.J. Hounslow, Impact deformation and rebound of wet granules, Powder Technology, 140 (2004) 248-257.

[10] J. Vercruysse, D. Córdoba Díaz, E. Peeters, M. Fonteyne, U. Delaet, I. Van Assche, T. De Beer, J.P. Remon, C. Vervaet, Continuous twin screw granulation: Influence of process variables on granule and tablet quality, European Journal of Pharmaceutics and Biopharmaceutics, 82 (2012) 205-211.

[11] C. Mendez Torrecillas, L.J. Gorringe, N. Rajoub, J. Robertson, R.G. Elkes, D.A. Lamprou, G.W. Halbert, The impact of channel fill level on internal forces during continuous twin screw wet granulation, International Journal of Pharmaceutics, 558 (2019) 91-100.

[12] R.M. Dhenge, J.J. Cartwright, M.J. Hounslow, A.D. Salman, Twin screw wet granulation: Effects of properties of granulation liquid, Powder Technology, 229 (2012) 126-136.

[13] A. Kumar, M. Alakarjula, V. Vanhoorne, M. Toiviainen, F. De Leersnyder, J. Vercruysse, M. Juuti, J. Ketolainen, C. Vervaet, J.P. Remon, K.V. Gernaey, T. De Beer, I. Nopens, Linking granulation performance with residence time and granulation liquid distributions in twin-screw granulation: An experimental investigation, European Journal of Pharmaceutical Sciences, 90 (2016) 25-37.

[14] R.M. Dhenge, J.J. Cartwright, D.G. Doughty, M.J. Hounslow, A.D. Salman, Twin screw wet granulation: Effect of powder feed rate, Advanced Powder Technology, 22 (2011) 162-166.

[15] S.V. Muddu, L. Kotamarthy, R. Ramachandran, A Semi-Mechanistic Prediction of Residence Time Metrics in Twin Screw Granulation, Pharmaceutics, 2021.

[16] ICH Guideline Q10 on Pharmaceutical Quality System, https://www.ema.europa.eu/en/documents/scientific-guideline/international-conference-harmonisation-technical-requirements-registration-pharmaceuticals-human-guideline-q10-pharmaceutical-quality-system-step-5_en.pdf, 2008.

[17] A.A. Gowen, C.P. O'Donnell, P.J. Cullen, S.E.J. Bell, Recent applications of Chemical Imaging to pharmaceutical process monitoring and quality control, European Journal of Pharmaceutics and Biopharmaceutics, 69 (2008) 10-22.

[18] S. Grassi, C. Alamprese, Advances in NIR spectroscopy applied to process analytical technology in food industries, Current Opinion in Food Science, 22 (2018) 17-21.

[19] A.S. Mali, M. Jagtap, P. Karekar, A. Maruška, A brief review on process analytical technology (PAT), Int. J. Curr. Pharm. Res, 8 (2016) 10-15.

[20] C. Pasquini, Near Infrared Spectroscopy: fundamentals, practical aspects and analytical applications, Journal of the Brazilian Chemical Society, 14 (2003).

[21] J. Zhao, G. Tian, H. Qu, Pharmaceutical Application of Process Understanding and Optimization Techniques: A Review on the Continuous Twin-Screw Wet Granulation, Biomedicines, 2023.

[22] G. Févotte, J. Calas, F. Puel, C. Hoff, Applications of NIR spectroscopy to monitoring and analyzing the solid state during industrial crystallization processes, International Journal of Pharmaceutics, 273 (2004) 159-169.

[23] C.V. Liew, A.D. Karande, P.W.S. Heng, In-line quantification of drug and excipients in cohesive powder blends by near infrared spectroscopy, International Journal of Pharmaceutics, 386 (2010) 138-148.

[24] D. Bär, H. Debus, S. Brzenczek, W. Fischer, P. Imming, Determining particle size and water content by near-infrared spectroscopy in the granulation of naproxen sodium, Journal of Pharmaceutical and Biomedical Analysis, 151 (2018) 209-218.

[25] W. Meng, A.D. Román-Ospino, S.S. Panikar, C. O'Callaghan, S.J. Gilliam, R. Ramachandran, F.J. Muzzio, Advanced process design and understanding of continuous twin-screw granulation via implementation of in-line process analytical technologies, Advanced Powder Technology, 30 (2019) 879-894.

[26] V. Pauli, Y. Roggo, P. Kleinebudde, M. Krumme, Real-time monitoring of particle size distribution in a continuous granulation and drying process by near infrared spectroscopy, European Journal of Pharmaceutics and Biopharmaceutics, 141 (2019) 90-99.

[27] Y.M. Colón, J. Vargas, E. Sánchez, G. Navarro, R.J. Romañach, Assessment of Robustness for a Near-Infrared Concentration Model for Real-Time Release Testing in a Continuous Manufacturing Process, Journal of Pharmaceutical Innovation, 12 (2017) 14-25.

[28] G.M. Troup, C. Georgakis, Process systems engineering tools in the pharmaceutical industry, Computers & Chemical Engineering, 51 (2013) 157-171.

[29] F. De Leersnyder, V. Vanhoorne, A. Kumar, C. Vervaet, T. De Beer, Evaluation of an in-line NIR spectroscopic method for the determination of the residence time in a tablet press, International Journal of Pharmaceutics, 565 (2019) 358-366.
[30] A.T. Tok, X. Goh, W.K. Ng, R.B.H. Tan, Monitoring Granulation Rate Processes Using Three PAT Tools in a Pilot-Scale Fluidized Bed, AAPS PharmSciTech, 9 (2008) 1083-1091.
[31] E.-A. Jung, Y.-J. Park, J.-E. Kim, Application of continuous manufacturing for solid oral dosage forms, Journal of Pharmaceutical Investigation, 53 (2023) 457-474.
[32] A.F.T. Silva, A. Burggraeve, Q. Denon, P. Van der Meeren, N. Sandler, T. Van Den Kerkhof, M. Hellings, C. Vervaet, J.P. Remon, J.A. Lopes, T. De Beer, Particle sizing measurements in pharmaceutical applications: Comparison of in-process methods versus off-line methods, European Journal of Pharmaceutics and Biopharmaceutics, 85 (2013) 1006-1018.
[33] L. Madarász, Á. Köte, B. Hambalkó, K. Csorba, V. Kovács, L. Lengyel, G. Marosi, A. Farkas, Z.K. Nagy, A. Domokos, In-line particle size measurement based on image analysis in a fully continuous granule manufacturing line for rapid process understanding and development, International Journal of Pharmaceutics, 612 (2022).
[34] O. Péterfi, L. Madarász, M. Ficzere, K. Lestyán-Goda, P. Záhonyi, G. Erdei, E. Sipos, Z.K. Nagy, D.L. Galata, In-line particle size measurement during granule fluidization using convolutional neural network-aided process imaging, European Journal of Pharmaceutical Sciences, 189 (2023) 106563.

[35] A.S. Hagrasy, P. Cruise, I. Jones, J.D. Litster, In-line Size Monitoring of a Twin Screw Granulation Process Using High-Speed Imaging, Journal of Pharmaceutical Innovation, 8 (2013) 90-98.

[36] A. Kumar, J. Dhondt, F. De Leersnyder, J. Vercruysse, V. Vanhoorne, C. Vervaet, J.P. Remon, K.V. Gernaey, T. De Beer, I. Nopens, Evaluation of an in-line particle imaging tool for monitoring twin-screw granulation performance, Powder Technology, 285 (2015) 80-87.

[37] A. Kumar, J. Dhondt, F. De Leersnyder, J. Vercruysse, V. Vanhoorne, C. Vervaet, J.P. Remon, K.V. Gernaey, T. De Beer, I. Nopens, Evaluation of an in-line particle imaging tool for monitoring twin-screw granulation performance, Powder Technology, 285 (2015) 80-87.

[38] R. Sayin, L. Martinez-Marcos, J.G. Osorio, P. Cruise, I. Jones, G.W. Halbert, D.A. Lamprou, J.D. Litster, Investigation of an 11mm diameter twin screw granulator: Screw element performance and in-line monitoring via image analysis, International Journal of Pharmaceutics, 496 (2015) 24-32.

[39] M.A.P. McAuliffe, G.E. O'Mahony, C.A. Blackshields, J.A. Collins, D.P. Egan, L. Kiernan, E. O'Neill, S. Lenihan, G.M. Walker, A.M. Crean, The Use of PAT and Off-line Methods for Monitoring of Roller Compacted Ribbon and Granule Properties with a View to Continuous Processing, Organic Process Research & Development, 19 (2015) 158-166.

[40] M.R. Thompson, K.P. O'Donnell, "Rolling" phenomenon in twin screw granulation with controlled-release excipients, Drug Development and Industrial Pharmacy, 41 (2015) 482-492.

[41] D. Petrak, Simultaneous measurements of particle size and velocity with spatial filtering technique in comparison with Coulter multisizer and laser doppler velocimetry, (2001).

[42] P. Dieter, D. Stefan, E. Günter, K. Michael, In-line particle sizing for real-time process control by fibre-optical spatial filtering technique (SFT), Advanced Powder Technology, 22 (2011) 203-208.

[43] A. Burggraeve, T. Van Den Kerkhof, M. Hellings, J.P. Remon, C. Vervaet, T. De Beer, Evaluation of in-line spatial filter velocimetry as PAT monitoring tool for particle growth during fluid bed granulation, European Journal of Pharmaceutics and Biopharmaceutics, 76 (2010) 138-146.

[44] S. Celikovic, J. Poms, J. Khinast, M. Horn, J. Rehrl, Control oriented modeling of twin-screw granulation in the ConsiGmaTM-25 production plant, International Journal of Pharmaceutics, 641 (2023) 123038.

[45] M. Fonteyne, J. Vercruysse, D.C. Díaz, D. Gildemyn, C. Vervaet, J.P. Remon, T.D. Beer, Real-time assessment of critical quality attributes of a continuous granulation process, Pharmaceutical Development and Technology, 18 (2013) 85-97.

[46] H.N.G. Wadley, R. Mehrabian, Acoustic emission for materials processing: a review, Materials Science and Engineering, 65 (1984) 245-263.

[47] J. Liu, C. Jiang, X. Yang, S. Sun, Review of the Application of Acoustic Emission Technology in Green Manufacturing, International Journal of Precision Engineering and Manufacturing-Green Technology, (2023).

[48] H. Tsujimoto, T. Yokoyama, C.C. Huang, I. Sekiguchi, Monitoring particle fluidization in a fluidized bed granulator with an acoustic emission sensor, Powder Technology, 113 (2000) 88-96.

[49] A. Crouter, L. Briens, The effect of granule moisture on passive acoustic emissions in a V-blender, Powder Technology, 299 (2016) 226-234.

[50] M.K. Papp, C.P. Pujara, R. Pinal, Monitoring of High-shear Granulation using Acoustic Emission: Predicting Granule Properties, Journal of Pharmaceutical Innovation, 3 (2008) 113-122.

[51] X. Xu, C. Mack, Z.J. Cleland, C.K.P. Vallabh, V.S. Dave, C. Cetinkaya, Correlation of solid dosage porosity and tensile strength with acoustically extracted mechanical properties, International Journal of Pharmaceutics, 542 (2018) 153-163.

[52] B. Scharf, Fundamentals of Auditory Masking, Audiology, 10 (1971) 30-40.

[53] W.A. Yost, R.R. Fay, A.N. Popper, Auditory perception of sound sources, Springer Science & Business Media2007.

[54] D.J. Buttle, C.B. Scruby, Characterization of particle impact by quantitative acoustic emission, Wear, 137 (1990) 63-90.

[55] M.F. Leach, G.A. Rubin, J.C. Williams, Particle size determination from acoustic emissions, Powder Technology, 16 (1977) 153-158.

[56] M. Uher, P. Beneš, Measurement of particle size distribution by the use of acoustic emission method, 2012 IEEE International Instrumentation and Measurement Technology Conference Proceedings, 2012, pp. 1194-1198.

[57] A. Bastari, C. Cristalli, R. Morlacchi, E. Pomponi, Acoustic emissions for particle sizing of powders through signal processing techniques, Mechanical Systems and Signal Processing, 25 (2011) 901-916.

[58] E.M. Hansuld, L. Briens, A. Sayani, J.A.B. McCann, An investigation of the relationship between acoustic emissions and particle size, Powder Technology, 219 (2012) 111-117.

[59] S. Matero, S. Poutiainen, J. Leskinen, K. Järvinen, J. Ketolainen, A. Poso, S.-P. Reinikainen, Estimation of granule size distribution for batch fluidized bed granulation process using acoustic emission and N-way PLS, Journal of Chemometrics, 24 (2010) 464-471.

[60] S. Poutiainen, S. Matero, T. Hämäläinen, J. Leskinen, J. Ketolainen, K. Järvinen, Predicting granule size distribution of a fluidized bed spray granulation process by regime based PLS modeling of acoustic emission data, Powder Technology, 228 (2012) 149-157.

[61] J.F. Gamble, A.B. Dennis, M. Tobyn, Monitoring and end-point prediction of a small scale wet granulation process using acoustic emission, Pharmaceutical Development and Technology, 14 (2009) 299-304.

[62] N.J. Watson, M.J.W. Povey, G.K. Reynolds, B.H. Xu, Y. Ding, Acoustic emission monitoring from a lab scale high shear granulator—A novel approach, International Journal of Pharmaceutics, 465 (2014) 262-274.

[63] W.J. Stronge, Impact Mechanics, 2 ed., Cambridge University Press, Cambridge, 2018.

[64] D.E. Stewart, Rigid-Body Dynamics with Friction and Impact, SIAM Review, 42 (2000) 3-39.

[65] A. Aryaei, K. Hashemnia, K. Jafarpur, Experimental and numerical study of ball size effect on restitution coefficient in low velocity impacts, International Journal of Impact Engineering, 37 (2010) 1037-1044.

[66] B. Yildirim, H. Yang, A. Gouldstone, S. Müftü, Rebound mechanics of micrometre-scale, spherical particles in high-velocity impacts, Proceedings of the Royal Society A: Mathematical, Physical and Engineering Sciences, 473 (2017) 20160936.

[67] Y.A. Khulief, Modeling of Impact in Multibody Systems: An Overview, Journal of Computational and Nonlinear Dynamics, 8 (2012).

[68] K. Hashiguchi, Multiplicative Hyperelastic-Based Plasticity for Finite Elastoplastic Deformation/Sliding: A Comprehensive Review, Archives of Computational Methods in Engineering, 26 (2019) 597-637.

[69] M.K. Yazdi, V. Vatanpour, A. Taghizadeh, M. Taghizadeh, M.R. Ganjali, M.T. Munir, S. Habibzadeh, M.R. Saeb, M. Ghaedi, Hydrogel membranes: A review, Materials Science and Engineering: C, 114 (2020) 111023.

[70] R.Y. Choi, A.S. Coyner, J. Kalpathy-Cramer, M.F. Chiang, J.P. Campbell, Introduction to Machine Learning, Neural Networks, and Deep Learning, Translational Vision Science & Technology, 9 (2020) 14-14.

[71] F. Mumali, Artificial neural network-based decision support systems in manufacturing processes: A systematic literature review, Computers & Industrial Engineering, 165 (2022) 107964.

[72] A.D. Rasamoelina, F. Adjailia, P. Sinčák, A Review of Activation Function for Artificial Neural Network, 2020 IEEE 18th World Symposium on Applied Machine Intelligence and Informatics (SAMI), 2020, pp. 281-286.

[73] M.G.M. Abdolrasol, S.M.S. Hussain, T.S. Ustun, M.R. Sarker, M.A. Hannan, R. Mohamed, J.A. Ali, S. Mekhilef, A. Milad, Artificial Neural Networks Based Optimization Techniques: A Review, Electronics, 2021.

[74] K.Z. He, Xiangyu; Ren,Shaoqing; Sun, Jian, Delving Deep into Rectifiers: Surpassing Human-Level Performance on ImageNet Classification, ICCV15, (2015).

[75] A. Krizhevsky, G. Hinton, Convolutional deep belief networks on cifar-10, Unpublished manuscript, 40 (2010) 1-9.

[76] D.-A. Clevert, T. Unterthiner, S. Hochreiter, Fast and accurate deep network learning by exponential linear units (elus). arXiv 2015, arXiv preprint arXiv:1511.07289, (2020).

[77] G. Klambauer, T. Unterthiner, A. Mayr, S. Hochreiter, Self-normalizing neural networks, Advances in neural information processing systems, 30 (2017).

[78] P. Ramachandran, B. Zoph, Q.V. Le, Searching for activation functions, arXiv preprint arXiv:1710.05941, (2017).

[79] D. Misra, Mish: A self regularized non-monotonic activation function, arXiv preprint arXiv:1908.08681, (2019).

[80] I. Goodfellow, Y. Bengio, A. Courville, Deep learning, MIT press2016.

[81] M. Roodschild, J. Gotay Sardiñas, A. Will, A new approach for the vanishing gradient problem on sigmoid activation, Progress in Artificial Intelligence, 9 (2020) 351-360.

[82] X. Wang, Y. Qin, Y. Wang, S. Xiang, H. Chen, ReLTanh: An activation function with vanishing gradient resistance for SAE-based DNNs and its application to rotating machinery fault diagnosis, Neurocomputing, 363 (2019) 88-98.

[83] S.J. Prince, Understanding Deep Learning, MIT press2023.

[84] K.-B. Kim, D.-J. Yoon, J.-C. Jeong, S.-S. Lee, Determining the stress intensity factor of a material with an artificial neural network from acoustic emission measurements, NDT & E International, 37 (2004) 423-429.

[85] Z. Taha, K. Widiyati, Artificial neural network for bearing defect detection based on acoustic emission, The International Journal of Advanced Manufacturing Technology, 50 (2010) 289-296.

[86] K. Laxman, A. Ross, L. Ai, A. Henderson, E. Elbatanouny, M. Bayat, P. Ziehl, Determination of vehicle loads on bridges by acoustic emission and an improved ensemble artificial neural network, Construction and Building Materials, 364 (2023) 129844.

Chapter 3: Predicting the Particle Size Distribution in Twin Screw Granulation through Acoustic Emissions

Predicting the Particle Size Distribution in Twin Screw Granulation through Acoustic Emissions

H.A. Abdulhussain[a], M.R. Thompson[a,*]

[a] *CAPPA-D/MMRI, Department of Chemical Engineering,*

McMaster University, Hamilton, Ontario, Canada

[*] Author to whom correspondence should be addressed.

Tel: (905) 525-9140 x 23213

mthomps@mcmaster.ca

3.1. Abstract

A non-destructive process analytical technology for monitoring the complex particle size distributions inherent to twin screw granulation (TSG) was presented, based on acoustic emissions (AE). AE spectra were collected during the wet granulation of lactose monohydrate at different liquid to solid ratios from 8-14% and correlated with the particle size distributions (PSD) to train a neural network model. Predicted PSD for particle sizes from 44 to 7000 μm based on the AE spectra showed the largest root mean squared error of 4.25 wt% at 2230 μm. After transforming the AE data with a newly created digital filter based on particle impact mechanics to address auditory masking, the maximum error for predicting fractions was reduced to below 1 wt%. This technology shows great promise in predicting the complex size distributions present in TSG in real time.

Keywords: Acoustic Emission, Process analytical technology, Twin screw granulation, Impact mechanics, Artificial neural network

3.2. Introduction

The concept of continuous manufacturing has been gaining momentum in the pharmaceutical industry over the past two decades. The publications of the United States Food and Drug Administration (FDA) on process analytical technologies (PAT) along with the harmonized tripartite Q8 guideline of the International Council for Harmonization (ICH) of 'Technical Requirements for Pharmaceuticals for Human Use' paved the way for regulatory acceptance of novel manufacturing technologies to be used in the production of solid oral dosage forms[1, 2]. The advantages of continuous, in comparison to batch, manufacturing for drug products rely upon its higher product consistency, reduced costs associated with product scale-up, and ability to readily implement PAT [2, 3].

Twin screw granulation (TSG) has gained much attention over the past decade as a continuous manufacturing technology for wet, foam, heat-assisted and hot melt granulation [3-5]. The advantages of TSG over other manufacturing technologies are its closely confined mixing characteristics, short residence time (seconds compared to minutes or hours), and modular process configuration, which dramatically reduce its equipment footprint [6, 7]. One key difference between TSG and its batch counterpart is the particle size distribution (PSD) produced. A batch granulation process is expected to produce a unimodal (Gaussian) distribution whereas TSG typically produces a bimodal distribution for the same formulation [6, 8-10]. The PSD is vital to determining tablet properties, such as strength and porosity, which ultimately affect the rate that this type of dosage form disintegrates upon ingestion [11, 12].

From a monitoring perspective, the challenges associated with a bimodal distribution are unique, since simple numerical descriptors such as the mean particle size or the span of the distribution have little correlated meaning with tabletting, unlike for a Gaussian distribution. This presents a unique need for PAT within TSG to show correlation with the PSD, not just simple particle size descriptors, to monitor for quality consistency. PAT currently examined for in-line granulation monitoring include near infrared (NIR) spectroscopy [13, 14] and image processing [11, 14, 15], though the latter is more prevalent industrially for particle sizing at the moment. Both of these approaches have the advantage of being non-destructive and can be integrated directly into the manufacturing process[13, 14]. However, NIR spectroscopy requires a large amount of data for calibration and it is subject to sensor fouling which can lead to spurious results [16]. Image processing (ex. the commercial Horiba Eyecon^{TM} system) is also subject to fouling/dust accumulation around its optics and exhibits resolution issues when looking at extremes in particle sizes [17, 18]. Both are good non-destructive technologies with no risk of interfering with or contaminating the granulation process but a more robust approach that was immune to fouling would be advantageous if it could address the aforementioned complexities of the PSD for TSG. Other potential techniques such as laser diffraction, mechanical vibrations, and electrostatic sensing have been shown to be feasible to predict particle size but are difficult to implement in a manufacturing setting due to their high costs, lower perceived sensor durability, accuracy, and reliability [19-21].

Acoustic Emissions (AE) is an approach not yet considered for TSG monitoring but conceivably well suited to the process based on its advantages of needing no calibrations, greater immunity to the influences of fouling/dust accumulation, and low implementation costs [22]. It would not be a completely novel approach since AE has been used for monitoring in the past of other particulate process operations, both within [23-26] and outside [27-29] of the pharmaceutical industry. The associated technique relate features of a detected signal to the particle impacts or collisions that generated these acoustic emissions. Most notable examples have been reported for high shear batch granulation, in order to determine the endpoint of the process and to predict a Gaussian particle size distribution [26, 30]. Outside the pharmaceutical industry, multiple studies have involved pneumatic conveyers, fluidized beds, and milling units, using AE analysis to once again predict a Gaussian distribution [19-22, 29]. Approaches for applying AE to monitor much more complex particle size distributions have yet to be disclosed in the literature.

In this regard, the present study investigates the means for developing a robust non-destructive non-contact PAT capable of monitoring the complex PSD produced by continuous granulation via TSG. To predict weight fractions for a broad range of anticipated granule sizes, it is postulated that the intensity of a set of frequencies in an acquired AE spectrum can be correlated to the impact mechanics of specific particle sizes. Furthermore, it is postulated that with appropriate signal processing and selection of a neural network model that bimodal PSD may be predicted in real-time for this continuous process.

3.3. Materials and Methods

3.3.1. Materials and Process Setup

Granulation was completed in a 27 mm 40 L/D Model ZSE-27HP corotating twin screw extruder (Leistritz Extrusion; Somerville, NJ, USA). The barrel consisted of a water-cooled feed zone (Z0) and nine barrel zones (Z1–Z9) actively controlled at 35℃. The screw speed for all experiments was 200 RPM. Flowlac® 100 α-lactose monohydrate (Meggle Pharma; Wasserburg, Germany) was chosen as the placebo formulation for the study due to its low water solubility, minimizing the effects of moisture on the acoustics during this preliminary stage of PAT development. The lactose was introduced into the extruder at a constant flow rate of 4 kg/h for all experiments using a Brabender T20 twin-screw gravimetric feeder (Mississauga, ON, Canada). An aqueous solution of 4 wt% METHOCEL™ E3PLV (DuPont Nutrition & Biosciences; Midland, MI, USA) was used as the liquid binder in this work and injected into the extruder at zone Z2 using an ISCO 260D high pressure syringe pump (Teledyne-ISCO Inc.; Lincoln, NE, USA) at varying liquid-to-solids (L/S) ratios of 8, 10, 12, 13, and 14% [31, 32]. The liquid was injected in the intermeshing region between the two screws. Experiments for each L/S ratio were repeated 10 times to build a sizeable dataset for the modeling technique described in a later section. The screw design employed for these experiments consisted of multiple conveying elements with pitches of 30 and 20 mm from Z1-Z7 followed by two kneading blocks with discs at 60 degrees offset in Z8 and then subsequent conveying elements in Z9; the screw design is typical for twin-screw wet granulation.

3.3.2. Particle Size Analysis

The granules produced from the extruder were air-dried at room temperature for 48 hours to below 5 % (w/w) moisture content before being analyzed for their size; moisture content was determined using an HG63 moisture analyzer (Mettler-Toledo; Columbus, OH). PSD data was determined using a Ro-Tap RX-29 sieve shaker (W.S. Tyler; Mentor, OH, USA). A granulated sample of 100 g for each L/S ratio was originally classified into eight size fractions (using sieves of 2100, 1700, 1400, 1180, 850, 500, and 300 μm nominal openings, as well as the bottom pan) by mechanically agitating for five minutes. The weight difference before and after sieving was used to find the wt% for each bin in the distribution. The mass on the 2100 μm sieve was subsequently classified further by reconfiguring the shaker with sieves of 8000, 6300, 4760, 3350, 2360, 2100, and 1700 μm nominal openings and mechanically agitating for another five minutes. Similarly, the mass in the bottom pan from the original agitation was subsequently classified further by reconfiguring the shaker with sieves of 500, 300, 250, 180, 150, 53, and 44 μm nominal opening and once more, mechanically agitating for five minutes. During the TSG experiments, granule sizes changed from very fine to very coarse, much more broadly than normal granulation operations. The sieving of the granules on the 2100 μm sieve and pan was done in order to capture all possible changes across different L/S ratios for the neural network model implemented in the subsequent section.

3.3.3. Acoustic Signal Acquisition

To record the continuous particle impacts exiting from the extruder, a F15α broadband sensor that was most sensitive to frequencies between 100 to 450 kHz (Physical Acoustics; Princeton, NJ, USA) was attached to a 25.4 mm x 25.4 mm tab that extended from a SAE 304 stainless steel (SS) impact plate with dimensions of 44.5 mm x 76.2 mm; seating the sensor on the tab, off to the side of the plate, was preferred since the envisioned PAT design positions the plate inside the exit chute of a TSG but ready access to the sensor will demand that it be positioned outside of the chute walls. The sensor was fitted to the impact plate using high vacuum grease (Dow Corning) to improve contact. Figure 3-1 shows the sensor and impact plate assembly.

The detected signal with the sensor was amplified using a Physical Acoustics 2/4/6c amplifier set to +60 dB and collected using a National Instruments 3.5 MHz 12-bit 4-channel data acquisition system. For each experiment, 30 seconds of data was collected from the collisions of granules onto the plate at a sampling rate of 3 MHz. The vertical distance of the plate relative to the exit of the extruder was based on an analysis of apparent terminal velocity to ensure consistency of the impacts. Approximately 97% of the particles for Flowlac® 100 were below 250 μm [33] and so, the smallest particle chosen to be a 'granule' in the model was 300 μm based on the minimum sieve size in the study unlikely to capture ungranulated solids. The drop distance for a 300 μm particle to reach terminal velocity was found to be roughly 20 cm below the exit of the extruder, which is where the plate was positioned. This was done for all experiments mentioned below. The terminal velocity analysis was done to ensure the impacts of particles at the top or bottom of the plate would be relatively consistent with one another. Figure 3-2 shows a schematic for the experimental setup with the extruder and impact plate assembly.

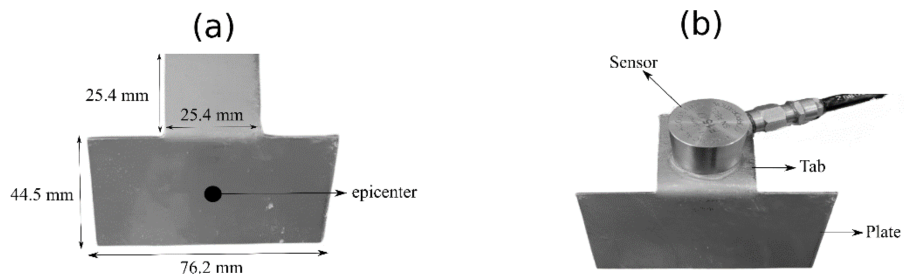

Figure 3-1. Top-down view of the impact plate inclined at 60 degrees relative to the horizontal plane (a) without and (b) with the acoustic emission sensor.

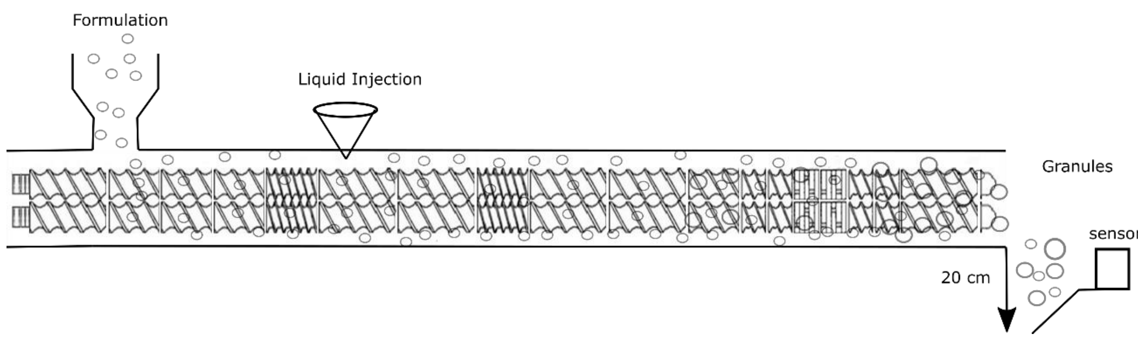

Figure 3-2. Schematic of the PAT setup for particle size monitoring, showing the twin-screw granulator and impact plate assembly positioned after its exit in the experiments.

3.3.4. Studies of Plate Angle and Plate Thickness

Initially, the impact plate setup was examined for differing inclinations of 10, 30, 45, and 60 degrees relative to the horizontal plane with a fixed plate thickness of 0.7 mm. Only granulation at 8% L/S ratio was tested in this case. AE sampling for a 30 s duration was repeated three times, for every angle to account for statistical and acoustic variance. The trajectory and mechanical integrity of granules colliding with the plate was observed at a distance of 10 mm away from the edge of the plate by high speed image analysis taken using a FASTCAM SA-Z type 2100k camera (Photron Limited, Tokyo, Japan) operating at 20,000 frames per second. Analysis of videos was done using Photron FastCam Viewer 4 software.

In the second stage of experiments analyzing the impact plate setup, *g*ranule collisions were recorded for 30 s for plates with thicknesses of 0.7, 1, and 1.5 mm at a fixed inclination of 60°. In this case, more extensive granulation was performed at 8, 10, 12, 13, and 14% L/S ratios for each plate thickness. The AE sampling for 30 s was repeated three times for every L/S ratio to account for statistical and acoustic variance.

3.3.5. Granulation Experiments for Model Training and Validation

AE monitoring of particle collisions on the 1.5 mm thick impact plate angled at 60 degrees inclination relative to the horizontal plane, were recorded according to Sec 3.3.3. TSG trials were performed at L/S ratios of 8, 10, 12, 13, and 14%. At 8% it was found there was a large amount of ungranulated particles whereas 14% was found to be the maximum saturation before the granules turned into sludge. This range ensured AE spectra was collected from very fine to very coarse granules. AE sampling for 30 s was repeated ten times per L/S ratio to generate a large training dataset for modeling and to account for statistical and acoustic variance.

With an estimated flowrate of 1.1 g/s, a sampled signal of 30 s duration corresponded to thousands or tens of thousands of collisions depending on the selected operating conditions with the extruder. Factoring in repeats, more than 4,800 sampled signals were recorded for the training and validation experiments. A discrete Haar wavelet filter was used to reduce noise followed by Fast Fourier Transform (FFT) to view each processed signal in the frequency domain. With no visible peaks roughly above 600 kHz, the chosen frequency range of analysis was 0-700 kHz in this study. Each signal dataset was reduced in size for the model, decreasing the frequency resolution from 3 Hz to 67 Hz.

A granular sample of roughly 300 g was collected for each L/S ratio after the 10 sampled signals were collected. The PSD for the trial was determined by analyzing 100 g of the collected granules. Three repeats were done to assess the error in the sieving measurement. Following the characterization method in Sec 3.3.2, weight fractions were determined for the corresponding average particle sizes (>8000, 7150, 5530, 4055, 2855, 2230, 1900, 1550, 1290, 1015, 675, 400, 275, 215, 165, 102, 49, and <44 μm). Weight fractions above 7150 μm and below 49 μm were zero wt%, and did not change as the L/S ratio increased. As a result, the size fractions of >8000 and <44 μm were not included in the final dataset to reduce redundancies, making the final distribution composed of 16 weight fractions in the model.

3.3.6. Designing an AE Impact Filter

A particle monitoring system based on impacts, where granules spanning a wide range of sizes (and strengths) presents a challenge known as auditory or spectral masking. The “sound” produced by a large particle impacting a plate will overshadow the sound produced by a smaller particle colliding at the same time or closely thereafter. Since the principle of an acoustic monitoring method is to relate the amplitude of a signal (or specific frequencies in the signal) to a count of particles, masking may have a detrimental effect on the predicted PSD. To address this issue, a digital signal filter was conceived to alleviate auditory masking at the impact plate, derived from Hertz theory for single particle impacts.

The work by Rao describes the transverse response, normal modes, along with the force response when an impact force is applied to a metal plate at rest [34]. They are shown in Equations (3-1), (3-2), (3-6), and (3-7) below. The transverse response of the plate shown in Equation (3-1) below is a function of both the normal modes of the plate along with the plate response to the force applied.

$$w(x, y, t) = \sum_{m=1}^{\infty} \sum_{n=1}^{\infty} W_{mn}(x, y)\eta_{mn}(t) \tag{3-1}$$

where W_{mn} represents the normal modes of the plate and η_{mn} is the plate response to the force applied. M and n correspond to the modal numbers for the x and y direction. The normal modes are of the plate are:

$$W_{mn} = \frac{2}{\sqrt{\rho hab}} \sin\left(\frac{m\pi x}{a}\right) \sin\left(\frac{n\pi y}{b}\right) \tag{3-2}$$

where ρ, h, a, b are the density, thickness, length, and width of the plate, respectively. Assuming the particles are spherical and collisions are elastic, the force can be modelled with the Hertz theory of impact as shown [35, 36]:

$$F(t) = F_0 \sin\left(\frac{\pi t}{t_c}\right) = F_0 \sin(\pi \Omega \mathrm{t}) \tag{3-3}$$

with F_0 being the maximum force and t_c being the contact time of a collision, and Ω is the frequency of the impact force. Expressions for the maximum force and contact time are given in Equations (4) and (5), respectively:

$$F_0 = 1.917 \rho_1^{\frac{3}{5}} \left(\frac{1 - v_1}{\pi E_1} + \frac{1 - v_2}{\pi E_2}\right)^{-2/5} R^2 V_0^{6/5} \tag{3-4}$$

$$t_c = 4.53 \left(\frac{4\rho_1 \pi \left(\frac{1 - v_1}{\pi E_1} + \frac{1 - v_2}{\pi E_2}\right)}{3}\right)^{2/5} R V_0^{6/5} \tag{3-5}$$

where ρ_1 is the density of the particle, v_1 and E_1 refer to the Poisson ratio and Young's Modulus of lactose monohydrate. R is the particle radius and V_0 is its impact velocity. Knowing the impact force, the response of the plate to the force can be determined and is shown as:

$$\eta_{mn}(t) = \frac{2F_0}{(\omega_{mn}^2 - \Omega^2)\sqrt{\rho hab}} \sin\left(\frac{m\pi x_0}{a}\right) \sin\left(\frac{n\pi y_0}{b}\right) (\omega_{mn} \sin \Omega \mathrm{t} - \Omega \sin \omega_{mn} t) \tag{3-6}$$

where x_0 and y_0 are the points of impact on the plate, and ω_{mn} is the natural frequency of the plate:

$$\omega_{mn} = \pi^2 \left[\left(\frac{m}{a}\right)^2 + \left(\frac{n}{b}\right)^2\right] \sqrt{\frac{E_2 h^3}{12(1 - v_2)\rho h}} \tag{3-7}$$

where E_2 and v_2 are the Young's Modulus and the Poisson's ratio for the plate, respectively. The plate compression for a single particle dropping onto a plate was then computed from Equation (3-1). The parameters used in Equations (3-1) – (3-7) are shown in Table 3-1.

Table 3-2. List of constants and corresponding values for granulation of lactose monohydrate.

Description	Parameter	Value	Unit	Reference
Young's Modulus (Lactose)	E_1	3.33×10^9	Pa	[37, 38]
Young's Modulus (SS)	E_2	193×10^9	Pa	[39]
Poisson's Ratio (Lactose)	v_1	0.25	No unit	[40, 41]
Poisson's Ratio (SS)	v_2	0.29	No unit	[42]
Impact velocity (Lactose)	v_0	0.74	m/s	
Density (SS)	ρ	7900	kg/m^3	[39, 42]
True density (Lactose)	ρ_1	1547	kg/m^3	[43]
Impact location (x-coordinate)	x_0	0.022225	m	

Impact location (y-coordinate)	y_0	0.0381	m	

Figure 3-3 (a) shows the plate response, on a frequency basis, for the impact of a 100 μm particle. The plate response of a single granule of 49 to 7150 μm size impacting a stainless steel plate at its epicenter, on a frequency basis, is shown in Figure 3-3 (b). As particle size increases, the plate is seen to vibrate at a lower frequency, giving an inverse relationship. This trend was also noted by others [44-46] and allows the user to understand and roughly correlate peaks in the spectrum with their particle size.

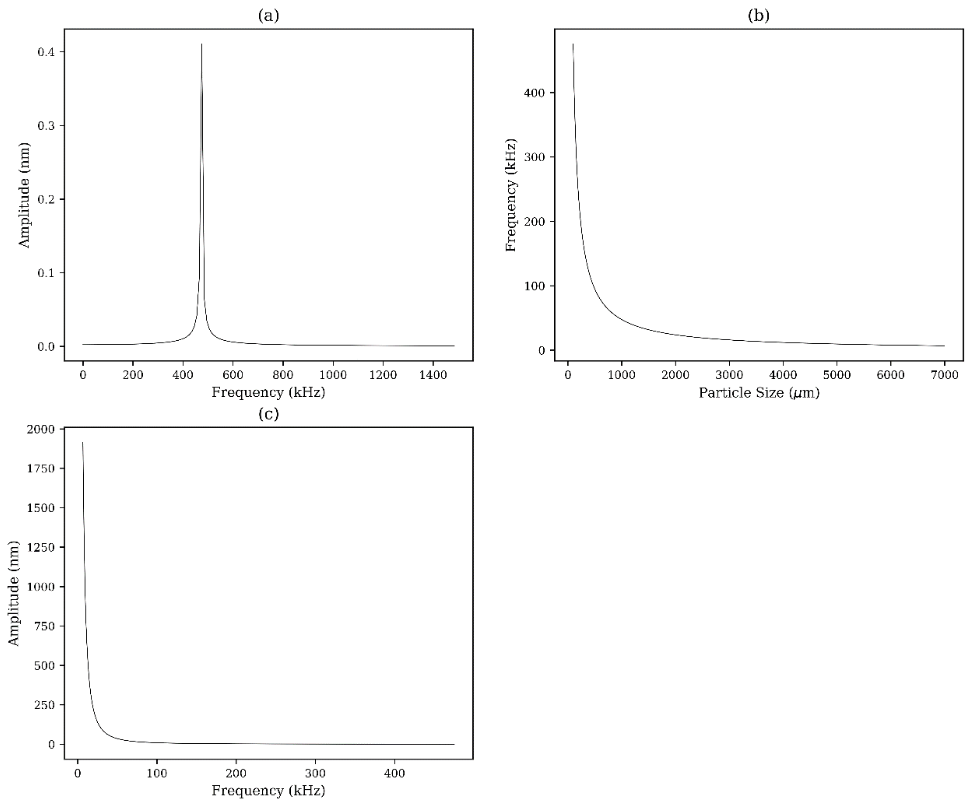

Figure 3-3. (a) Frequency spectrum for the plate response corresponding to a 100 μm particle collision. (b) Calculated frequencies corresponding to particles between 100 and 7150 μm particle collision with the plate at its epicenter. (c) Maximum amplitude and recorded frequency of particles between 100 and 7150 μm.

Assuming granules impacting the plate are spherical in nature, the mass of a single granule is calculated per particle size (49 – 7150 μm). It is assumed that the maximum mass of any particle that will strike the plate is equal to the flowrate in g/s over a one second basis (1.1 g in this study). The maximum mass is divided by the mass of every particle to obtain an approximate number of granules per particle size. The theoretical amplitude for each particle size is then scaled by the number of granules for its respective size. The measured amplitude from the AE experiments is then divided by the maximum amplitude at the theoretical impact frequency found in Figure 3-3 (c) to filter for auditory masking and produce the final spectrum.

3.3.7. Neural Network Model

To relate the data-intensive impact acoustic signal to particle sizes, an artificial neural network (ANN) model was employed due to the exhibited nonlinearity in the modelled environment. These types of models have been shown to be superior to statistical modeling when looking at highly non-linear systems [47-49], making them attractive for the purposes of predicting PSD from an AE signal. Before modeling, stratified splitting was used to ensure the training and testing sets contained an equal proportion of data for each L/S ratio. Each L/S ratio dataset was split into 80% training and 20% testing. Then 10% of the training data was used for validation during model training. Principal component analysis (PCA) was used on the training set to reduce the dataset dimensions down to 12 components which contain 64.5% of the variance in the original data. Both PCA and the ANN were setup in Python using the *sklearn* library.

For the case of the testing set, the acoustic signal from granule collisions for each L/S ratio were averaged in the testing set giving one representative spectrum for each L/S ratio. This strategy allows for simplicity when performing new experiments as well as gives the opportunity to see the prediction error for each distribution. When predicting PSD with the testing set, loadings from a PCA model were used to convert the dataset into scores. The scores are then fed into the ANN to predict the PSD. The ANN employed an input layer with 12 nodes, which correspond to the number of components from PCA. This was followed by 3 hidden layers at 500 nodes, 250, and 100 nodes, respectively along with one output layer with 16 nodes, corresponding to each particle size. The Rectified Linear Unit activation function (ReLU) was used for the input and first hidden layer. The second and third hidden layers had the hyperbolic tangent (tanh) and sigmoid function, respectively, while the output layer had a linear activation function. 50% dropout regularization was employed between layers to minimize overfitting. The chosen Loss function was the mean squared error (MSE). To quantify prediction error in the model, the root mean squared error (RMSE) was used.

For the case when the model used the AE Impact Filter, the training, testing, and validation datasets were identical to the original approach. In this case, PCA was not used to compress the AE data since it was found to worsen predictions when the filter was used. The ANN architecture was identical to the case without the filter, both in terms of the activation functions and number of layers. The only difference being the input layer had 10395 nodes due to PCA not being used to reduce the dataset.

3.4. Results and discussion

3.4.1. Effect of Plate Angle

Exiting granules from the extruder were targeted to collide at the epicenter of the plate to optimally minimize both plate vibrations and AE signal attenuation. The incline angle of the impact plate will have a strong influence on the amplitude of acoustic emissions due to the contact mechanics present. Figure 3-4 plots the average maximum amplitude in the spectra collected for inclined plate angles of 10, 30, 45, and 60 degrees relative to the horizontal plane. The maximum amplitude was seen to increase as the incline angle increased until 45 degrees, reflecting the gain in AE signal intensity associated with particle impacts. This seems contrary to expectation, at least following the theory of single particle impacts which anticipates the amplitude of AE associated with a collision should be greater for smaller inclinations [46]. The trend seen for amplitude was attributed to the accumulated mass observed on the plate over time at angles of 10 and 30 degrees, dampening the impact force of subsequent colliding particles. Conditions at 45 and 60 degrees showed no accumulated mass on the plate but as expected, the amplitude decreased for the steeper angle in these two cases due to decreasing normal collision forces by falling particles.

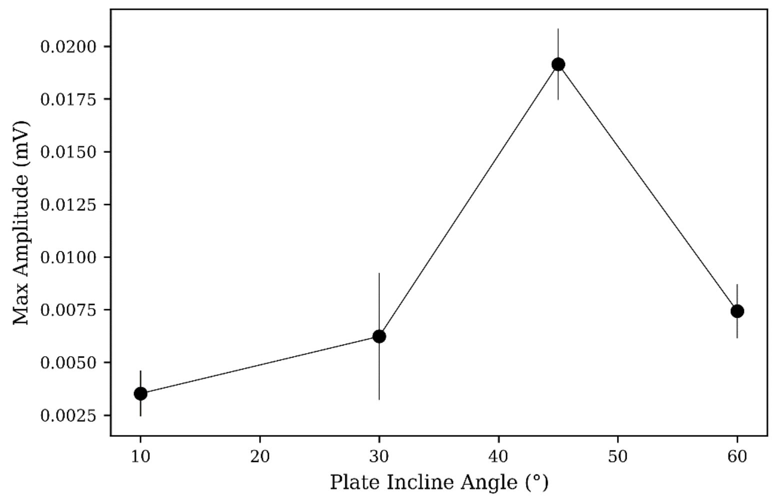

Figure 3-4. Average maximum amplitude of the AE spectra corresponding to changing incline plate angle.

Based on the trend in maximum amplitude, it might be naturally assumed that the choice for plate inclination in the setup would have been at 45 degrees; however, the effects of granular breakage and secondary collisions on the spectra must also be considered. Figure 3-5 shows the captured motion of granules colliding with the impact plate at 45 and 60 degrees inclination, as observed by high speed image analysis. At 45 degrees, more granular damage was observed during the primary collision with the plate and rebounding particles had a greater chance of striking the plate again, potentially inflating the amplitude for a certain particle size. At 60 degrees, the decreased normal force reduced the damage seen by granules as they collided with the plate and since they departed the field of view by ‘sliding or rolling’, there was little likelihood of a detectable secondary impact. Despite the lower signal amplitude at 60 degrees, this condition was chosen as the preferred plate incline angle.

It is expected that some granule breakage will always occur regardless of the inclination angle of the plate. Such breakage has more influence on a rebounding rather than an impacting particle and hence, more significantly affect the PSD rather than acoustic emission in our study. Fortunately, the absence of detectable breakage in the captured video of impacts at 60 degrees inclination gave increased confidence that the signal was being correlated to an accurate representation of the particles that produced the acoustic emissions.

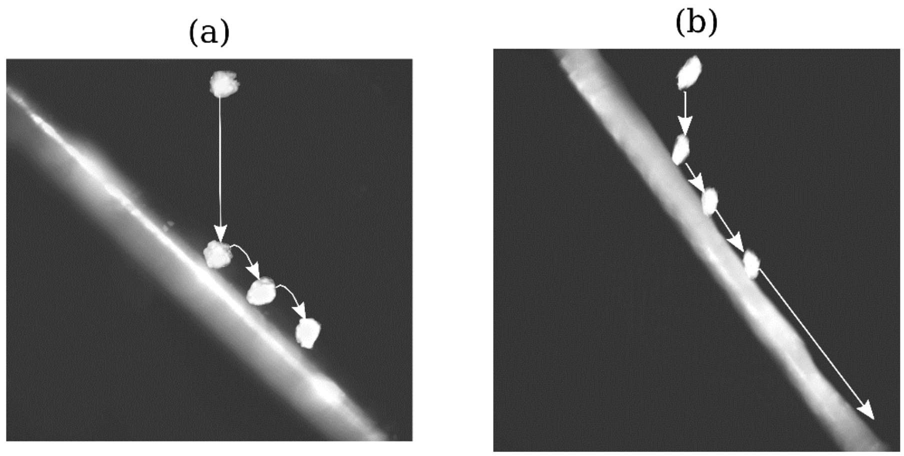

Figure 3-5. Trajectory of a particle on the impact plate with (a) 45 and (b) 60 degrees angle relative to the horizontal plate shown by super-imposing images over time. Arrows were shown to highlight the observed particle path followed.

3.4.2. Effect of Impact Plate Thickness

The other setup parameter studied was plate thickness. Figure 3-6 shows AE spectra for plates of different thicknesses, constantly inclined at 60 degrees to the horizontal plane. There was generally no change in the nature of the spectra for the same L/S ratio as the thickness increased from 0.7 to 1.5 mm; however, the signal amplitude decreased as the thickness of the plate increased, most notably seen for the spectra at 13 and 14% L/S ratios. Particle impacts onto the 0.7 mm plate were creating detectable vibrations in the plate itself during experiments implying particles might contact onto the plate multiple times during a single collision event due to the rebound motion of the plate, thereby increasing the measured amplitude. As its thickness increased the plate vibrated less from the particle impacts. A thickness of 1.5 mm was considered acceptable for the final setup since no motion from the plate was observed during experiments, and yet the signal strength was sufficient for the model to distinguish different particle collisions.

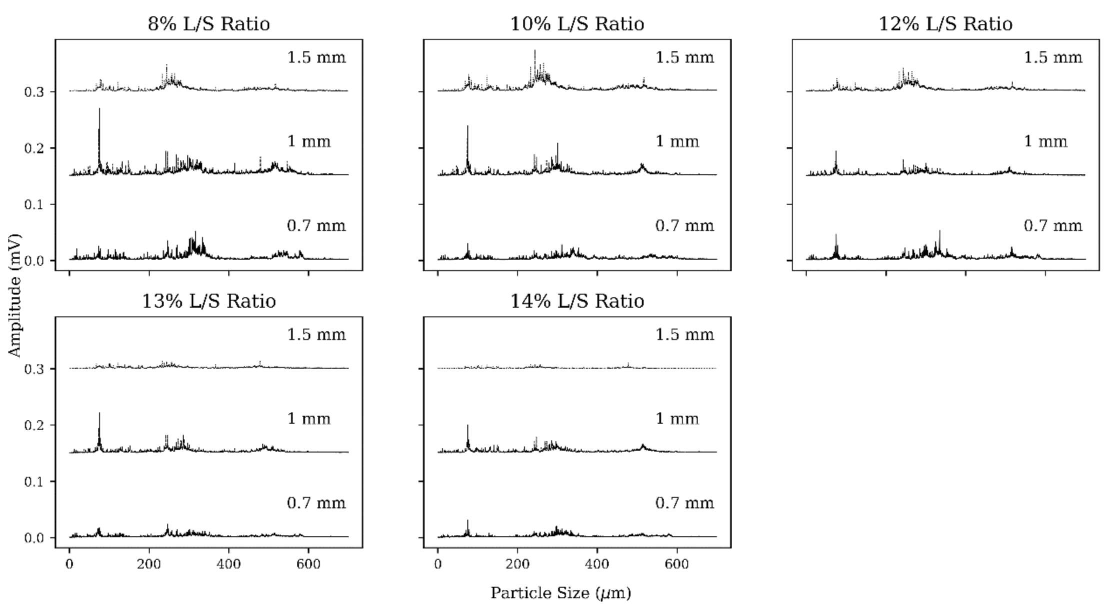

Figure 3-6. AE spectra for each L/S ratio for the impact plate inclined at 60 degrees for thicknesses of 0.7, 1, and 1.5 mm.

3.4.3. Signal Analysis based on Particle Size

Figure 3-7 shows the average acoustic spectra from the TSG experiments for each L/S ratio along with their respective PSDs. The observable trend in AE spectra, shown in Figure 3-7(a), was a decrease in the amplitude as L/S ratio increased, with the main regions of interest being 50-150 kHz and 200-300 kHz. From plate response calculations in Figure 3-3(b), the 50-150 kHz region corresponds to 300 – 1000 μm particle impacts and the 200-300 kHz region relates to 150 – 240 μm particle impacts. Correspondingly, Figure 3-7(b) shows that as the L/S ratio increased, the weight fraction of granules between 49 – 1550 μm decreased substantially, seeming to corroborate the decrease in amplitude in the AE spectra. While the plate response frequency assignments were derived only for single particle impacts, they appear to be suitably correlated with the particle sizes under this study from TSG. Impacts of particles above 2200 μm in size were predicted to produce plate responses around 20-50 kHz, beyond the ideal sensitivity range of the broadband sensor. AE associated with these larger particles still exhibited detected frequencies (harmonics) in the experiments that could be discriminated by the model but the current setup should be considered reasonable for monitoring particles below 3000 μm. Since the largest granule size suitable for tableting is 1.25 mm [15, 50, 51], the current setup was considered suitable for the purposes of introducing the ANN model. Future studies will consider the advantages of a two sensor system to acquire a broader range of frequencies so that the model might have a better capacity to predict very coarse granules via TSG.

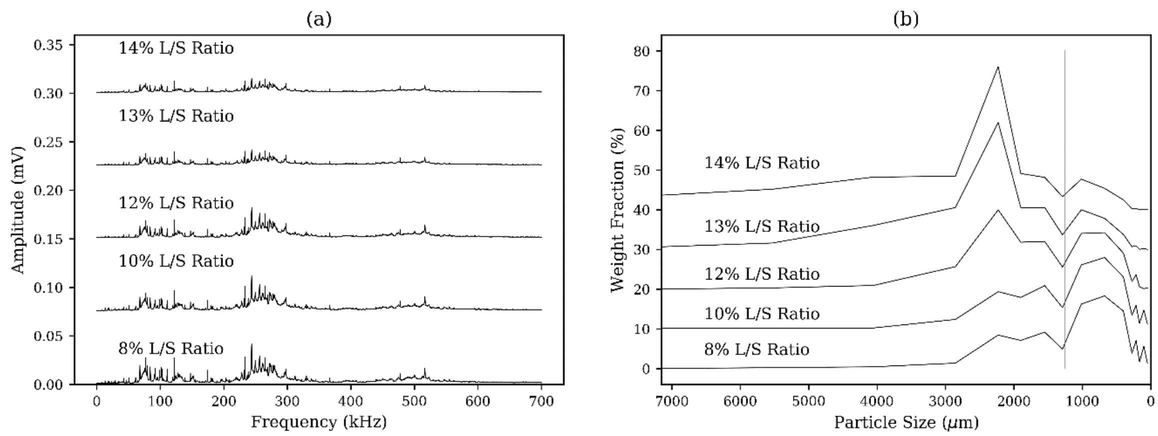

Figure 3-7. (a) Acoustic spectra of particle impacts for each L/S ratio. (b) PSDs for each L/S ratio. The vertical line indicates the often considered ideal size (1250 μm) suitable for tableting.

3.4.4. Model Training and Validation

Confidence in the model predictions was evaluated based on RMSE calculated for the testing AE spectra corresponding to granulation at each L/S ratio, as shown in Figure 3-8. Predicted PSDs based on the testing datasets processed without and with the impact filter are shown in Figure 3-9 and 3-10, respectively along with their experimentally measured PSD for each L/S ratio. For the case of processing the AE data without the impact filter, the RMSE for the majority of particle sizes was below 2 wt% for all L/S ratios. This is reflected in Figure 3-9 where the model was able to fit each PSD fairly well. The particle size with the highest error was 2230 μm for PSD at 12% L/S ratio, which goes up to 4.25 wt% RMSE as seen in Figure 3-8 (a). This high RMSE is attributed to the PSD being strongly bimodal with both peaks being nearly equal to one another, which likely increased the difficulty in predictions. In general, the model without the filter was considered to have satisfactorily learned to associate the AE spectra to sets of particles colliding with the impact plate, at least for the specific case of lactose monohydrate which granulates at much lower degrees of saturation than most pharmaceutical formulations. Future studies will be required to understand how formulations and degree of saturation affect the AE spectra and the model's ability to associate acoustics to particle size. This will enable the prediction error for each particle size to be tracked for different formulations making this potentially a very powerful monitoring tool when producing multiple products from the same TSG.

For the case of processing the AE spectral data with the impact filter, a significant decrease was seen in the prediction error in comparison to Figure 3-8(a), now at or below 1 wt% RMSE for all particle sizes being considered. This improved accuracy in predicted PSD is reflected in Figure 3-10 where the model and experimental sieved weight fractions are much closer in value. With the impact filter, the loss error was no longer localized around 2230 μm, highlighting the effect that auditory masking was having on the AE signal in the original model. Diminishing auditory masking of the signal allowed the model to more equally consider the contribution of all frequencies (and particle collisions) in the response.

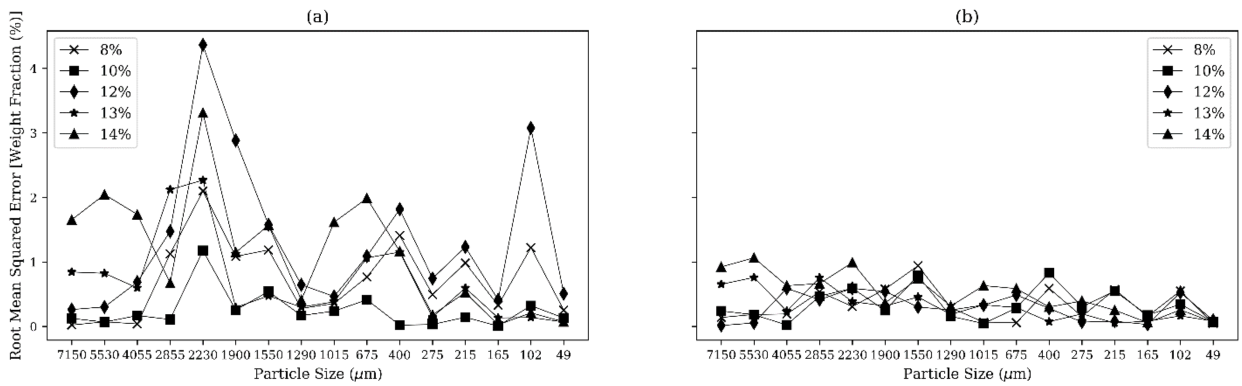

Figure 3-8. RMSE for every particle size at different L/S ratios for AE data (a) without and (b) with the impact filter.

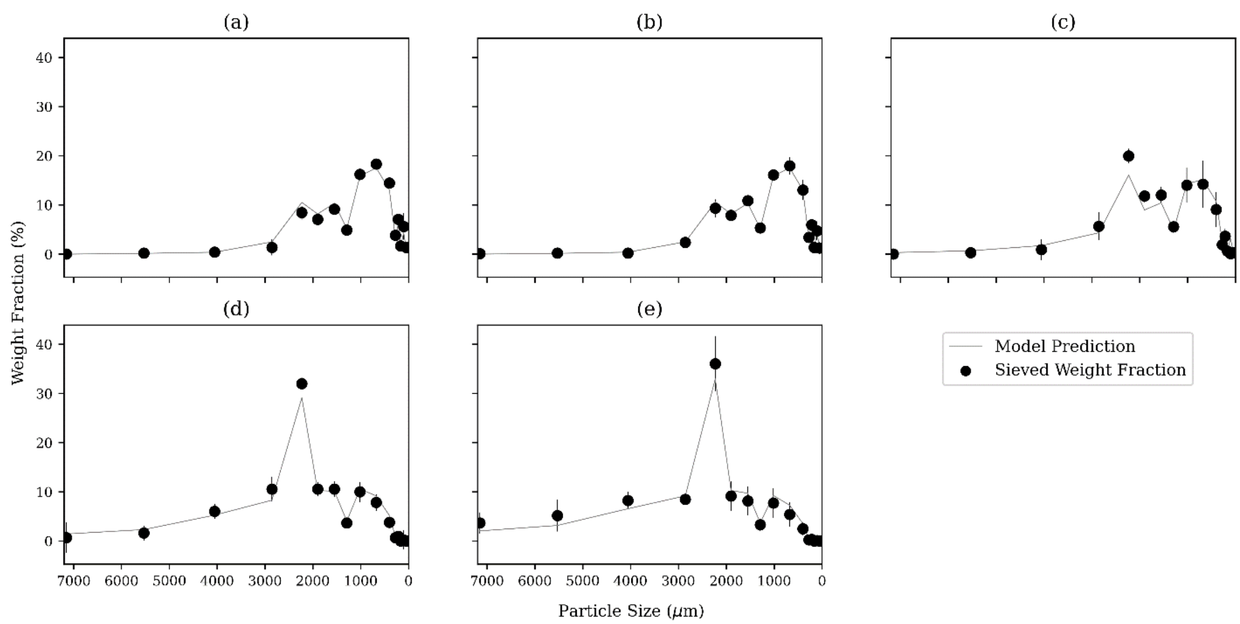

Figure 3-9. PSD predictions for (a) 8% (b) 10% (c) 12% (d) 13% and (d) 14% L/S ratio for AE spectral data without the impact filter. Error bars represent the standard deviation (n=3).

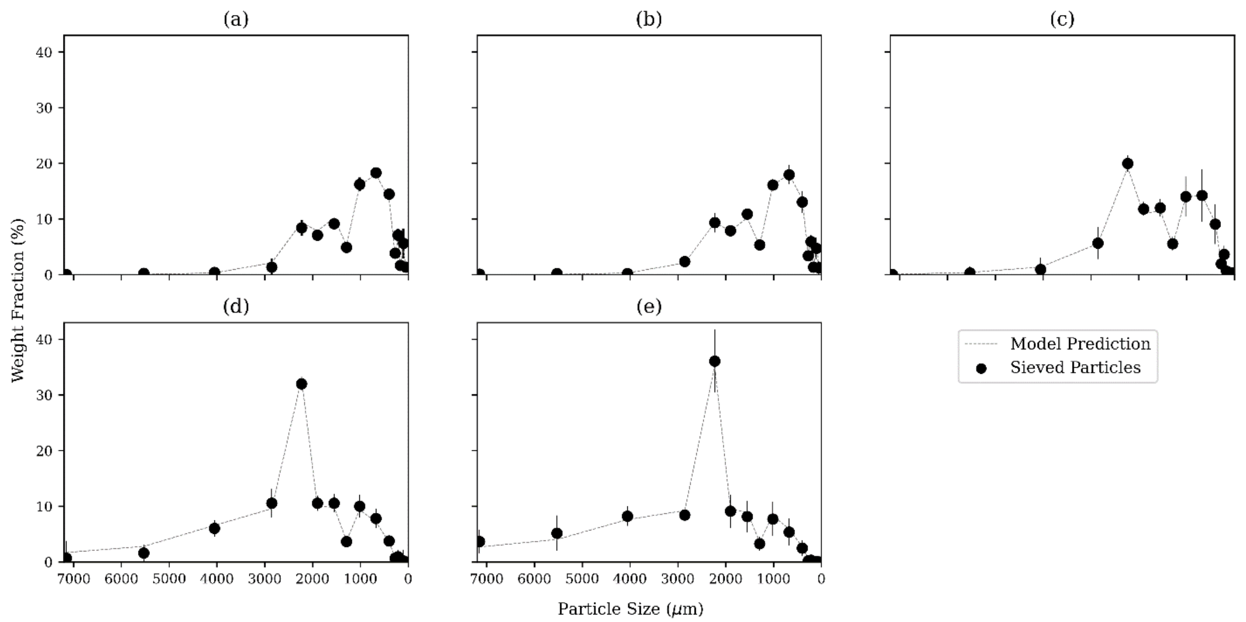

Figure 3-10. PSD predictions for (a) 8% (b) 10% (c) 12% (d) 13% and (d) 14% L/S ratio for AE spectral data with the impact filter. Error bars represent the standard deviation (n=3).

3.5. Conclusion

Ultrasonic acoustic emissions were explored as an approach for PAT to monitor the exiting particle size from a twin screw granulator, a continuous granulation method noted for producing complex size distributions. The elements of the approach consisted of a 1.5 mm thick stainless steel impact plate, ideally inclined at 60 degrees to minimize powder accumulation and ensure rebounding trajectories did not allow for secondary collisions by granules from the granulator. Using an artificial neural network model and PCA to reduce the dimensions of the dataset, error analysis showed the model experienced the most difficulty predicting the distribution when it was strongly bimodal, with the highest reported error of 4.25 wt% for the 2230 μm fraction. Applying a newly introduced impact filter to the AE data to minimize auditory masking, the model error decreased significantly below 1 wt% and became evenly distributed amongst all particle sizes rather than being localized to the larger particles in the exiting distribution. For this preliminary study for an AE-based PAT approach, the training was done with lactose monohydrate, but future studies will follow to examine how formulation and level of saturation affects acoustic emissions of impacting granules. It is anticipated that plate design and the auditory masking filter will require revisions as fracture strength and cohesiveness change the nature of particle impacts. Practically speaking, the accuracy of the approach will also need study as the flow rate increases to production levels and only a fraction of the exiting mass is impacting the plate.

3.6. Acknowledgements

The authors would like to thank Kevin O' Donnell from Dupont Biosciences and Nutrition for providing the materials used in this study and the Natural Sciences and Engineering Research Council (NSERC) for funding the work. The authors would also like to thank Austin Bedrosian and Vladimir Gritsichine for their helpful insights in the early stages of data analysis.

3.7. References

[1] M. Fonteyne, A. Correia, S. De Plecker, J. Vercruysse, I. Ilic, Q. Zhou, C. Vervaet, J.P. Remon, F. Onofre, V. Bulone, T. De Beer, Impact of microcrystalline cellulose material attributes: a case study on continuous twin screw granulation, Int J Pharm, 478 (2015) 705-717.

[2] C. Portier, K. Pandelaere, U. Delaet, T. Vigh, A. Kumar, G. Di Pretoro, T. De Beer, C. Vervaet, V. Vanhoorne, Continuous twin screw granulation: Influence of process and formulation variables on granule quality attributes of model formulations, Int J Pharm, 576 (2020) 118981.

[3] E.I. Keleb, A. Vermeire, C. Vervaet, J.P. Remon, Twin screw granulation as a simple and efficient tool for continuous wet granulation, Int J Pharm, 273 (2004) 183-194.

[4] B. Mu, M.R. Thompson, Examining the mechanics of granulation with a hot melt binder in a twin-screw extruder, Chemical Engineering Science, 81 (2012) 46-56.

[5] K.E. Rocca, S. Weatherley, P.J. Sheskey, M.R. Thompson, Influence of filler selection on twin screw foam granulation, Drug Dev Ind Pharm, 41 (2015) 35-42.

[6] A. Ito, P. Kleinebudde, Influence of granulation temperature on particle size distribution of granules in twin-screw granulation (TSG), Pharm Dev Technol, 24 (2019) 874-882.

[7] J. Vercruysse, A. Burggraeve, M. Fonteyne, P. Cappuyns, U. Delaet, I. Van Assche, T. De Beer, J.P. Remon, C. Vervaet, Impact of screw configuration on the particle size distribution of granules produced by twin screw granulation, Int J Pharm, 479 (2015) 171-180.

[8] A.S. El Hagrasy, J.D. Litster, Granulation rate processes in the kneading elements of a twin screw granulator, AIChE Journal, 59 (2013) 4100-4115.

[9] R.M. Dhenge, K. Washino, J.J. Cartwright, M.J. Hounslow, A.D. Salman, Twin screw granulation using conveying screws: Effects of viscosity of granulation liquids and flow of powders, Powder Technology, 238 (2013) 77-90.

[10] B. Van Melkebeke, C. Vervaet, J.P. Remon, Validation of a continuous granulation process using a twin-screw extruder, Int J Pharm, 356 (2008) 224-230.

[11] B. Presles, Novel image analysis method for in situ monitoring the particle size distribution of batch crystallization processes, Journal of Electronic Imaging, 19 (2010) 031207.

[12] A.F. Silva, A. Burggraeve, Q. Denon, P. Van der Meeren, N. Sandler, T. Van Den Kerkhof, M. Hellings, C. Vervaet, J.P. Remon, J.A. Lopes, T. De Beer, Particle sizing measurements in pharmaceutical applications: comparison of in-process methods versus off-line methods, Eur J Pharm Biopharm, 85 (2013) 1006-1018.

[13] T. De Beer, A. Burggraeve, M. Fonteyne, L. Saerens, J.P. Remon, C. Vervaet, Near infrared and Raman spectroscopy for the in-process monitoring of pharmaceutical production processes, Int J Pharm, 417 (2011) 32-47.

[14] J. Huang, C. Goolcharran, J. Utz, P. Hernandez-Abad, K. Ghosh, A. Nagi, A PAT Approach to Enhance Process Understanding of Fluid Bed Granulation Using In-line Particle Size Characterization and Multivariate Analysis, Journal of Pharmaceutical Innovation, 5 (2010) 58-68.

[15] V. Pauli, Y. Roggo, L. Pellegatti, N.Q. Nguyen Trung, F. Elbaz, S. Ensslin, P. Kleinebudde, M. Krumme, Process analytical technology for continuous manufacturing tableting processing: A case study, J Pharm Biomed Anal, 162 (2019) 101-111.

[16] C. BUSCHMILLLER, W. Wiedey, C. Doescher, M. Plitzko, J. Breitkreutz, In-line Monitoring of Granule Moisture and Temperature throughout the entire Fluidized-bed Granulation Process using Microwave Resonance Technology Part I, Pharmazeutische Industrie, 71 (2009).

[17] P. Suresh, I. Sreedhar, R. Vaidhiswaran, A. Venugopal, A comprehensive review on process and engineering aspects of pharmaceutical wet granulation, Chemical Engineering Journal, 328 (2017) 785-815.

[18] A. Kumar, J. Dhondt, F. De Leersnyder, J. Vercruysse, V. Vanhoorne, C. Vervaet, J.P. Remon, K.V. Gernaey, T. De Beer, I. Nopens, Evaluation of an in-line particle imaging tool for monitoring twin-screw granulation performance, Powder Technology, 285 (2015) 80-87.

[19] A. Bastari, C. Cristalli, R. Morlacchi, E. Pomponi, Acoustic emissions for particle sizing of powders through signal processing techniques, Mechanical Systems and Signal Processing, 25 (2011) 901-916.

[20] Y. Hu, X. Qian, X. Huang, L. Gao, Y. Yan, Online continuous measurement of the size distribution of pneumatically conveyed particles by acoustic emission methods, Flow Measurement and Instrumentation, 40 (2014) 163-168.

[21] A. Boschetto, F. Quadrini, Powder size measurement by acoustic emission, Measurement, 44 (2011) 290-297.

[22] C.-j. Ren, J.-d. Wang, D. Song, B.-b. Jiang, Z.-w. Liao, Y.-r. Yang, Determination of particle size distribution by multi-scale analysis of acoustic emission signals in gas-solid fluidized bed, Journal of Zhejiang University-SCIENCE A, 12 (2011) 260-267.

[23] S. Matero, S. Poutiainen, J. Leskinen, K. Järvinen, J. Ketolainen, S.P. Reinikainen, M. Hakulinen, R. Lappalainen, A. Poso, The feasibility of using acoustic emissions for monitoring of fluidized bed granulation, Chemometrics and Intelligent Laboratory Systems, 97 (2009) 75-81.

[24] M. Whitaker, G.R. Baker, J. Westrup, P.A. Goulding, D.R. Rudd, R.M. Belchamber, M.P. Collins, Application of acoustic emission to the monitoring and end point determination of a high shear granulation process, Int J Pharm, 205 (2000) 79-92.

[25] M.J. Waring, M.H. Rubinstein, J.R. Howard, Acoustic emission of pharmaceutical materials during compression, International Journal of Pharmaceutics, 36 (1987) 29-36.

[26] M.K. Papp, C.P. Pujara, R. Pinal, Monitoring of High-shear Granulation using Acoustic Emission: Predicting Granule Properties, Journal of Pharmaceutical Innovation, 3 (2008) 113-122.

[27] H. Yonghui, W. Lijuan, H. Xiaobin, Q. Xiangchen, G. Lingjun, Y. Yong, On-line Sizing of Pneumatically Conveyed Particles Through Acoustic Emission Detection and Signal Analysis, IEEE Transactions on Instrumentation and Measurement, 64 (2015) 1100-1109.

[28] C. Aldrich, D.A. Theron, Acoustic estimation of the particle size distributions of sulphide ores in a laboratory ball mill, Journal of the Southern African Institute of Mining and Metallurgy, 100 (2000) 243-248.

[29] H. Warren Shen, H. Reginald Hardy, A. Wahab Khair, Laboratory study of acoustic emission and particle size distribution during rotary cutting, International Journal of Rock Mechanics and Mining Sciences, 34 (1997) 121.e121-121.e116.

[30] E.M. Hansuld, L. Briens, A. Sayani, J.A.B. McCann, An investigation of the relationship between acoustic emissions and particle size, Powder Technology, 219 (2012) 111-117.

[31] E.I. Keleb, A. Vermeire, C. Vervaet, J.P. Remon, Continuous twin screw extrusion for the wet granulation of lactose, International Journal of Pharmaceutics, 239 (2002) 69-80.

[32] M.R. Thompson, J. Sun, Wet Granulation in a Twin‐Screw Extruder: Implications of Screw Design, Journal of Pharmaceutical Sciences, 99 (2010) 2090-2103.

[33] M. Pharma, Flowlac (r) 100 Product Detail - MEGGLE Pharma - Excipients & Technology.

[34] S.S. Rao, Transverse Vibration of Plates, Vibration of Continuous Systems2006, pp. 457-540.

[35] G.C. McLaskey, S.D. Glaser, Hertzian impact: experimental study of the force pulse and resulting stress waves, J Acoust Soc Am, 128 (2010) 1087-1096.

[36] J. Reed, Energy losses due to elastic wave propagation during an elastic impact, Journal of Physics D: Applied Physics, 18 (1985) 2329.

[37] M. Perkins, S.J. Ebbens, S. Hayes, C.J. Roberts, C.E. Madden, S.Y. Luk, N. Patel, Elastic modulus measurements from individual lactose particles using atomic force microscopy, International Journal of Pharmaceutics, 332 (2007) 168-175.

[38] F. Bassam, P. York, R.C. Rowe, R.J. Roberts, Young's modulus of powders used as pharmaceutical excipients, International Journal of Pharmaceutics, 64 (1990) 55-60.

[39] A. Steels, Stainless Steel 304, 304L, 304H Grade Data Sheet - Stainless-Steel-304-304L-304H-Grade-Data-Sheet, 2013.

[40] V. Busignies, P. Tchoreloff, B. Leclerc, C. Hersen, G. Keller, G. Couarraze, Compaction of crystallographic forms of pharmaceutical granular lactoses. II. Compacts mechanical properties, European Journal of Pharmaceutics and Biopharmaceutics, 58 (2004) 577-586.

[41] F. Podczeck, Theoretical and experimental investigations into the delamination tendencies of bilayer tablets, International Journal of Pharmaceutics, 408 (2011) 102-112.

[42] A. Materials, Properties: Stainless Steel - Grade 304 (UNS S30400).

[43] S.-Y. Chang, C. Wang, C.C. Sun, Relationship between hydrate stability and accuracy of true density measured by helium pycnometry, International Journal of Pharmaceutics, 567 (2019) 118444.

[44] G. Carson, A.J. Mulholland, A. Nordon, M. Tramontana, A. Gachagan, G. Hayward, Particle sizing using passive ultrasonic measurement of particle–wall impact vibrations, Journal of Sound and Vibration, 317 (2008) 142-157.

[45] M. Guo, Y. Yan, Y. Hu, D. Sun, X. Qian, X. Han, On-line measurement of the size distribution of particles in a gas–solid two-phase flow through acoustic sensing and advanced signal analysis, Flow Measurement and Instrumentation, 40 (2014) 169-177.

[46] D.J. Buttle, S.R. Martin, C.B. Scruby, Particle Sizing by Quantitative Acoustic Emission, Research in Nondestructive Evaluation, 3 (1991) 1-26.

[47] T.B. Blank, S.D. Brown, Nonlinear multivariate mapping of chemical data using feed-forward neural networks, Analytical Chemistry, 65 (2002) 3081-3089.

[48] V. Prasad, B.W. Bequette, Nonlinear system identification and model reduction using artificial neural networks, Computers & Chemical Engineering, 27 (2003) 1741-1754.

[49] M. Blanco, J. Coello, H. Iturriaga, S. Maspoch, J. Pagès, NIR calibration in non-linear systems: different PLS approaches and artificial neural networks, Chemometrics and Intelligent Laboratory Systems, 50 (2000) 75-82.

[50] M. Santl, I. Ilic, F. Vrecer, S. Baumgartner, A compressibility and compactibility study of real tableting mixtures: the effect of granule particle size, Acta Pharm, 62 (2012) 325-340.

[51] M. Khorasani, J.M. Amigo, C.C. Sun, P. Bertelsen, J. Rantanen, Near-infrared chemical imaging (NIR-CI) as a process monitoring solution for a production line of roll compaction and tableting, Eur J Pharm Biopharm, 93 (2015) 293-302.

Chapter 4: Considering Inelasticity in the Real-Time Monitoring of Particle Size for Twin-Screw Granulation via Acoustic Emissions

Considering Inelasticity in the Real-Time Monitoring of Particle Size for Twin-Screw Granulation via Acoustic Emissions

H.A. Abdulhussain[a], M.R. Thompson[a,*]

[a]*CAPPA-D/MMRI, Department of Chemical Engineering,*

McMaster University, Hamilton, Ontario, Canada

[*] Author to whom correspondence should be addressed.

Tel: (905) 525-9140 x 23213

mthomps@mcmaster.ca

4.1. Abstract

A recently developed process analytical technology (PAT) using artificial intelligence to form the framework of its model, combining frequency-domain acoustic emissions (AE) and elastic impact mechanics to accurately predict complex particle size distributions (PSD) in real-time. This model was modified in this study to give more accurate predictions for the more highly cohesive granules typical of pharmaceutical solid oral dosage formulations. AE spectra were collected from the granulated impacts of various formulations with ranging characteristics from largely elastic to highly inelastic collision responses. A viscoelastic (Hertzian spring-dashpot) and elastoplastic (Walton-Braun) contact force model were compared to understand how these different micro-mechanical approaches would affect the prediction accuracy of particle sizes relevant to granulation. Retraining the artificial intelligence model with the Walton-Braun transformation and a more comprehensive dataset of AE spectra spanning a broad range of granulated formulations showed the prediction error drop to as low as 2% compared to the original elastic version showing errors as large as 18.6% with representative formulations of the industry. The improved PAT shows good applicability to monitoring bimodal PSD that are typical of continuous twin-screw granulation.

Keywords: Acoustic Emissions, Process analytical technology, Micro-mechanical models, Artificial intelligence, Twin screw granulation

4.2. Introduction

Continuous manufacturing in the pharmaceutical industry has been a topic of major discussion for the past two decades. The United States Food and Drug Administration's (FDA) revised guidance on Good Manufacturing Practices has encouraged manufacturers to look into alternate manufacturing technologies beyond current batch operations to improve the supply and consistency of drugs. A challenge for implementing continuous manufacturing is loss of the hold-time studies associated with quality assessment between the steps of batch production. Equipment design and its operations for continuous manufacturing does not offer similar mid-process access to sampling and testing of the product, and hence the ability to recognize quality issues and then correct them quickly is paramount, especially considering how quickly waste can be generated at these new higher rates of production when specifications are not being met. To maintain (or improve) product quality within a continuous production platform, inline process analytical technologies (PAT) are necessary to provide real-time assessments of how well the system is operating [1, 2].

Twin screw granulation (TSG) has gained much interest in the pharmaceutical industry as a continuous manufacturing technology, capable of multiple modes of solids handling including wet, dry and hot melt granulation. Its advantages over other technologies lie in its flexible equipment design, closely confined space for uniform mixing, and decades of use in the food and plastics industries, making it simpler to apply process control techniques once presented with a robust PAT [3, 4]. A major difference between TSG and batch granulation technologies is the particle size distribution (PSD) produced. Batch granulation often produces a Gaussian particle size distribution (PSD) [5-8], whereas samples by TSG typically exhibit a bimodal PSD [9-12]. Due to this more complex distribution shape, single descriptors like d_{50} are not appropriately representative of the product quality for TSG and thus, any PAT for this application should be capable of providing more details describing the size of exiting particles in real-time.

Acoustic Emissions (AE) is a non-destructive ultrasonic technique that has been shown in its prior art to be a good predictor of Gaussian PSD [13-16]. In those cases, a parameter like maximum amplitude of the time-domain AE signal, which was being generated by moving particle colliding with rigid surfaces, is correlated with particle size to predict a single descriptor, typically d_{50}. To improve the applied methods of AE to now predict a bimodal PSD we turned to frequency-domain signal analysis aided with artificial intelligence (AI) techniques but we also found it necessary to create a new digital signal filter[17]. This filter addressed a difficult problem hindering AE implementation with TSG, specifically when multiple particles strike a surface simultaneously, auditory masking occurs where the amplitude of larger particles overshadow the amplitude of smaller ones. Since particle counts are associated with frequency amplitude in determining the PSD by AE, the filter corrects the signal based on impact mechanics to ensure all particles of any size are correctly represented in the correlations. With this filter, our AE-based PAT showed excellent predictive accuracy for near-elastic collisions based on lactose monohydrate granulation[17].

In comparison to lactose monohydrate granules, most pharmaceutical granulates produced by TSG are better described as moderate-to-highly inelastic in their collision behavior. Inelastic collisions will exhibit significantly different stress waves captured by an acoustic sensor in terms of both wave pattern and amplitude. Surface moisture and the cohesive nature of the solids (excipients and actives) making up a granule will create protractedly long contact times during a collision, as well as dampen the intensity of the signal generated [18]. As a result, our original PAT showed high prediction errors with these typical extended-release formulations, highlighting the need to make further modifications to the digital filter.

To improve the scope of applications for the new AE-based PAT, a more descriptive impact filter was sought to expand the method's predictive nature to formulations of higher saturation and/or cohesion while retaining the original auditory masking correction. The aim of this work was to develop a new filter that accounts for cohesive forces through the use of micromechanical descriptors of the impacts to monitor the PSD with improved accuracy for a broader range of formulations being processed by TSG. The focus on micromechanics, and more broadly inelasticity, was to ensure that improvements in predictive accuracy could be described by physical attributes generating the impact, including the degree of inelasticity associated with water's influence on the different components of the granule, affecting both cohesiveness and stiffness, as well as the production of viscous liquid bridges of the granules. The alternative of directly training the AI model with acoustic data from the different formulations and thereby following a black-box approach, was not considered in this study because it would provide no information on why the correlated fit of this new model was better or worse.

4.3. Materials and methods

4.3.1. Materials

Four formulations were granulated for model training with the excipients Flowlac® 100 (Meggle Pharma; Germany), Avicel PH102 (Dupont Nutrition & Biosciences; Midland, MI), METHOCEL™ K4M, METHOCEL™ F4M (Dupont Nutrition & Biosciences; Midland, MI) and Kollidon SR® (BASF). The latter three excipients give extended-released drug properties to a tablet and were chosen to alter the impact behavior of exiting granules from the TSG. All excipients besides Flowlac® 100 (Lactose Monohydrate) required much higher quantities of binding liquid (over 20% compared to 4% [19]) before pendular saturation occurred for granulation; the concern for this extra water was our expectation that it would affect the stiffness of the granular components and shift in its distribution within a granule upon impact. From these materials, three formulations were tested in this study consisting of 60% lactose, 20% Avicel PH102 (Microcrystalline Cellulose, MCC), along with 20% METHOCEL™ F4M, 20% METHOCEL™ K4M, or 20% Kollidon SR®, respectively. All formulations were dry mixed prior to being granulated in the extruder. A pure lactose formulation was used in addition as a control, being more elastic-like in impact behavior compared to the three studied formulations and the granules for which the original PAT [17] was trained. The binding liquid in this work consisted of 2% METHOCEL™ E3PLV (DuPont Nutrition & Biosciences; Midland, MI) dissolved in distilled water.

4.3.2. Twin Screw Granulation Experiments

Wet granulation studies were completed in a 27 mm 40 L/D Model ZSE-27HP corotating twin screw extruder (Leistritz Extrusion; Somerville, NJ, USA). The extruder consisted of a water-cooled feed zone (Z0) in the beginning and nine heated barrel zones (Z1–Z9) actively controlled for temperature, set according to the list of experiments shown in Table 4-1. The use of different temperatures for different formulations was to control the water-absorption behavior of their extended-release excipients and ensure they could be granulated at the same range of liquid-to-solid (L/S) ratios. The L/S ratios of 25, 30, and 35% were chosen to produce broad PSDs with ample amounts of fines (<300 μm), granules of desired size for tableting (600-1500 μm), and coarse particles (>2000 μm). In the pure lactose formulation, a L/S ratio of 6, 8, and 10% were used to produce PSDs with similar shapes to the METHOCEL™ and Kollidon® SR formulations. Formulations K4M and F4M could not be granulated at room temperature, producing a gel-like paste, likely due to the hydrogel nature of these hydroxypropyl methylcelluloses (HPMC)[20]. Increasing the barrel temperature to 40℃ reduced swellability of these HPMC and allowed them to be granulated at the higher L/S ratios. For the formulation KSR, a barrel temperature of 15 ℃ was used as it was more susceptible to dry granulation due to the low glass transition temperature (~35 ℃ in its dry state[21]) of Kollidon® SR.

Table 4-1. Wet granulation experimental design.

Formulation	Name	Experiment	L/S Ratio (%)	Temperature (℃)
Flowlac ® 100	Lac	1	6	25
		2	8	25
		3	10	25
60% Flowlac® 100 + 20% Avicel PH102 + 20% METHOCEL™ K4M	K4M	1	25	40
		2	30	40
		3	35	40
60% Flowlac® 100 + 20% Avicel PH102 + 20% METHOCEL™ F4M	F4M	1	25	40
		2	30	40
		3	35	40
60% Flowlac® 100 + 20% Avicel PH102 + 20% Kollidon® SR	KSR	1	25	15
		2	30	15
		3	35	15

The screw speed and mass flow rate for all experiments was 300 RPM and 3 kg/hr, respectively. The formulations were added into the extruder using a Brabender T20 twin-screw gravimetric feeder (Mississauga, ON, Canada). The liquid binder was injected into the extruder at zone Z2 using an ISCO 260D high pressure syringe pump (Teledyne-ISCO Inc.; Lincoln, NE, USA) at varying L/S ratios depending on the formulation and experiment shown in Table 4-1. The screw design for these experiments was composed of conveying elements from Z1-Z7 followed by two kneading elements in Z8 and then conveying elements in Z9. The granules produced from the extruder were spread out on large trays to air-dry at room temperature for 48 hours before being analyzed for their size. The moisture content before and after granulation was measured using a HG63 moisture analyzer (Mettler-Toledo; Columbus, OH), with recorded data shown in Tables S.4-1. and S.4-2 in Sec 4.9. It was found after drying, the moisture content of the granules regardless of formulation was between 4-5%, which lies in the typical range of moisture for retarding static charge buildup during tabletting."

4.3.3. Particle Size Characterization

PSD data was determined using a Ro-Tap RX-29 sieve shaker (W.S. Tyler; Mentor, OH, USA). A sample of 100 g for each experiment was classified into eight size fractions using sieves of 2100, 1700, 1400, 1180, 850, 500, and 300 μm nominal openings, and the bottom pan by mechanically agitating for five minutes. The mass on the 2100 μm sieve was then classified further with sieves of 8000, 6300, 4760, 3350, 2360, 2100, and 1700 μm nominal openings and mechanically agitating for another five minutes. The mass in the bottom pan from the original agitation was also classified further by with sieves of 500, 300, 250, 180, 150, 53, and 44 μm nominal openings followed by mechanically agitating for five minutes. This extent of classification was done to report highly detailed size distributions for the neural network model described in Section 4.4., collecting more information beyond the ideally sought sizes (500-1500 μm) from the granulator to ensure the PAT could monitor extremes as the L/S ratio varied.

Three repeats were completed to assess the error in the PSD measurement. Weight fractions were reported for the average particle sizes: >8000, 7150, 5530, 4055, 2855, 2230, 1900, 1550, 1290, 1015, 675, 400, 275, 215, 165, 102, 49, and <44 μm. The fractions above 7150 μm and below 49 μm were always 0 wt% in these trials, fixing the distribution shape to the baseline at both ends and allowing the size fractions of >8000 and <44 μm to be ignored in the final datasets to minimize redundancies. Therefore, the PSD used in the modelling was composed of weight fractions for sixteen particle sizes.

4.3.4. Acoustic Emission Analysis

A F15α broadband sensor (Physical Acoustics; Princeton, NJ, USA) was attached to a 25.4 mm x 25.4 mm tab that extended from the top edge of a SAE 304 stainless steel (SS) impact plate with a length, width, and thickness of 44.5, 76.2, and 1.5 mm, respectively [17]. The sensor was attached to the impact plate using high vacuum grease (Dow Corning) to improve contact. No part of the AE setup was connected to the extruder, making the measurements unaffected by the vibrations present in the process. This was confirmed by running the AE system while the screws were rotating with no material present in the machine.

The detected signal with the sensor was amplified using a Physical Acoustics 2/4/6c amplifier set to +60 dB and collected using a National Instruments 3.5 MHz 12-bit 4-channel data acquisition system. In every TSG experiment, collisions of granules onto the plate at a sampling rate of 3 MHz were collected for one minute. The vertical distance of the plate relative to the exit of the extruder was based on an estimation of the terminal velocity to ensure consistency of the impacts. The vertical distance for a 300 μm particle, the smallest size considered to be a 'granule' in this study, to reach terminal velocity was found to be roughly 20 cm below the exit of the extruder. Figure 4-1 shows the experimental setup of the extruder and plate assembly.

An average of ~200 signals granule impacts (often occurring simultaneously) were recorded by the sensor over a one minute period for a selected operating condition in the extruder corresponding to Table 4-1. A discrete Haar wavelet filter was applied to a trial signal to reduce noise before applying a Fast Fourier Transform (FFT). No significant peaks were detected too much above 600 kHz and as the main peaks of interest are mainly in the ultrasound range, ambient noise from the extruder had no effect on the PAT. Thus, the analyzed frequency range was chosen as 0-700 kHz to reliably describe the signal but limit extraneous data in the training data set for the model (described in Section 4.4.) [22] . This meant that a single trial signal was an array composed of approximately 230,000 data points. To reduce computational complexity, the frequency resolution was reduced to lower the memory requirements needed to load the data, from the original 3 Hz to 87 Hz, to reach a similar resolution of the signal from the previous work [17], which reduced the signal to a length of 8065.

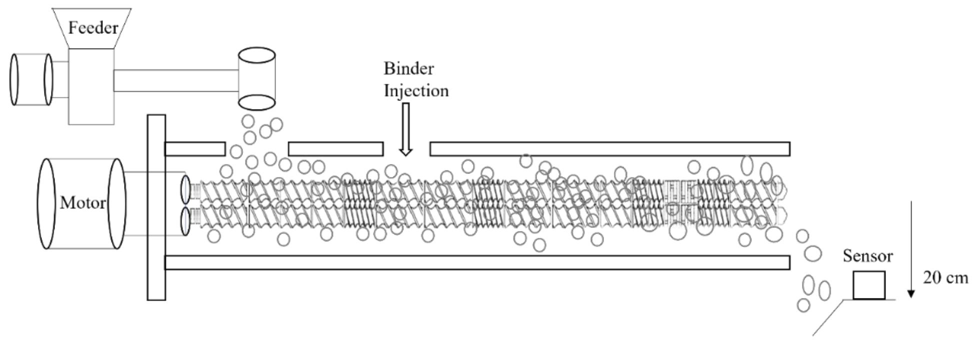

Figure 4-1. Experimental setup for real time monitoring of particle size, showing the formulation going into the twin screw extruder impact plate, and AE sensor assembly positioned 20 cm below the exit.

4.3.5. Coefficient of Restitution

A FASTCAM SA-Z type 2100k camera (Photron Limited, Tokyo, Japan) operating at 20,000 frames per second was positioned 10 mm away from the edge of the plate to record the normal displacement of particles upon impact. Video was recorded during granulation at the lowest and highest L/S ratio for each formulation in Table 4-1, to estimate the coefficient of restitution (COR) at the point of impact over a range of typical conditions; the varied formulations used in the study were intended to observe how sensitive the PAT system was to cohesion, represented by COR, though we hoped for good robustness since a commercial PAT would unlikely have access to such difficult data to collect. The supplied Photron FastCam Viewer 4 software was used to analyze the videos for particle velocities. In this work, the COR was assumed to be constant. The coefficient of restitution was found by taking the ratio of the velocity of the rebounding particle over its impact velocity. The coefficient of restitution for each formulation is shown in Table 4-2. A COR close to unity implied a near-elastic collision whereas a decreasingly smaller COR value corresponded to an increasingly inelastic collision. Table 4-2 showcases how the chosen formulations varied from being mostly elastic to highly inelastic, ensuring the PAT was trained with particles experiencing properties typical of pharmaceutical granulate. Adjusting the L/S ratio did not change the COR significantly (with the exception of K4M), thus the chosen approach for improving this PAT was by adjusting the formulations, rather than liquid content. Each condition was repeated three times to estimate the uncertainty of the measurement.

Table 4-2. Coefficient of restitution for each formulation tested.

Formulation	L/S Ratio (%)	Coefficient of Restitution	Standard Deviation	Percent change between low and high L/S ratio’s (%)
Lac	6	0.78	0.06	1.30
	10	0.79	0.11	
K4M	25	0.52	0.16	51.2
	35	0.24	0.05	
F4M	25	0.66	0.04	3.03
	35	0.68	0.08	
KSR	25	0.72	0.04	1.40
	35	0.71	0.04	

4.4. Modelling

To account for inelastic forces related to the chemistry and water content of exiting granules, a more accurate descriptor of the dampened impact behavior of different formulations was desired for the PAT system. For the previously disclosed auditory masking filter[17], it was assumed that all granules impacting the steel plate were perfectly elastic, represented by Hertz theory, which produced corresponding vibrations of a specific frequency in the plate that could be detected. To improve the predictive nature of the PAT, a modified filter was considered based on micromechanical theories so that the changes in impact behavior with the different tested formulations could be explained and a user might reasonably change the model without detailed data of the particle-surface interactions. Sections 4.4.1. and 4.4.2. will cover the viscoelastic and elastoplastic collision mechanics used to develop an updated impact filter.

4.4.1. Viscoelastic Micromechanics

A non-linear Hertzian spring and dashpot model was assumed considered to represent the impact force of particles striking the plate by assuming these collisions exhibited a viscoelastic response. The contact force (F_c) is composed of spring and dashpot contributors, as shown in Equation (1),

$$F_c = F_s + F_d \tag{1}$$

where F_s, and F_d are the spring and dashpot forces, respectively. The expressions for F_s and F_d are shown in Equations (2) and (3),

$$F_s = k_{Hz}\alpha^{\frac{3}{2}} \tag{2}$$

$$F_d = \eta_{Hz}\alpha^{\frac{1}{4}}\dot{\alpha} \tag{3}$$

where k_{Hz} is the Hertzian spring constant and η_{Hz} is the Hertzian damping coefficient. α and $\dot{\alpha}$, refers to a particle's overlapping contact area and rate at which a granule is overlapping during its impact with a flat plate. k_{Hz} and η_{Hz} are defined in Equation (4) and (5),

$$k_{Hz} = \frac{4}{3}\left(\frac{(1-\sigma_1^2)}{\pi E_1} + \frac{(1-\sigma_2^2)}{\pi E_2}\right)^{-1}\sqrt{R} \tag{4}$$

$$\eta_{Hz} = -\sqrt{5}\sqrt{\rho_1 V k_{Hz}}\frac{\ln e}{\sqrt{(\ln e)^2 + \pi^2}} \tag{5}$$

where V is the volume of the particle, E is the elastic modulus, σ is the possions ratio, ρ is the density, R is the particle radius, and e is the coefficient of restitution. The subscripts 1 and 2 refer to the particle and the plate, respectively.

With this design, η_{Hz} was tested with values between 1×10^{-6} and 1000 to assess the overall fit of the PSD of formulations with varying COR; the range of 1×10^{-6} to 1000 was chosen to showcase the effects of viscoelasticity with negligible dampening to fully dampened conditions based on the particle size range, moduli, and Poisson's ratio shown in Table 4-3. To compute the new contact force, the overlapping contact area between the particles must be found to compute the spring force. To find the particle overlap as a function of time, the equation of motion of a dropping particle based on spring and dashpot theory must be solved, and is shown in Equation (6),

$$\ddot{\alpha}(t) = -\frac{k_{Hz}}{\rho_1 V}\alpha^{\frac{3}{2}} - \frac{\eta_{Hz}}{\rho_1 V}\delta(t)^{\frac{1}{4}}\dot{\alpha} \tag{6}$$

where $\ddot{\alpha}$ is the acceleration of the particle. This differential equation was solved using the initial conditions $\alpha(0) = 0$ and $\dot{\alpha}(0) = V_0$, with V_o being the impact velocity. The impact velocity was assumed to be 1.5 m/s based on the terminal velocity analysis developed in the previous work[17]. The contact time was estimated by finding the time where maximum overlap occurred.

Table 4-3. List of constants used in the development of the viscoelastic filter.

Variable	Symbol	Value	Unit	Reference
Young's Modulus (Lactose)	E_1	3.33×10^9	Pa	[23, 24]
Young's Modulus (Stainless Steel)	E_2	199×10^9	Pa	[25]
Poisson's Ratio (Lactose)	v_1	0.25	No unit	[26, 27]
Poisson's Ratio (Stainless Steel)	v_2	0.29	No unit	[25]

4.4.2. Elastoplastic Micromechanics

For comparison to the viscoelastic approach, the inelastic collision of a particle with the plate was also considered to be described by the Walton-Braun model [28], which assumes the particle impact can be described as an elastoplastic response. The Walton-Braun model consisted of a loading (F_L) and unloading (F_{UL}) forces, along with the characteristic time of the impact (τ) (which was chosen as the contact time), and coefficient of restitution (e), shown in Equations (7) - (10) [29],

$$F_L = K_L\alpha \tag{7}$$

$$F_{UL} = K_{UL}(\alpha - \alpha_o) \tag{8}$$

$$\tau = \frac{\pi}{2}\sqrt{\frac{m}{K_{UL}}}\left(1 + \sqrt{\frac{K_{UL}}{K_L}}\right) \tag{9}$$

$$e = \sqrt{\frac{K_L}{K_{UL}}} \tag{10}$$

where α is the particle overlap, α_o is the overlap where the unloading force is zero, K_L and K_{UL} are the loading and unloading spring constants, respectively, and m is the mass of the particle.

In this approach K_L is fitted and kept at a constant value for all formulations, and K_{UL} was varied to adjust the coefficient of restitution for each formulation. Physically, this assumes that the impact velocities of all particles striking the plate were the same and only the rebounding behavior could possibly differ based on differing granule composition. In this work, when computing the loading force for each particle size, 5% of the particle radius was chosen as the maximum overlap to be able to produce changes in the AE spectra as a result of varying K_{UL} in the proposed auditory digital filter. Having the particle overlap below 1% of the particle radius was found to produce negligible changes in the resultant spectra, whereas Walton showed in their own work that going above 10% of the particle radius made the model overly sensitive to the elastic constant [30], which would counter the robustness sought in the PAT.

Equations (1) and (7) were applied for every particle size, and the maximum contact force and contact time were recorded in each case. These force and time values were then fed into the previous auditory masking filter [17] to compute the frequency resonance and amplitude of the plate for each particle size to create two new auditory masking filters.

4.4.3. Neural Network Modelling

After completing all experiments, the processed AE dataset from Sec. 4.3.4 contained ~2400 rows (signals) with 8065 columns (corresponding to frequencies from 0 to 700 kHz in 87 Hz increments). The PSD dataset obtained from Sec. 4.3.3 contained ~2400 rows (samples) with 16 columns (different particle sizes). To relate the AE spectra (after digital filtering) to PSD, an artificial neural network (ANN) model was utilized. Before the data was trained, stratified splitting was applied to the AE data to allow the training and testing datasets to contain an equal proportion of data for each formulation and L/S ratio. The data was split into 80% training and 20% testing. 10% of the training data was used for validation during model training. The ANN were setup in Python using the *keras* library.

The ANN employed an input layer with 8065 nodes, corresponding to the length of the AE spectra. This was followed by four hidden layers at 500 nodes, 250, 100, and 50 nodes respectively along with one output layer with 16 nodes, corresponding to each particle size. The Rectified Linear Unit activation function (ReLU) was used for the first and fourth hidden layer. The second and third hidden layers had the hyperbolic tangent (tanh) and sigmoid function, respectively. The output layer had a linear activation function, making this architecture identical to the one proposed in the previous PAT and allowing reasonable comparisons on the prediction error as parameter sensitivity was considered with the impact micromechanics. The mean squared error was used as the loss function. To quantify prediction error in the model, the root mean squared error (RMSE) was used. To quantify prediction error in the model, the root mean squared error (RMSE) was used. The high number of hidden layers was not anticipated to increase the risk of the model overfitting but rather give it more flexibility for future industrial training. Though a larger dataset in the future will help improve the predictive accuracy of this model, it was shown in this study to already be quite robust with the current training dataset by comparing its accuracy with a unique formulation it had never seen before in its training, with the PSD results showing a similar RMSE to other trial data.

The first ANN model was trained with all AE signals collected only from granulating lactose monohydrate at 6-10 wt% L/S, after being passed through the auditory masking filter modified with either the viscoelastic or elastoplastic micromechanics. Treating this data as the elastic case, a dampening coefficient of 1×10^{-6} or coefficient of restitution value of 0.8 was used in the filter during training (taken from Table 4-2).

Examples of the RMSE vs particle size plots shown in Figure 4-2 used to evaluate the ANN model were calculated with test lactose cases (6%, 8%, and 10% L/S) with the viscoelastic and elastoplastic filters applied in this first model (lactose ANN model). The reported RMSE with the original auditory masking filter [17] was 1.1 wt% across all these L/S ratios tested, and it is evident from the plots in Figure 4-2 that both viscoelastic and elastoplastic filters did not increase the maximum error, just as we would have hoped comparing the filters configured for the elastic case.

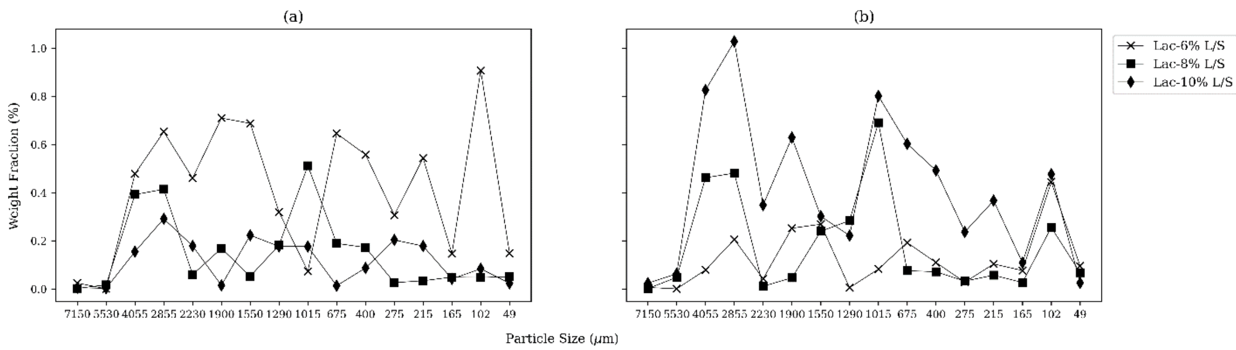

Figure 4-2. RMSE values for lactose monohydrate as the elastic case with the (a) viscoelastic filter at an η value of 1×10^{-6}, and (b) elastoplastic filter at e value of 0.8.

The first ANN model was used for testing the influence of the dampening and unloading parameters in the two filters. Experimental AE data for each of the three ‘inelastic' formulations (K4M, F4M, KSR) was transformed using either the spring-dashpot and Walton-Braun modification to the auditory masking filter and then processed by the first ANN model to predict PSDs for comparison with experimental PSD results. The purpose of experiments at this stage was to examine how the dampening and unloading parameters of the two filters each improved the predictions relative to the elastic case; this approach was followed to explain improvements in the overall model’s capacity to better understand cohesion, done so based on micromechanical analogies. The average RMSE from each of those predictions was then used to plot the trend of improvement associated with the corrective cohesive nature as a function of the changing parameter.

Finally, the performance of the filters was evaluated with a retrained AI model, now developed based on the AE spectra of all formulations. The goal was to demonstrate the best predictive accuracy with the modified PAT. Results with the retrained ANN model were compared with the original lactose trained ANN model to show the capabilities of this PAT for real-time monitoring of twin-screw granulation.

4.5. Results and discussion

The retarding agents used for extended-release formulations, namely hydroxypropyl methyl cellulose (HPMC, e.g. K4M and F4M) and polyvinyl acetate/povidone (e.g. KSR) tend to absorb considerably higher quantities of water compared to lactose [31, 32] and can also display a tacky nature depending on their molecular weight and functionality [33], with both of these traits affecting the inelastic response of a particle as it impacted the metal plate of our PAT system. While no impacting granule will be solely comprised of any of these extended-release excipients, they do represent a significant portion of its mass and contribute notably to its mechanical integrity and response to forces. Compared to the diluents used in wet granulation for solid oral dosage products, these retarding agents were selected for testing as being more extreme examples of inelastic particles. These pharmaceutical excipients are typically used at concentrations of 10-30 wt% in solid oral dosage formulations, and hence were selected at

20 wt% for this study to produce contact responses that would be indicative of actual manufacturing conditions.

The relatively high COR reported in Table 4-2 and notably good fit using an elastic filter [17] were the basis for choosing lactose granule impacts as the baseline elastic case in this study. Training with only AE data from the lactose granulation experiments to create the first ANN model also meant that water had minimal influence on the correlation with particle size because so little (<10 wt%) is required to granulate this excipient. This meant the correlation tool was developed without an awareness of how higher amounts of bound water or the stickiness of an excipient could affect the force and duration of a granule impact, and the resulting acoustics produced by that impact. As a result, differences for the predicted PSD using the first ANN as we studied the extended-release formulations could be attributed to the micromechanical filter, especially as the inelasticity was adjusted.

4.5.1. Influence of liquid-to-solid ratio on the AE spectra

Figure 4-3 presents the frequency-domain AE spectra for the lowest and highest L/S ratio cases examined for each of the four formulations. Impacts by all formulations produced AE in similar frequency bands, namely 60–150 kHz, 200–300 kHz, and smaller intensity peaks between 480–500 kHz. These bands will correspond to particle size ranges between 400–1000 μm, 150–240 μm, and less 100 μm, respectively[17]. Lactose particles produced the largest signal amplitude due to their relatively high elasticity, though peak intensity diminished as water content increased from 6 wt% to 10 wt% from the increased inelasticity. The amplitude was generally largest with the formulation Lac followed by

KSR, then F4M and finally K4M producing the most inelastic particles impacting the plate. As the L/S ratio increased, the peaks between 450-500 kHz were more significantly decreased in intensity as seen in Figure 4-3, which from the analysis of particle size can be attributed to a declining number of fines exiting the extruder.

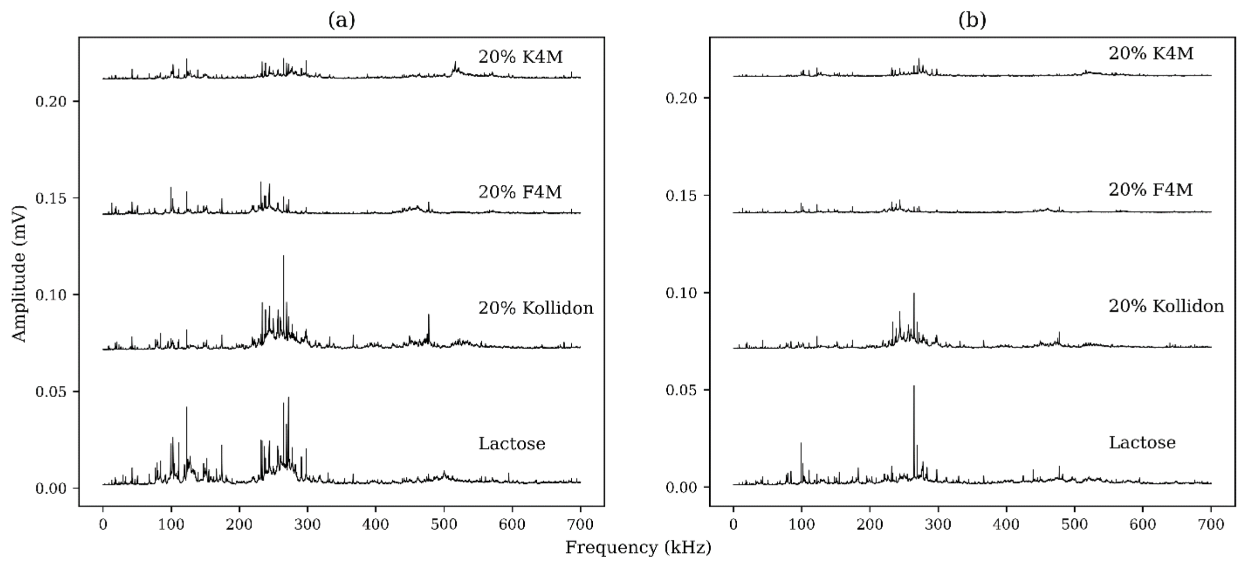

Figure 4-3. Frequency-domain AE Spectra for (a) lowest and (b) highest L/S ratios for samples of Lac, K4M, F4M and KSR.

4.5.2. Comparing viscoelastic and elastoplastic contact model responses

To assess which micromechanical contact response was most descriptive of cohesive granules exiting the twin-screw granulator, experimental particle size data for K4M, F4M, and KSR formulations was compared to the predicted PSD derived from the measured AE signal being input into the first ANN model using the two modified filters.

Figure 4-4 showcases the relationship between predicted impact force and particle size for several different dampening parameter and coefficient of restitution values using

Equations (1) and (7). With increasing value of the dampening parameter, there was an increase in the calculated impact force by the smaller particles and decrease for the larger particles. The viscoelastic nature of the contact model assumes that the impact force will be distributed over a longer period of time in comparison to an elastic collision corresponding to the time-dependent mechanical response of the granule [34]. The increase in the dampening parameter value appeared to match the same general changes mentioned in Sec 4.5.1, causing decreasing intensity of the impact force with greater inelasticity.

Figure 4-5 shows an example of how the filter, whose behavior was shown in Figure 4-4, adjusted the spectra of KSR, F4M, and K4M formulations with a low or high value for the dampening parameter; original spectra were shown in Figure 4-3. Increasing the dampening value in the cases of KSR and F4M caused a steady increase in amplitude with increasing frequency, making the 300 – 550 kHz regions (corresponding to smaller particles) where there was more signal information, to now appear with more intensity in the adjusted spectra. Only minor differences were noted in the adjusted spectra of K4M between low and high dampening values, indicating a similar level of amplification/attenuation by the filter regardless of the dampening parameter.

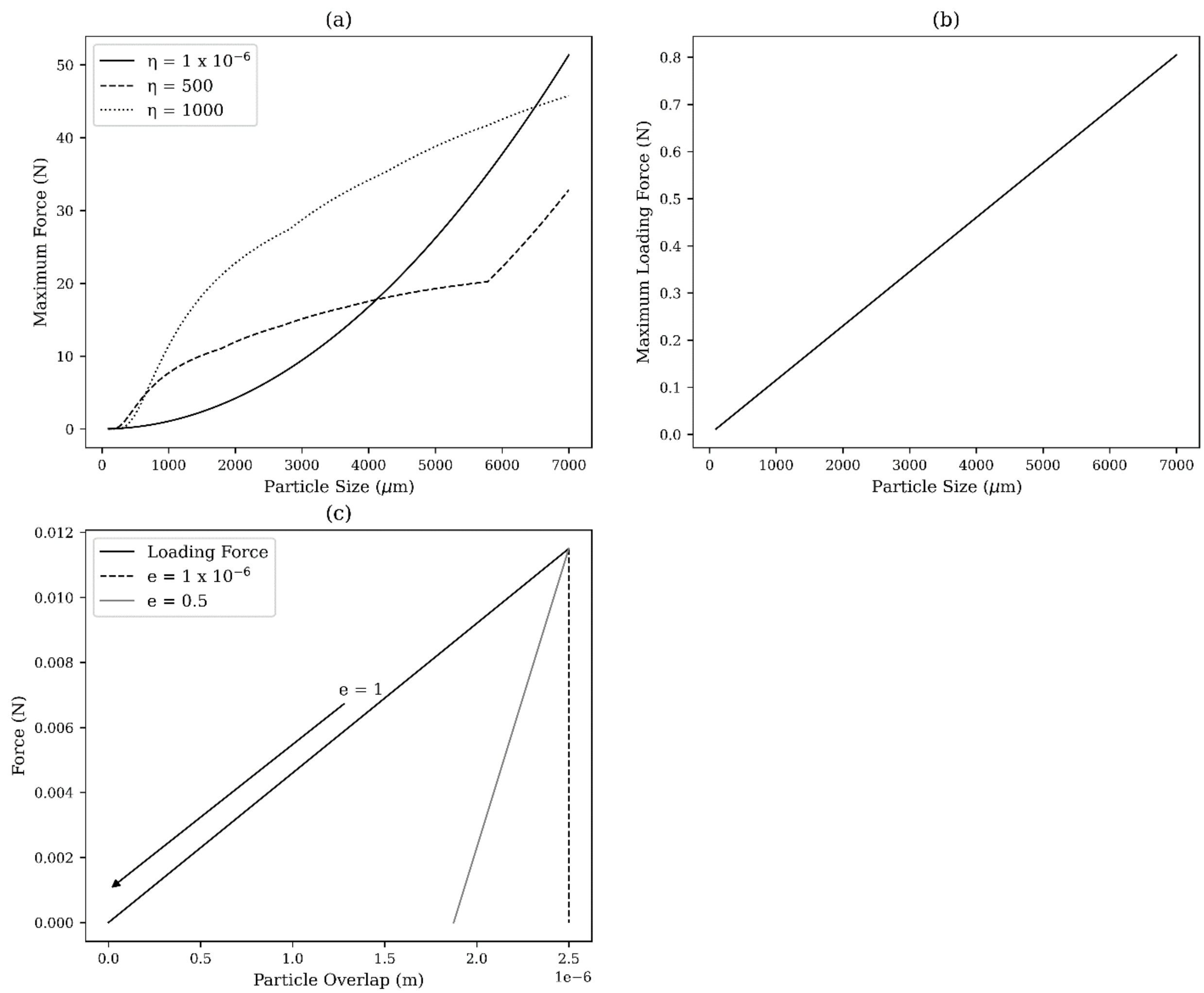

Figure 4-4. Predicted maximum contact force of a particle impacting a metal plate as a function of its size for (a) the spring and dashpot model at different dampening parameters and (b) the Walton and Braun model. Part (c) shows the response of a 100 μm particle to an elastoplastic impact at low and high unloading spring constants in the Walton and Braun model.

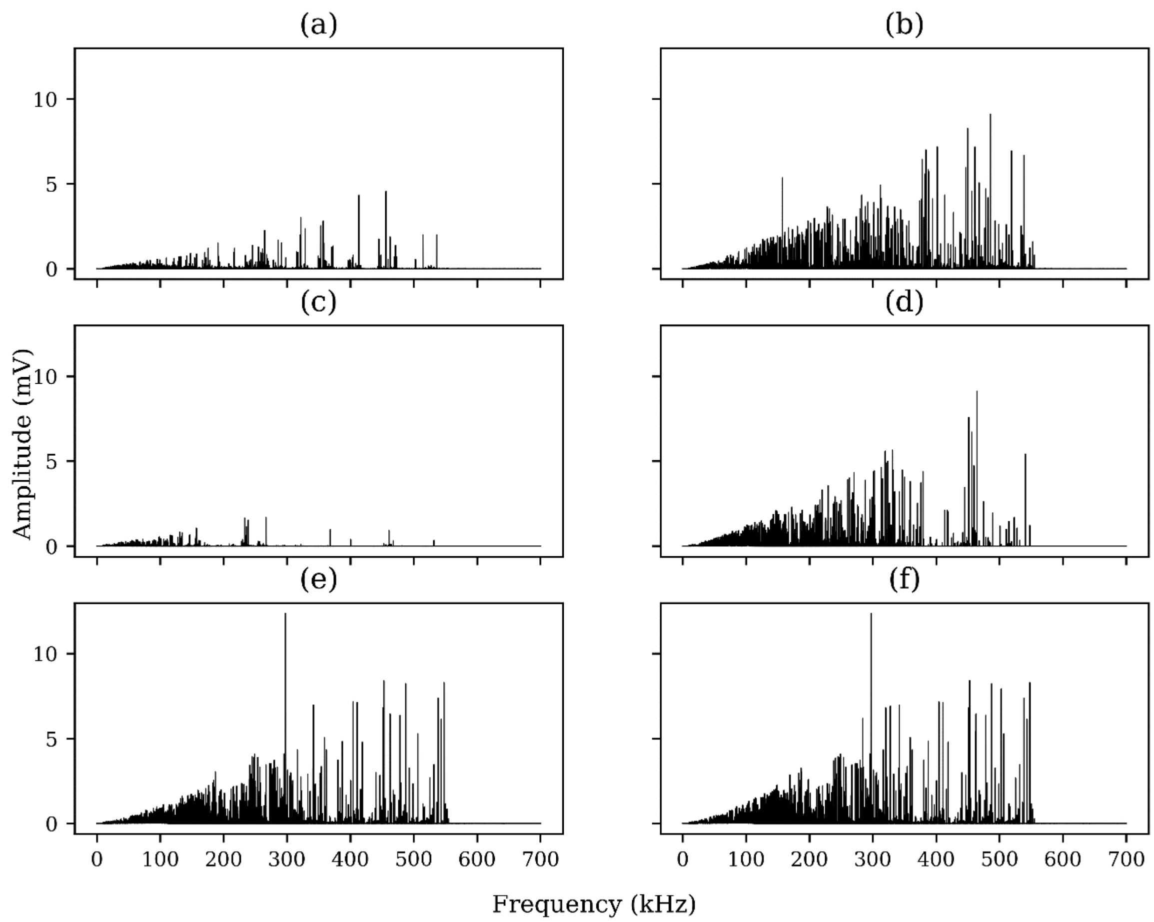

Figure 4-5. Examples of filtered spectra for KSR (a, b,), F4M (c, d), and K4M (e, f) at 35% L/S ratio. Subplots (a), (c), and (e) correspond to spectra being amplified for viscoelastic impact micromechanics with $\eta = 1 \times 10^{-6}$ whereas subplots (b), (d), (f) corresponded to $\eta = 1000$.

Considering the function of the elastoplastic filter, Figure 4-4(b) shows a linear increase in the maximum loading force with respect to particle size in comparison to the parabolic relationship observed with the spring and dashpot model. The unloading spring constant adjusted the rebounding behaviour in the form of a normal force offset, as seen in Figure 4-4(c) and as the coefficient of restitution increased, the loading and rebounding curves corresponded more closely to each other and then became identical at $e = 1$. Similar to the viscoelastic contact model, contact time with the plate increased as the collision was treated as more inelastic but considering the impact as plastic in nature meant that permanent deformation occurred to a granule during a collision, which is different from a viscoelastic model which generally assumes contact deformation is reversible but time dependent. Since the contact time produced by the Walton and Braun model is orders of magnitude higher than produced by the spring and dashpot model, there was a decrease in the maximum range of frequencies experiencing amplification, now between 0-230 kHz, in comparison to 0-550 kHz with the viscoelastic filter. Figure 4-6 shows how the elastoplastic filter amplifies the spectra for KSR, F4M, and K4M formulations.

Contrary to the viscoelastic auditory masking filter, increasing the coefficient of restitution in the elastoplastic auditory masking filter, amplified the spectra for all formulations. When the formulations were processed with a coefficient of restitution of e = 1×10^{-6}, the amplification of the spectra was at its minimum, due to the long enduring contact time attenuating the impact force to such a degree that minimal correction occurred to the measured AE spectrum. On the other end of the range when $e = 1$, the highest amplification was observed to the corrected AE spectra for samples of KSR, followed by F4M and K4M, as seen in Figure 4-6.

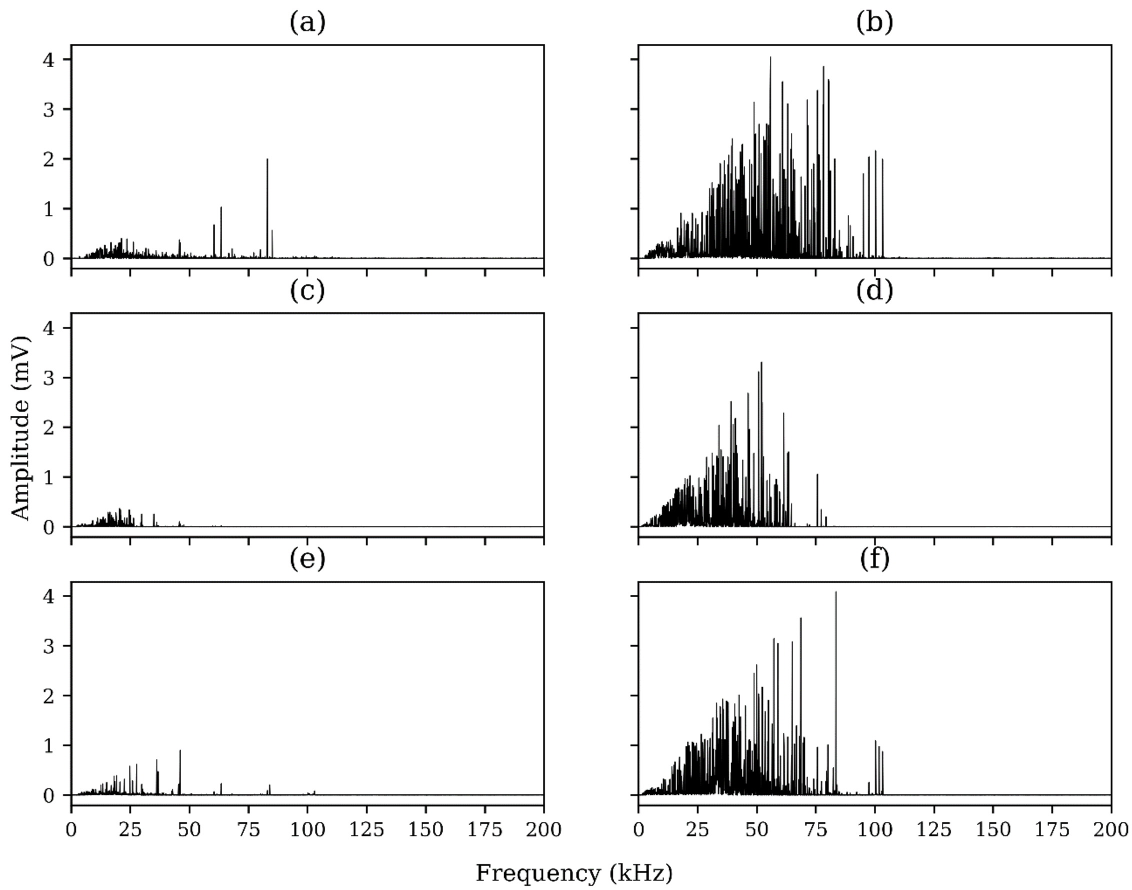

Figure 4-6. Example amplitude spectra for KSR (a, b), F4M (c, d), and K4M (e, f) at 35% L/S ratio. Subplots (a), (c), (e) correspond to spectra processed with the elastoplastic auditory masking filter with an e value of 1×10^{-6} whereas subplots (b), (d), and (f) correspond to spectra processed with an e of 1.

The error (reported as the average RMSE) was plotted in Figure 4-7 with changing dampening parameter (η) for the viscoelastic filter or COR (e) for the elastoplastic filter. Based on the measured coefficient of restitution in Table 4-2, results with K4M will represent the most inelastic case, while F4M and KSR should be quite similar but still show responses more inelastic than the elastic case. The consistently higher average RMSE with K4M, for both filters, showed that neither micromechanics could adequately correct the impact mechanics with the ANN model derived on lactose alone, for such inelasticity imparted to the granules. The lowest average RMSE was consistently found with KSR, for both models, even though its measured COR was similar to F4M.

The viscoelastic transformation with the lactose ANN model showed in Figure 4-7 no effect on K4M, a decrease in error with KSR and an increase in the error with F4M as the dampening parameter increased. These differing trends with the different formulations indicated the viscoelastic filter could not be robustly applied to improve PSD predictions. Needing different dampening parameter values based on particle size and coefficient of restitution of the formulation would be far too complicated for a suitable PAT. The fact that there was no dampening parameter value when COR of a formulation was sufficiently low was also problematic, considering the goal of a low RMSE. With these findings, this filter was not deemed to be an improvement for the PAT.

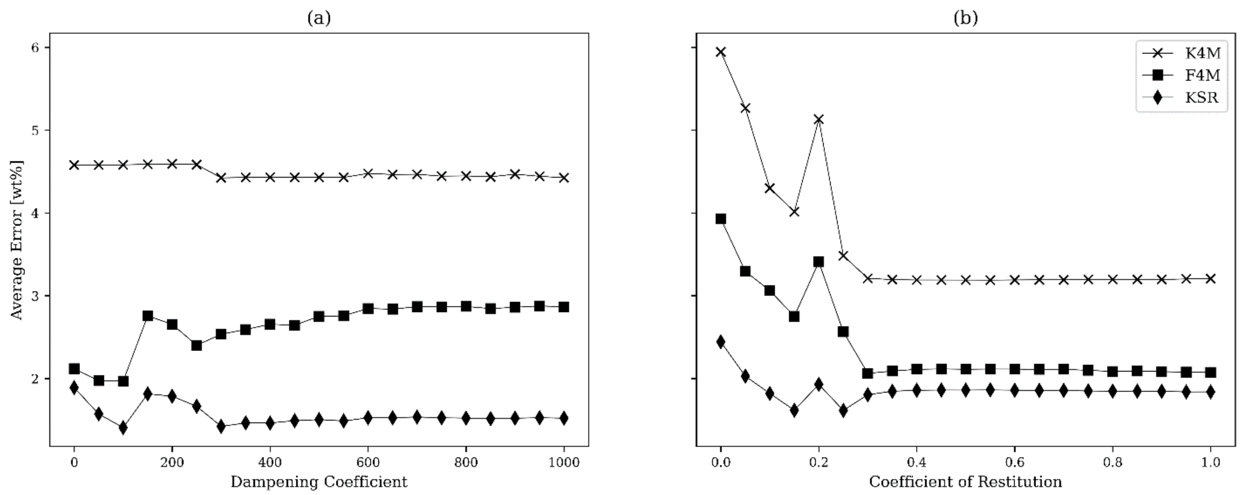

Figure 4-7. Average RMSE of all L/S ratios for K4M, F4M, and KSR in (a) a viscoelastic model with varying dampening coefficient and (b) an elastoplastic model with varying coefficient of restitution.

The elastoplastic transformation with the lactose ANN showed a more consistent response to all formulations tested, with the highest RMSE being at $e = 1 \times 10^{-6}$ in all cases, likely due to the transformation overestimating the plastic nature of the impacts, which caused minimal amplification of the spectra (relative to $e = 1$ as seen in Figure 4-6), likely causing a miscount of the number of particle collisions. An inverse trend for RMSE was seen for all formulations with a plateau present for a COR above ~0.3, with the KSR formulation being the least sensitive and K4M formulation being the most sensitive as e was varied. The consistency in trend and improvement in error with COR were seen as a positive indicator that the elastoplastic model could be a better fit with the nature of these formulations being granulated. The plateau was also very meaningful since it appeared that there would be broad robustness towards the set value of e in the filter provided it was above 0.3. Therefore, the Walton-Braun model was chosen as the preferred transformation for the improved PAT and retrained ANN results discussed in the next section.

The errors using the first ANN for predicting PSD, with all formulations, were too high for reliable real-time monitoring, especially with more inelastic formulations like K4M. RMSE values closer to 1% were desirable and would be more comparable to what was achieved with the elastic model with purely lactose granules. To improve the information used by the ANN model to predict PSD, it was retrained with new data from all four formulations.

4.5.3. Updated Model

In this section, the ANN model was retained with the AE data from all tested formulations and its prediction accuracy compared to the original lactose ANN model, using the original (elastic) auditory masking filter and modified (inelastic) filter based on the elastoplastic contact model. As shown in Figure 4-8, applying the original PAT (lactose ANN and elastic filter) to the entire set of formulation showed large deviations except with lactose granules. The RMSE was particularly high for KSR and F4M at 25% L/S ratio, reaching as high as 18.6 wt% and 17.5 wt%, respectively for the particle sizes of 2855 and 2230 μm, respectively. Applying the elastoplastic filter to the data and using a trained lactose ANN with the elastoplastic filter reduced the RMSE on average in comparison to the elastic filter, but unacceptably large RMSE were seen, especially for K4M at 35% L/S ratio where the error was as high as 15.8 wt% at 2230 μm. The retrained ANN model showed dramatically decreased prediction error on average in comparison to the lactose

ANN with the original elastic filter; Figure 4-8(c) shows the retrained model with elastic filter had difficulties mainly predicting the distributions associated with F4M and K4M, reaching as high as 3 and 9 wt% for the F4M and K4M formulations at 35% L/S ratio, respectively. Switching to use of the elastoplastic filter with the retrained ANN model, the error distribution in Figure 4-8(d) is shown to be more evenly distributed in comparison to the RMSE predictions of original auditory masking filter in Figure 4-8(c), with the maximum RMSE being 2 wt% across all particle sizes. This outcome matches our findings with the original PAT while studying lactose granulation [17], where training the ANN model had the most profound overall effect on lowering RMSE but only with the correct filter used was it possible to reduce the error for all particle sizes. To challenge the model and test its predictive accuracy, AE data was collected for a completely new formulation of 40% KSR (where the higher KSR content replaced a portion of lactose in the mixture) granulated at 30% L/S ratio. The formulation was not used in the retraining of the AI model yet the predicted PSD included in Figure S4-1 showed a good fit, especially for an acoustic pattern the system had never seen before, though it appears to be slightly underpredicting the coarse fraction. The maximum RMSE was found to be 2.8 wt%, corresponding to the coarse fraction as shown in Figure S4-2 of the supplementary file.

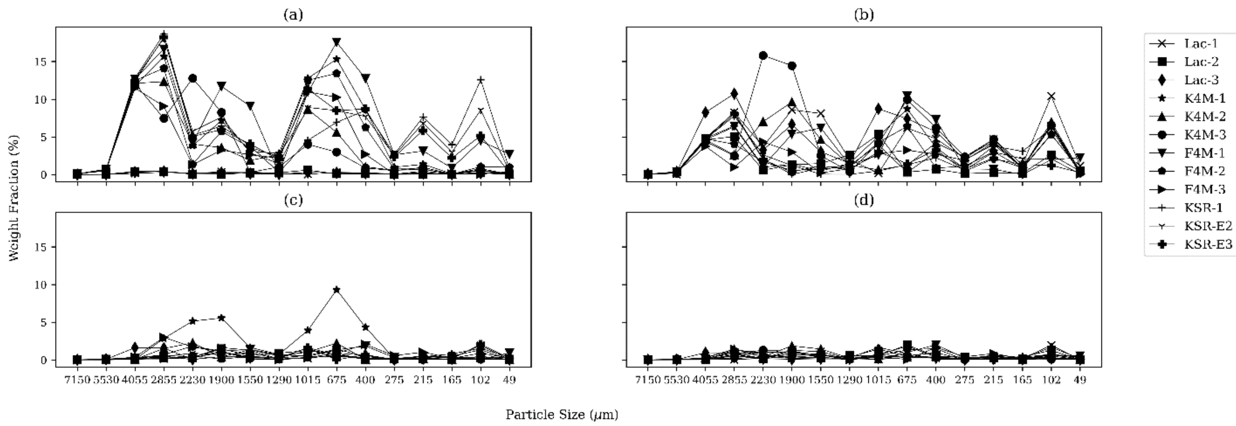

Figure 4-8. RMSE plot of particle size weight fractions of the testing set consisting of data from lactose, KSR, F4M, and K4M with (a) trained lactose ANN with the original filter, (b) trained lactose ANN with the elastoplastic filter (e = 0.8), (c) retrained ANN with the original filter, and (d) retrained ANN the elastoplastic auditory masking filter (e = 0.6). Subplots (a) & (c) used data pre-processed with the original auditory masking filter and data used in subplots (b) & (d) were pre-processed with the elastoplastic auditory masking filter.

The PSD predictions with the elastoplastic filter and retrained ANN model are shown in Figure 4-9, for the four formulations at three L/S ratios; the significant variation in the experimental bimodal PSD shape among the four formulations gave a good sense of the extremes in granulation by twin-screw granulation and the capacity of the modified PAT to predict such extremes. The newly trained model is now able to predict a PSD from formulations that exhibit both very elastic and inelastic impact behaviours. The experiments conducted ensured the PSD ranged from very fine to very coarse for every formulation tested, as shown in Figure 4-9.

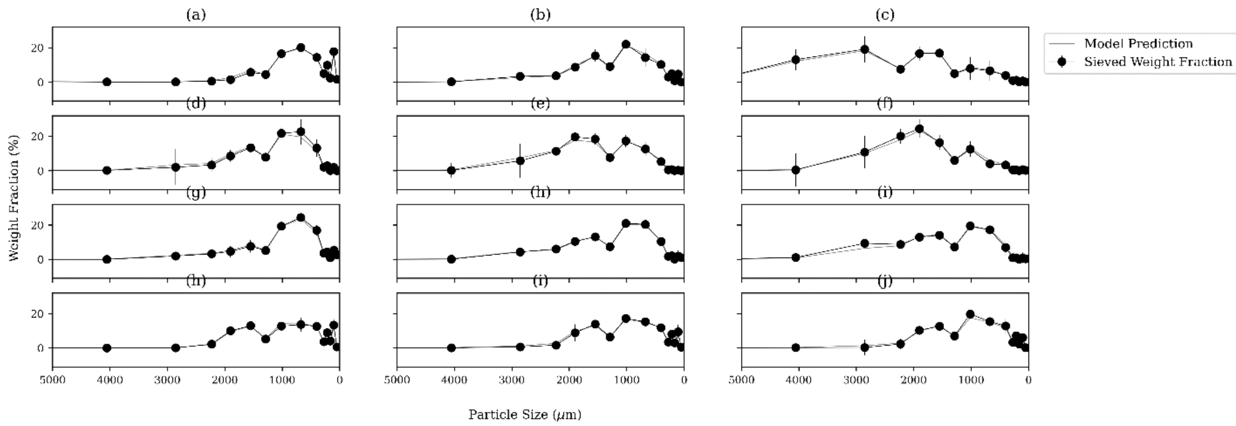

Figure 4-9. Model predictions with the dampening filter with lactose at (a) 6%, (b) 8%, and (c) 10% L/S ratio. The second row are predictions for K4M at (d) 25%, (e) 30%, and (f) 35% L/S ratio. The third row's predictions are for F4M at (g) 25%, (h) 30%, and (i) 35% L/S ratio. The last row predictions are for KSR at (j) 25%, (k) 30%, and (l) 35% L/S ratio.

4.6. Conclusion

Differing inelastic granule impact behaviours were explored to develop a modified auditory masking filter to more accurately predict the PSD of typical cohesive pharmaceutical formulations produced in a twin-screw granulator. Two micromechanical models were tested to transform acoustic emissions data produced from impact collisions with a plate that were varying in their inelasticity based on the water content and nature of the excipients. It was found the Walton and Braun model which describes an elastoplastic behaviour was more robust than a non-linear spring and dashpot model which describes viscoelasticity. The error from the trained lactose models showed as the formulations became increasingly inelastic the average value of the prediction error increased. However, the viscoelastic ANN model showed little change for 20% K4M, whereas the elastoplastic

ANN model showed a consistent trend regardless of formulation, showing more robustness in comparison to the viscoelastic ANN. Retraining the model with the Walton and Braun transformation with all the data showed a maximum RMSE of 2 wt% in comparison to the ANN with the original auditory masking filter with a maximum of 18.6 wt%. Future work will focus on adapting the filter to account to particles with non-spherical shapes along with expanding it to different processes such as hot melt or dry granulation.

4.7. Acknowledgements

The authors would like to thank Kevin O'Donnell and International Flavors and Fragrances Inc. (formerly Dow Chemical) for donating the HPMC and lactose monohydrate, and Shaukat Ali and BASF for donating the Kollidon SR used in this study. In addition, we would like to thank the Natural Sciences and Engineering Research Council (NSERC) for its funding of the work.

4.8. References

[1] F. Destro, I. Hur, V. Wang, M. Abdi, X. Feng, E. Wood, S. Coleman, P. Firth, A. Barton, M. Barolo, Z.K. Nagy, Mathematical modeling and digital design of an intensified filtration-washing-drying unit for pharmaceutical continuous manufacturing, Chemical Engineering Science, 244 (2021) 116803.

[2] M. Jelsch, Y. Roggo, P. Kleinebudde, M. Krumme, Model predictive control in pharmaceutical continuous manufacturing: A review from a user's perspective, European Journal of Pharmaceutics and Biopharmaceutics, 159 (2021) 137-142.

[3] U. Nandi, V. Trivedi, S.A. Ross, D. Douroumis, Advances in Twin-Screw Granulation Processing, Pharmaceutics, 2021.

[4] M.R. Thompson, Twin screw granulation – review of current progress, Drug Development and Industrial Pharmacy, 41 (2015) 1223-1231.

[5] M. Bardin, P.C. Knight, J.P.K. Seville, On control of particle size distribution in granulation using high-shear mixers, Powder Technology, 140 (2004) 169-175.

[6] T. Närvänen, T. Lipsanen, O. Antikainen, H. Räikkönen, J. Yliruusi, Controlling granule size by granulation liquid feed pulsing, International Journal of Pharmaceutics, 357 (2008) 132-138.

[7] T. Schæfer, D. Johnsen, A. Johansen, Effects of powder particle size and binder viscosity on intergranular and intragranular particle size heterogeneity during high shear granulation, European Journal of Pharmaceutical Sciences, 21 (2004) 525-531.

[8] A.C. Scott, M.J. Hounslow, T. Instone, Direct evidence of heterogeneity during high-shear granulation, Powder Technology, 113 (2000) 205-213.

[9] M. Fonteyne, A. Correia, S. De Plecker, J. Vercruysse, I. Ilić, Q. Zhou, C. Vervaet, J.P. Remon, F. Onofre, V. Bulone, T. De Beer, Impact of microcrystalline cellulose material attributes: A case study on continuous twin screw granulation, International Journal of Pharmaceutics, 478 (2015) 705-717.

[10] A. Ito, P. Kleinebudde, Influence of granulation temperature on particle size distribution of granules in twin-screw granulation (TSG), Pharmaceutical Development and Technology, 24 (2019) 874-882.

[11] R. Meier, M. Thommes, N. Rasenack, K.P. Moll, M. Krumme, P. Kleinebudde, Granule size distributions after twin-screw granulation – Do not forget the feeding systems, European Journal of Pharmaceutics and Biopharmaceutics, 106 (2016) 59-69.

[12] J. Vercruysse, A. Burggraeve, M. Fonteyne, P. Cappuyns, U. Delaet, I. Van Assche, T. De Beer, J.P. Remon, C. Vervaet, Impact of screw configuration on the particle size distribution of granules produced by twin screw granulation, International Journal of Pharmaceutics, 479 (2015) 171-180.

[13] Y. Hu, L. Wang, X. Huang, X. Qian, L. Gao, Y. Yan, On-line Sizing of Pneumatically Conveyed Particles Through Acoustic Emission Detection and Signal Analysis, IEEE Transactions on Instrumentation and Measurement, 64 (2015) 1100-1109.

[14] Y. Hu, X. Huang, X. Qian, L. Gao, Y. Yan, Online particle size measurement through acoustic emission detection and signal analysis, 2014 IEEE International Instrumentation and Measurement Technology Conference (I2MTC) Proceedings, 2014, pp. 949-953.

[15] C.-j. Ren, J.-d. Wang, D. Song, B.-b. Jiang, Z.-w. Liao, Y.-r. Yang, Determination of particle size distribution by multi-scale analysis of acoustic emission signals in gas-solid fluidized bed, Journal of Zhejiang University-SCIENCE A, 12 (2011) 260-267.

[16] M. Uher, P. Beneš, Measurement of particle size distribution by the use of acoustic emission method, 2012 IEEE International Instrumentation and Measurement Technology Conference Proceedings, 2012, pp. 1194-1198.

[17] H.A. Abdulhussain, M.R. Thompson, Predicting the particle size distribution in twin screw granulation through acoustic emissions, Powder Technology, 394 (2021) 757-766.

[18] H. Tsujimoto, T. Yokoyama, C.C. Huang, I. Sekiguchi, Monitoring particle fluidization in a fluidized bed granulator with an acoustic emission sensor, Powder Technology, 113 (2000) 88-96.

[19] T.M. Chitu, D. Oulahna, M. Hemati, Rheology, granule growth and granule strength: Application to the wet granulation of lactose–MCC mixtures, Powder Technology, 208 (2011) 441-453.

[20] V. Vanhoorne, B. Vanbillemont, J. Vercruysse, F. De Leersnyder, P. Gomes, T.D. Beer, J.P. Remon, C. Vervaet, Development of a controlled release formulation by continuous twin screw granulation: Influence of process and formulation parameters, International Journal of Pharmaceutics, 505 (2016) 61-68.

[21] "BASF Pharma", Kollidon® SR | Coprocessed Excipients | BASF Pharma, BASF Pharma, 2023.

[22] "Physical Acoustics", F30a - 150-750 kHz High-Sensitivity Flat Frequency Response AE Sensor, by Physical Acoustics, Physical Acoustics, 2023.

[23] F. Bassam, P. York, R.C. Rowe, R.J. Roberts, Young's modulus of powders used as pharmaceutical excipients, International Journal of Pharmaceutics, 64 (1990) 55-60.

[24] M. Perkins, S.J. Ebbens, S. Hayes, C.J. Roberts, C.E. Madden, S.Y. Luk, N. Patel, Elastic modulus measurements from individual lactose particles using atomic force microscopy, International Journal of Pharmaceutics, 332 (2007) 168-175.

[25] H.M. Ledbetter, N.V. Frederick, M.W. Austin, Elastic-constant variability in stainless-steel 304, Journal of Applied Physics, 51 (2008) 305-309.

[26] V. Busignies, P. Tchoreloff, B. Leclerc, C. Hersen, G. Keller, G. Couarraze, Compaction of crystallographic forms of pharmaceutical granular lactoses. II. Compacts mechanical properties, European Journal of Pharmaceutics and Biopharmaceutics, 58 (2004) 577-586.

[27] F. Podczeck, Theoretical and experimental investigations into the delamination tendencies of bilayer tablets, International Journal of Pharmaceutics, 408 (2011) 102-112.

[28] O.R. Walton, R.L. Braun, Viscosity, granular-temperature, and stress calculations for shearing assemblies of inelastic, frictional disks, Journal of Rheology, 30 (1986) 949-980.

[29] A.B. Stevens, C.M. Hrenya, Comparison of soft-sphere models to measurements of collision properties during normal impacts, Powder Technology, 154 (2005) 99-109.

[30] M. Paulick, M. Morgeneyer, A. Kwade, Review on the influence of elastic particle properties on DEM simulation results, Powder Technology, 283 (2015) 66-76.

[31] M.R. Thompson, K.P. O'Donnell, "Rolling" phenomenon in twin screw granulation with controlled-release excipients, Drug Development and Industrial Pharmacy, 41 (2015) 482-492.

[32] V. Vanhoorne, L. Janssens, J. Vercruysse, T. De Beer, J.P. Remon, C. Vervaet, Continuous twin screw granulation of controlled release formulations with various HPMC grades, International Journal of Pharmaceutics, 511 (2016) 1048-1057.

[33] E.I. Keleb, A. Vermeire, C. Vervaet, J.P. Remon, Twin screw granulation as a simple and efficient tool for continuous wet granulation, International Journal of Pharmaceutics, 273 (2004) 183-194.

[34] E. Falcon, C. Laroche, S. Fauve, C. Coste, Behavior of one inelastic ball bouncing repeatedly off the ground, The European Physical Journal B - Condensed Matter and Complex Systems, 3 (1998) 45-57.

4.9. Supplementary Section

Table S.4-1. Moisture content of granules after exiting from the extruder.

Formulation	Moisture Content at Low L/S (%)	Standard Deviation	Moisture Content at High L/S (%)	Standard Deviation
Lactose	6.40	0.7	9.47	1.5
20% K4M	20.3	0.6	17.3	1.4
20% F4M	17.5	1.1	22.2	1.5
20% Kollidon	16.3	1.2	20.3	1.8

Table S.4-2. Moisture content of granules after air drying for 48 hours.

Formulation	Moisture Content at Low L/S (%)	Standard Deviation	Moisture Content at High L/S (%)	Standard Deviation
Lactose	4.49	0.8	5.00	0.1
20% K4M	4.25	0.7	4.72	0.2
20% F4M	4.72	0.2	4.70	0.1

20% Kollidon	4.10	0.1	4.43	0.1

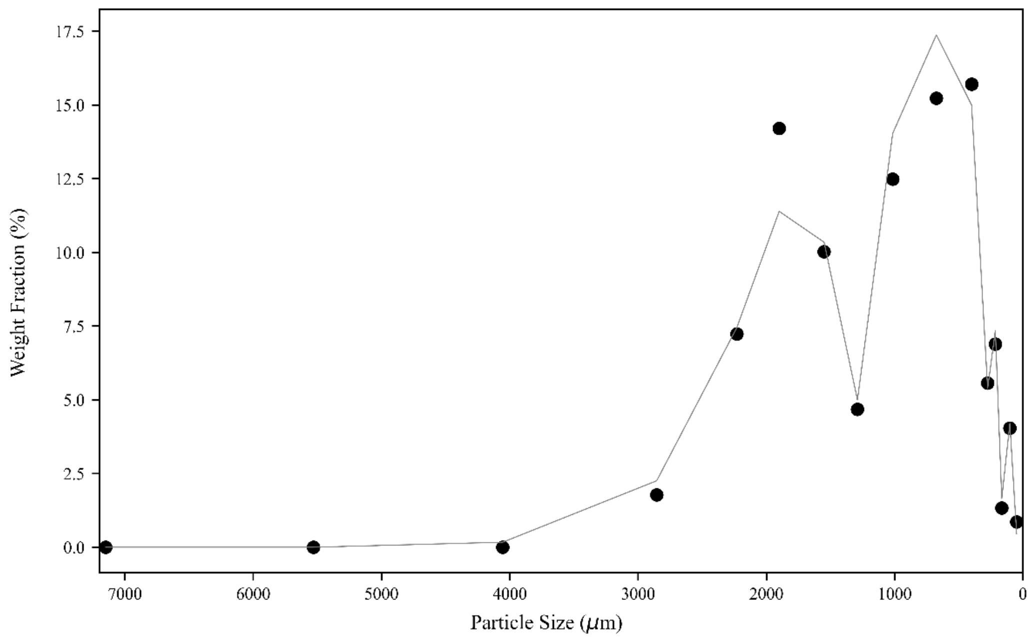

Figure S.4-1. Particle size distribution of a completely novel formulation, 40% KSR, granulated at 30% L/S ratio, with the symbols (circles) corresponding to measured data from the sieve shaker and the drawn line corresponding to the model prediction

Chapter 5: Examining the Evolution of the Particle Size Distribution from Startup to Steady State in Twin Screw Granulation with Acoustic Emissions

Examining the Evolution of the Particle Size Distribution from Startup to Steady State in Twin Screw Granulation with Acoustic Emissions

H.A. Abdulhussain[a], M.R. Thompson[a,*]

[a]*CAPPA-D/MMRI, Department of Chemical Engineering,*

McMaster University, Hamilton, Ontario, Canada

[*] Author to whom correspondence should be addressed.

Tel: (905) 525-9140 x 23213

mthomps@mcmaster.ca

5.1. Abstract

An investigation was conducted with a newly created inline process analytical technology (PAT) to study the evolution of granulation by monitoring the particle size distribution (PSD) in real-time for the continuous twin-screw granulator during its startup. The PAT uses an artificial neural network model to correlate acoustic emissions (AE) of exiting granules to particle size. Onset of steady state was established based on PSD to be five times the mean residence time over a range of degrees of fill (12-30%) by comparison of sieve classification and the PAT. Greater insights were gained into the early stages of granulation by this inline PAT, showing different stages of granule growth for particle sizes ranging from 102-2230 μm as the process transitioned to steady operations. This study aimed to highlight how inline PAT could be used to learn more about this black-box process for the pharmaceutical community.

Topical Area: Particle Technology and Fluidization

Keywords: Acoustic emissions, Process analytical technology, Transient flow state, Twin screw granulation, Granulation mechanism.

5.2. Introduction

In the pharmaceutical industry, most global regulatory bodies are encouraging the development of advanced quality control strategies around the manufacturing of drug products, with specific focus on continuous processes. Twin screw granulation has gained significant interest from the pharmaceutical industry as one such process, over this past decade [1]. Twin screw granulation (TSG) offers significant advantages over comparable high shear batch processing, including systematic integration with other unit operations, increased throughput, shorter process (residence) time, and higher product consistency [2,3].

The transition to steady state in TSG has gone unstudied to date because the process operates as a black-box and most of our available characterization tools need substantial sample sizes to draw conclusions and yet this period of time may reveal significant details about the granulation mechanism. The TSG granulation mechanism is partially understood at present but mostly because it does somewhat follow the stages of nucleation, propagation and granule breakage seen in batch processes [4,5]. However, the present lack of scaling rules for this process highlights that there are still major gaps in our knowledge to be addressed. The complexity of the process is attributed to the confounding influences of its process variables, including formulation properties [6,7], screw design [7,8], screw speed [9], mass flowrate [4,10], and liquid-to-solids (L/S) ratio [9,11]. These variables are strongly affected by the degree of fill (DF), with the granulation mechanism seemingly changed as a result. By the process mapping done to date it has been observed that at lower DF, granules are thought to experience less frictional forces and are able to move freely in the barrel, which allows for increased growth and consolidation [6,12]. Conversely, at higher DF, granules are more constrained, moving in a plug-like manner, which is believed to reduce the amount of particles being wetted and yielding more fines produced [13-15]. Shi [16] confirmed this transition in the granulation mechanism was around a DF of 20%, observed in both 18 mm and 27 mm twin-screw granulators, where below it the impact of screw speed on the PSD is more prominent than the mass flow rate, and vice versa above this value. Seem et al.[14] also mentions in their review that screw speed does have an impact on granulation at very high DF (we estimate at 60% DF and onwards), which indicates that effects of screw speed may only be prominent at the extremes (very low or high DF), from a process mapping standpoint.

The only studies known to have been explicitly concerned with whether the process in a TSG was steady, relied on torque measurements and then only in a GEA ConSigma® machine [9,11,14,17]. While torque is a helpful variable to monitor operational consistency and will have some indirect correspondence to the state of the compression zone where binder spreading and particle agglomeration will primarily be occurring, it is not a direct descriptor for output performance such as end product responses like fracture strength and dissolution rate, or the more universally required information like particle size distribution (PSD). In fact, Ryckaret et al. [18], who provided some of the most thorough studies on the effects of torque in twin-screw granulation, measured torque along the length of the screw concluded that this inline measurement cannot be used to monitor particle size. Additionally, none of these studies were examining the transition period prior to steady state in their machines.

The purpose of this study was to explore the evolution of granulation during the transient start-up period after first establishing when steady state occurred for a generated

PSD. The work compares the capabilities of off-line sieve classification versus a recently developed inline PAT based on acoustic emission (AE) [19] on our understanding on how PSD evolves in a twin-screw granulator. The goals of the research were to assess the value of inline systems on their capacity to observe phenomena in a continuous process on a very short timescale. This study was also the first opportunity to relate mean residence time (MRT) to the time to reach steady state in a twin-screw granulator, which is commonly understood information for other chemical processes [20-23].

5.3. Materials and Methods

5.3.1. Materials

All trials were conducted with a placebo formulation of 60 wt% Flowlac® 100 lactose monohydrate (Meggle Pharma; Germany), 20 wt% Avicel® PH-102 microcrystalline cellulose (International Flavors and Fragrances; USA), and 20 wt% Kollidon SR® polyvinyl acetate/povidone (BASF; USA). The formulation was pre-mixed and then dried at 50℃ for 24 hours before use. The binder solution consisted of 2 wt% METHOCEL E3PLV (International Flavors and Fragrances; USA) dissolved in distilled water.

5.3.2. Twin Screw Granulation Experiments

Wet granulation was conducted in a 27 mm 40 L/D co-rotating twin-screw extruder, model ZSE-27HP from Leistritz Extrusion (Somerville, NJ). The extruder consisted of 10 barrel zones, the first (Z0) being water cooled followed by nine (Z1-Z9) temperature controlled zones. A standard granulation screw design was employed with conveying elements going from Z0 – Z7, two kneading blocks (60^{o} offset, medium thickness elements) in Z8 followed by another set of conveying elements in Z9, as seen in Figure 5-1. The barrel temperature was set to 15℃ as Kollidon SR® is more susceptible to dry granulation – with a glass transition temperature of 35℃ according to the manufacturer [24]. The formulation was fed into the extruder using a Brabender T20 twin screw gravimetric feeder (Missisauga, ON, Canada) and the liquid binder was added through an ISCO 260D high syringe pump (Teledyne-ISCO Inc; Lincoln, NE) at zone Z3.

The degree of fill was controlled at 12% (Low DF) and 30% (High DF), to operate the TSG on either side of one known granulation mechanism transition first noted by Seem et al. [14] and Tu et al.[15] and then further quantified by Shi [16] (~20% DF), for which our own studies have found to be quite accurate. The degree of fill was calculated according to the regression best fit model developed by Mozumder [25] in Equation (5-1) for our 27 mm 40 L/D extruder, who used a fixed L/S ratio of 26% while varying screw speed (SS) and powder (mass) flowrate (PFR):

$$DF = -0.07(SS) + 9.2\,(PFR) + 8.8 \tag{5-1}$$

The lower and upper bounds of the PFR were set as 3 kg/hr and 4.5 kg/hr (due to material constraints), respectively, and then using Equation (1), the screw speed was adjusted so that the DF was above and below the transition value of ~20%. The chosen DF for this work were 12% (349 RPM and 3 kg/hr) and 30% (288 RPM and 4.5 kg/hr).

For the trials to determine when steady state occurred, the L/S ratio was kept at 27%. The DF should not be significantly changed by the L/S being different from the operating state used to generate Equation (1), since it has been shown that DF is mainly a function of screw speed, mass flowrate, and screw design [14,26]. "Startup” procedure meant turning on the motor to the desired screw RPM, while simultaneously turning on the liquid pump and the feeder. Granules were collected from startup to 30 seconds (0-30 s), then the feeder, pump, and screw were then stopped. The machine was cleaned out of particle and then started again. This approach was used for startup to 1 minute (0-60 s or 0-1 min) and startup to 2 minutes (0-120 s or 0-2 min). For every period afterwards (namely 2-4 min, 4-6 min, 6-8 min, 8-10 min), granules were only collected for 2 min over the mentioned period. The reason for 2 min of sampling was that it was the minimum amount of time needed to collect approximately 100 g of granules for further sieve characterization at both DF conditions. Once the onset of steady state was determined for PSD, additional trials at 18% and 39% L/S ratio were conducted for artificial intelligence (AI) model training of the PAT (referring to Sec. 5.4. below) with granules collected at 2 and 4 min, respectively. The two L/S used for AI model training were selected to generate particle size distributions with larger amounts of fine (<300 μm) or coarse granules (>2100 μm).

All granule samples collected for offline analysis from the trials mentioned, were placed in trays and were left to air dry at room temperature for 48 hours before their PSDs were characterized. Approximately 1-2 g of granules collected before air drying was analyzed for their moisture content, collected from the trials at 0-30 s, 0-1 min, 0-2 min, and 2-4 min of runtime for all L/S ratios at both low and high DF, using a HG63 moisture analyzer (Mettler-Toledo; Columbus, OH). Only steady state residence time distributions were evaluated 10 min after startup for the 27% L/S ratio condition, by introducing a color tracer of 1 g cocoa powder into the extruder as a pseudo dirac pulse to calculate the MRT at 12 and 30% DF. Triplicates of the MRT were performed to determine uncertainty.

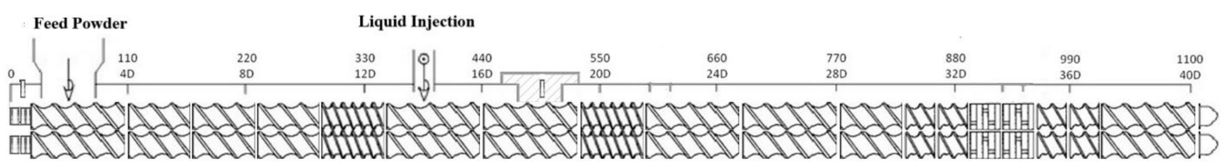

Figure 5-1. Screw design used for twin-screw granulation experiments.

5.3.3. Offline Particle Size Distribution Characterization

The offline PSD was characterized using a Ro-Tap RX-29 sieve shaker (W.S. Tyler; Mentor, OH). Unless otherwise stated, 100 g of granules from a trial were first classified into eight fractions using a set of sieves with nominal openings of 2100, 1700, 1400, 1180, 500, 300 μm along with the pan at the bottom. The sieve stack was mechanically agitated for 5 min before weighing the sieves to determine the PSD. The mass on the 2100 μm sieve was further classified with a second set of sieves with nominal openings of 8000, 6300, 4760, 3350, 2360, 2100, and 1700 μm and agitated for 5 min before weighing. Similarly, the mass in the bottom pan from the first classification was further classified with a third set of sieves with nominal openings of 500, 300, 250, 180, 150, 53, and 44 μm and agitated for 5 minutes before weighing. This procedure was done to obtain a well defined PSD. As a result, the weight fractions shown in this work are for the average sizes of 7150, 5530, 4055, 2855, 2230, 1900, 1550, 1290, 1015, 675, 400, 275, 215, 165, 102, and 49 μm.

For sample collection from 0-30 s or 0-1 min, the amount of mass being sieved was well below 100 g, and so a sensitivity test was conducted in this study to determine the minimum amount of mass needed to reproducibly measure the PSD using the sieving technique. Samples at 27% L/S collected at different time intervals were mixed together, making a total mass of 600 g. The sample was agitated manually for 2 min and then 100 g of material were immediately extracted and characterized using the first set of sieves mentioned above. This procedure was repeated by extracting either 50 g, 20 g, or 10 g of material and sieving to determine PSD.

5.3.4. Fracture Strength

Fracture strength of the granules was determined by uniaxial compression with an Instron 3366 benchtop mechanical testing system (Instron Corporation; Canton, MA) following the method by Adams [27]. A small quantity of granules (0.6 g) in the particle size range of 400 – 1900 μm was placed in a die press with a 11.09 mm bore diameter and were compressed at a 3.5 mm/min until a maximum load of 4200 N was reached. The stress-strain curve was then analyzed to obtain the fracture strength according to Equation (5-2) at high values of compressive strain (~20%):

$$\ln P = \ln\left(\frac{\tau'}{\alpha'}\right) + \alpha'\varepsilon + \ln(1 - \exp(-\alpha'\varepsilon)) \tag{5-2}$$

where P is the compressive stress, α' is the lateral stress pressure coefficient, τ' is the characteristic fracture strength, and ε is the compressive strain. The measurement was repeated three times to determine the uncertainty.

5.4. Inline Acoustic Emission PAT Validation

Inline detection of particle size distributions exiting the TSG used an acoustic emissions (AE) technique is described in earlier studies [19,28]. The acoustic sensor combined with AI model making up the PAT, can estimate the full bimodal size distribution indicative of TSG processing, giving much more information than just simple single value descriptors like d_{50}. Briefly, a stainless steel impact plate was positioned 20 cm below the outlet of the extruder with an F30α broadband AE sensor (Physical Acoustics, Princeton, NJ) attached using high vacuum grease (Dow Corning) to a tab protruding from the plate. The detected acoustic signal was amplified using a Physical Acoustics 2/4/6c amplifier set to +60 dB and collected at an acquisition rate of 3 MHz for all experiments. For the steady state determination trials at 27% L/S, the AE signal was continuously collected at the last trial from startup to 10 min whereas for the trials at 18 and 39% L/S, the signal was collected from startup to 6 min. An auditory masking filter coupled to a Walton-Braun impact model was used to correct for sound attenuation based on particle size and moisture content, as described in a previous study [19]. A neural network AI model translates the filtered amplitude-frequency signal in the 0-700 kHz range into a particle size distribution. To improve the accuracy of the model built on previous data [19,28] for the current formulation, 30 s sampled segments of the AE signal corresponding to times of granule collection for the current formulation were used for retraining along with their corresponding sieved particle size data. The collected granules corresponded to steady state from 2-4 min of runtime for 18%, 27%, and 39% L/S at both DFs for this placebo formulation. The AI model was trained for 300 iterations or epochs, with 80% of the data used for training and 20% for testing. The model was trained three times with different training and testing datasets to estimate the uncertainty of the PAT output. After training, the model was able to monitor the PSD accurately with the largest error corresponding to the 215 μm weight fraction (at a low degree of fill) with a root mean squared error (RMSE) of 0.61 wt% using data from the testing set. The uncertainty was presented as a standard deviation in reported PSD for this study.

In the earlier studies to develop the method [19,28], the AI model was established by analyzing 30-seconds segments of the signal to maximize the number of particle collisions used to estimate the PSD while providing timely updates to operators; the 30 s corresponded closely to the MRT in those cases. In the present study, the intent of using this method was to understand the nature of granules exiting the TSG well under the first minute of running the machine and that meant analyzing much smaller segments of the collected signal than even 30 s. Since the signal is a recording of every particle impact over time and therefore, records an accurate PSD corresponding to whatever time segment is analyzed, the concern here was to determine what is the minimum time segment needed for the AI model to output a representative PSD from the process. To explore the segment size of the signal required to match an offline characterization of PSD, a sensitivity analysis was performed. The PSD estimations of the AI model were compared using shorter signal segments from within the normal 30 s recording taken from the AE signal between 3.5-4 min after startup, namely segment intervals of 0-1 s, 0-5 s, 0-10 s, 0-20 s, and 0-30 s. The corresponding outputs of the model are shown in Figure 5-2 along with the offline sieved distribution for a sample taken between 2-4 min of run time at 27% L/S ratio and 12% DF.

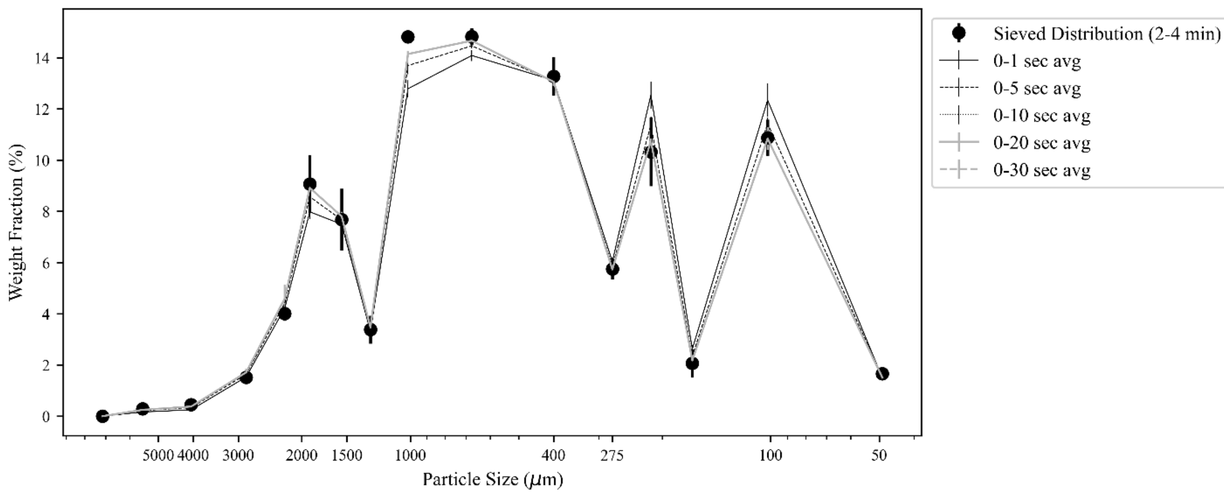

Figure 5-2. Estimated PSD generated by the AI model using varied time segments of an AE signal collected from 3.5 to 4 min after startup for the trial conditions of 12% DF and 27% L/S ratio. Error bars for the offline sieved data and PAT estimates represent the standard deviation (n=3).

The estimated distributions determined by the AI model showed the only major deviation from the sieved data when working with a time segment of 1 s duration (0-1 s interval), with the largest RMSE being for the ungranulated fractions, 215 μm and 102 μm at 3.1 wt% and 2.0 wt%, respectively. For a time segment of 5 s (0-5 s interval), the maximum RMSE decreased to 1.2 wt% and remained consistently below 1.0 wt% with the analysis of larger time segments from the AE signal; a RMSE value below 1 wt% is considered ideal for the model. In general, the larger the size of the signal segment analyzed by the AI model, the more accurate the estimation becomes. However, a segment of 10 s (or longer) was considered sufficiently close to match a sieved distribution collected over the span of 2 min, with a maximum RMSE below 1.0 wt% across all particle sizes. A signal segment of 10 s is recording 8.3 g of exiting granules corresponding to 58 screw revolutions, which appears sufficient to record enough particle collision to get the correct normalized distribution shape (at steady state).

Based on this analysis, there was confidence in using the PAT to analyze the transient period during startup, so long as the analysis was not less than 5 s and with good confidence when considering a period of at least 10 s.

5.5. Results and Discussion

No method of determining the particle size distribution of a sample is without limitations from measuring its true nature. The method of sieving requires a detectable quantity of mass on each tray, per the sensitivity of the weigh scale and weight of the sieves themselves, and even then, each tray is capturing particles covering a range of sizes assumed to be spherical in shape [29,30]. The new acoustic emissions PAT records the emitted elastic waves generated by wet granules exiting the extruder and impact a plate, even though its AI model to translate the signal into a PSD is trained with the classified samples obtained by sieving once dry. And so, neither was considered to more accurately representing the particle size distribution from the twin-screw granulator. The important difference in this study was that the PAT, as an accurate recording of every particle impact, could display distributions of very few particles and therefore analyze the time period during startup of the TSG before steady state was reached.

5.5.1. Sieving Technique Sensitivity

To use sieved data in this study, the reliability of the method to characterize PSD with samples below the traditional amounts of 80-100 g used [31-33] was assessed on account of the short run times being considered. Figure 5-3 shows multiple PSDs when the sample size was reduced from 100 g all the way down to 10 g, whereas Table 5-1 shows the d_{10}, d_{50}, and d_{90} for each of those distributions. Interestingly, the shape of the distribution showed little changes as the sample size decreased from 100 g to 50 g to 20 g, and only showed a significant difference at 10 g. A gradual decrease is seen in d_{10}, d_{50}, and d_{90} values from 100 g to 20 g, with the largest decrease of roughly 8.5% in the d_{50} over that range. Below 20 g, there was a shift in trend with the d_{50}, and d_{90} increasing whereas the d_{10} continued to decrease.

Based on these test results, from a reliability perspective, the minimum amount of mass that was considered for particle characterization in this study was 20 g. which is close to the amount that exits from the extruder over 30 sec at the chosen lower DF in this study.

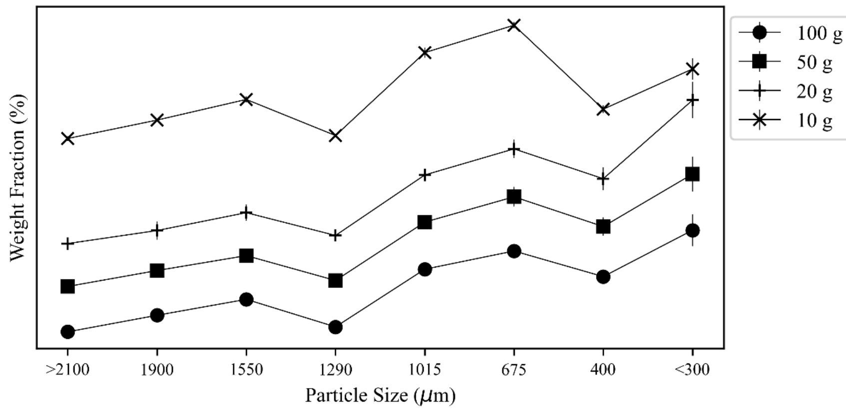

Figure 5-3. Particle size distribution sieved with 100, 50, 20, and 10 g of granulated material. Displayed distributions are incrementally shifted on the y-axis to clearly show the evolution of the distribution shape with sampled amount. Error bars represent the standard deviation (n=3).

Table 5-3. Single descriptors and their standard deviations for the particle size distributions sieved with varying masses.

Mass Sieved (g)	d_{10} (μm)	d_{50} (μm)	d_{90} (μm)
100	1901±30	859±57	342±5
50	1851±32	816±59	339±5
20	1771±68	786±47	332±4
10	1706±361	860±207	348±21

5.5.2. Steady State Determination

To examine the transient state, one must first determine when steady state occurs, at least covering the lower bounds of DF for wet granulation in the TSG. It was advantageous to describe the onset of steady operations relative to the residence time of the machine, following standard practices of Chemical Engineering [20-23]. Using offline and inline particle size characterizations of granules collected, Figure 5-4 compares the size distributions of samples from startup until 10 min at 27% L/S ratio while Figure 5-5 presents the d_{10}, d_{50}, and d_{90} of those distributions as a function of time, through sieving and AE PAT; due to the limits of sieve classification disclosed in Section 5.5.1, nothing was evaluated below 30 s for these specific trials but since reaching steady state took longer, it did not impact the analysis. Since the typical PSD is bimodal for TSG, the descriptors of d_{10}, d_{50}, d_{90} will not accurately reflect the changing distribution as they would for a mono-modal distribution but are beneficial nonetheless for denoting trends. For reference, the MRT determined at the two degrees of fill for this trial was 25 $\pm$1 s (12% DF - low) and 12 $\pm$1 s (30% DF - high). The faster process occurring with the higher degree of fill was attributed to the higher space velocity of the powder bed, which is a function of mass flow rate and inversely proportional to screw speed.

The analysis began with direct comparison of the particle size distributions. At 12% DF, the weight fractions of particles in the size range of 400-1900 μm increased between 30 s to 2 min after startup. By sieving, granules below 400 μm (mainly 102 and 215 μm) decreased in weight fraction after the first measurement at 30 s and then remained unchanged after 1 min (within the limits of uncertainty). After 2 min, which corresponded to five times (5x) MRT at this operating condition, the weight fractions of all particle sizes remained consistent within the limits of uncertainty for sieve classification. By the AE PAT, a decrease in the fine particles at 102 and 215 μm was noted past 1 min that ceased to change any further after 2 min whereas all size fractions larger than 400 μm show an increase over the same interval. At 30% DF (high DF), sieved particle sizes showed little variation in their weight fractions from 30 s onwards, with the exception of the 102 μm and 2855 μm sizes that took up to 1 min before they ceased to change further. At this higher DF, the onset of steady state corresponded to 5xMRT, just like at 12% DF. Using AE PAT, the estimates of weight fractions below 275 μm and above 1015 μm were the same for all time intervals tested with the exception of 9.5-10 min. For the particles sizes corresponding to 400 and 675 μm, the weight fractions increased slightly after 0-0.5 min and then remained constant for all time intervals used, with the exception of 9.5-10 min where another slight increase was observed for all particle sizes above 275 μm. However, the increase was within the uncertainty of the sieved measurements shown in Figure 5-4(b). The estimates by PAT corroborated the sieving results that steady state was 5xMRT at the high DF as well.

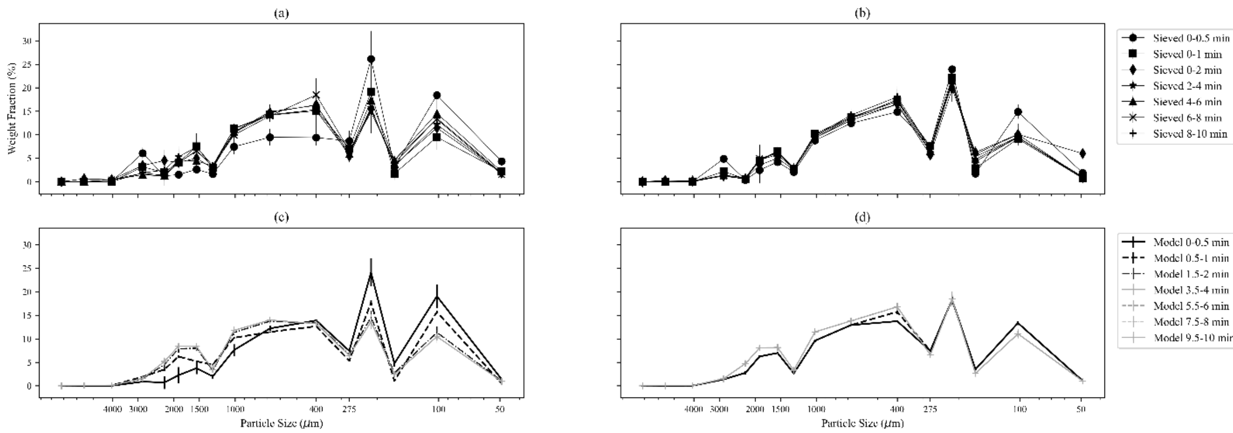

Figure 5-4. Particle size distribution by sieving at 27% L/S ratio with a degree of fill of (a) 12%, or (b) 30% with respect to time. Subplots (c) and (d) show the PSD at 27% L/S ratio from the AE PAT. Error bars for the offline sieved data and PSD estimates represent the standard deviation (n = 3).

The three descriptors, d_{10}, d_{50}, d_{90} in Figure 5-5 generally represent three distinct regions of the PSD, loosely characterized as fines, desired granules (for tabletting), and coarse particles, respectively from the granulator. Sieving results for the first 10 min of operation are given in Figures 5-5(column 'a') and it can be seen that larger versus smaller particle sizes evolved differently while the TSG process was starting up. At low DF, by sieving d_{90} and d_{50} increased until 2 min, before slightly decreasing and then no longer changing, whereas the d_{10} increased for 1 min then decreased before becoming constant. This makes some sense since it implies fines progressed through the machine at first with little alteration at this degree of fill, while granules took some time to grow but ultimately consumed the fines as would be expected. At high DF, a more consistent trend in the sieved results was observed across all descriptors where the particle size increased until 1 min then decreased before stabilizing. Applying the same mechanistic interpretation as above, this observation implies granule growth did not lag behind at the higher degree of fill, likely indicating less heterogeneity in the wetted state of powders at the site of injection. In comparison, the descriptors determined from the PAT results are given in Figures 5-5(column ‘b’) with smaller error bars. At both DF, d_{90} and d_{50} showed a steep rise in particle size over the first minute and then more gradual granule growth up to 2 min, while d_{10} showed only a gradual increase in size over the 2 min span. The descriptors were constant after 2 min for both DF from the PAT results.

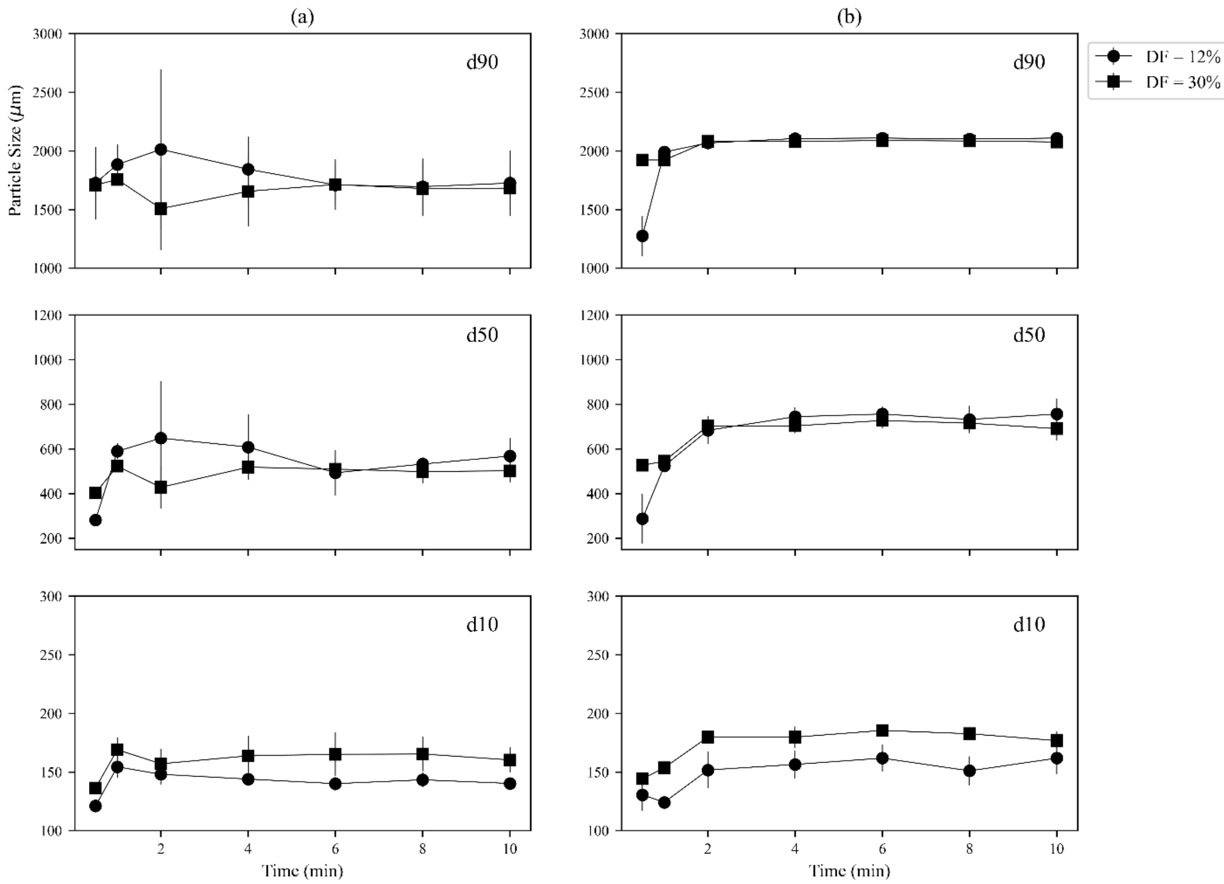

Figure 5-5. Plots of the change in d_{90}, d_{50}, and d_{10} with respect to time produced through (a) sieving and (b) AE PAT estimation for 27% L/S ratio. Error bars represent the standard deviation (n = 3) for both sieved and PAT data.

The singular descriptors, by both techniques, did not match the direct observations made of the PSD, with regards to onset of steady state. While the PAT descriptors showed smaller error bars and hence made it clearer as to the trend being seen compared to sieving, the onset of steady state would be much longer in both cases. Due to the bimodal nature of the characteristic PSD from a TSG, these descriptors were amplifying insignificant variances in particle sizes distributed between the two peaks. For this study, the preference was to rely on the findings from direct observation of the PSD and hence, it was concluded that 5xMRT was the most appropriate rule-of-thumb for anticipating the onset of steady state (based on particle size).

The finding of a near-identical onset of steady state with respect to MRT, by the two techniques, for the two DF conditions is ideal by being consistent with transport phenomena principles but was still a novel outcome since there is prior art showing that the granulation mechanism will differ on either side of a transition boundary, found to be ~20% DF for our process by Shi [16]; the transition boundary corresponds to where a difference has been noted in how screw speed affect particle size in the previous process mapping made by Tu et al [15] and Seem et al[14]. At 12% DF, particles are being dragged whereas at 30% DF, one sees tumbling and avalanching particulate motion. Since we are aware of another transition boundary at much higher DF(~60%) where above this state the powder bed becomes much more compressed and begins to move in a plug-like manner [8], one should not assume this rule-of-thumb of 5xMRT for PSD to reach steady conditions necessarily applies across all potential degrees of fill.

Moisture content and fracture strength measured for collected granules from trials at 27% L/S were examined as functions of time in Figure 5-6 to showcase other granule properties relevant for end use. The large error bars seen in Figure 5-6(b) are a result of the method of measurement, which involved sampling from a wide particle size range, so a large degree of variability was expected; the large error bars complicate definitively establishing the onset of steady conditions just as they did with the sieved particle size data in Figures 5-5 (column ‘a’). However, both properties are associated with the collision mechanics of our granules and so their trends helped to understand whether the determined onset of steady state applied to all particle properties. In Figure 5-6(a) and (b), at both DF, each analyzed property was found to increase, peak in value and then slightly decrease before becoming mostly constant within measurement variance. Moisture content became steady after 2 min whereas it was not possible to assess steady results for fracture strength. At 30% DF, both average moisture content and fracture strength seemed to reach a slightly higher peak value when compared to 12% DF, which would be reasonably expected by the increased compaction occurring to produce denser granules and are partition liquids from the interstitial regions to the more accessible surfaces of these granules [34,35]. Others have also noted an increase in moisture content at higher DF when studying in-barrel drying of granules within the TSG [36]. The error bars are quite large but with the same trends seen with particle size, we believe it is still reasonable to quote the onset of steady state corresponds to 5xMRT at 12 and 30% DF.

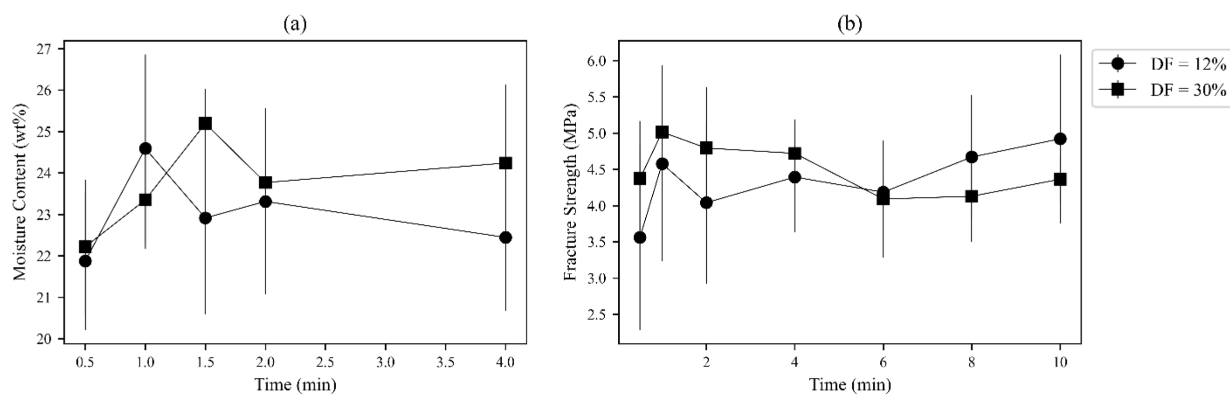

Figure 5-6. (a) Moisture content and (b) fracture strength of granules at 27% L/S ratio as a function of time. Error bars represent the standard deviation (n = 3).

5.5.3. Investigation of the transient period of continuous wet granulation by PAT

The studies in Section 5.5.2 concluded that steady state of the continuous wet granulation process was best approximated at 60-120 s from startup for the tested formulation, depending on the degree of fill. The analysis of particle classification by sieving in Sec. 5.5.1 found that at least 20 g of material was required to reliably produce a PSD by the method, which translates to a minimum of 16 or 24 s of material sampling at the high and low DF examined in this study, respectively. Comparably, a reliably produced PSD by AE PAT was found between 5-10 s of signal sampling. This meant offline sieving would provide a lower resolution of information, concerning evolving PSD during the transient period compared to the inline PAT. Despite this higher rate of process monitoring possible by PAT, neither PAT nor sieving can begin sample collection until material begins to leave the machine. For this study, time equivalent to 1xMRT was allowed to pass before analysis of the acoustic signal was considered, which meant the first PSD was estimated 5 s after MRT in the results of this section (30 s and 20 s for 12% and 30% DF, respectively). It is for this reason that many particle sizes in Figure 5-7, while changing over the remaining 4xMRT, appear to near instantly grow in weight fraction at time corresponding to 1xMRT; that jump in weight fraction will be ignored (data not shown) in the analysis since it is an artefact of the monitoring method. Figure 5-7 shows the change in two representative particle sizes over time for fractions identified as fines (102, 215 μm), desired granulates (675, 1015 μm), and coarse granules (1900, 2230 μm). The plot shows the evolving PSD for the well studied 27% L/S ratio as well as the PSDs for 18% L/S and 39% L/S using signal data collected from their trials to train the AI model.

Using 18% L/S ratio, at either degree of fill, one observed little-to-no variation in the PSD as a function of time. At the high DF, a little more variation was observed over 30-45 s, with the weight fraction of 102 μm (nominally) sized powder decreasing and then increasing until it remained essentially constant; whenever this particle size decreased, a small increase in weight fraction was observed for the 675, 1015, 1900, and 2230 μm sizes. The insignificant change at 18% L/S at both degrees was likely because the liquid content was too low for significant granule growth; at least ~60% of the particle sizes remained ungranulated (<400 μm) even at steady state.

At the two higher L/S ratios, there was much more variation in the different granule sizes over time making up the PSD and more distinction between the two degrees of fill. At 12% DF, the weight fraction of fines (102 μm and 215 μm) dominated the PSD over the period of 30-60 s (~1.0-2.0xMRT) for all L/S ratios. From 60-90 s (~2.0-4.2xMRT) the fines decreased in their weight fraction, down to about 7 wt% with 27% L/S ratio or 4 wt% with 39% L/S ratio, and then remaining constant at its steady state value from 105-120s (~4.2-5xMRT). For the desired granule sizes (675 and 1015 μm) and coarse sizes (1900 and 2230 μm) the weight fractions remained steady from ~1.0-2.0xMRT and then increased to its steady state values at ~16 and ~12 wt%, respectively, from 2-4.2xMRT at both L/S ratios. At 30% DF, the fines with 27% L/S ratio showed some variance between 20-50 s (~1.0-4xMRT) as but leveled off at ~15 wt%. The other size groups (675, 1015, 1900, and 2230 μm) showed small increases over this same period of time, with the coarse granule size corresponding to 1900 μm showing the greatest increase in weigh fraction up to 6 wt%. At 39% L/S ratio, the fine fractions underwent a drastic decrease from 40-50s from ~20 wt% to 6 wt%. All other weight fractions shown in Figure 5-7 underwent a sharp growth at this binder concentration after 40 s and then remained constant after 50 s, with the largest particle fractions being at 675 and 1015 μm (both around 14-15 wt%) followed by 2230 and 1900 μm (9-11 wt%).

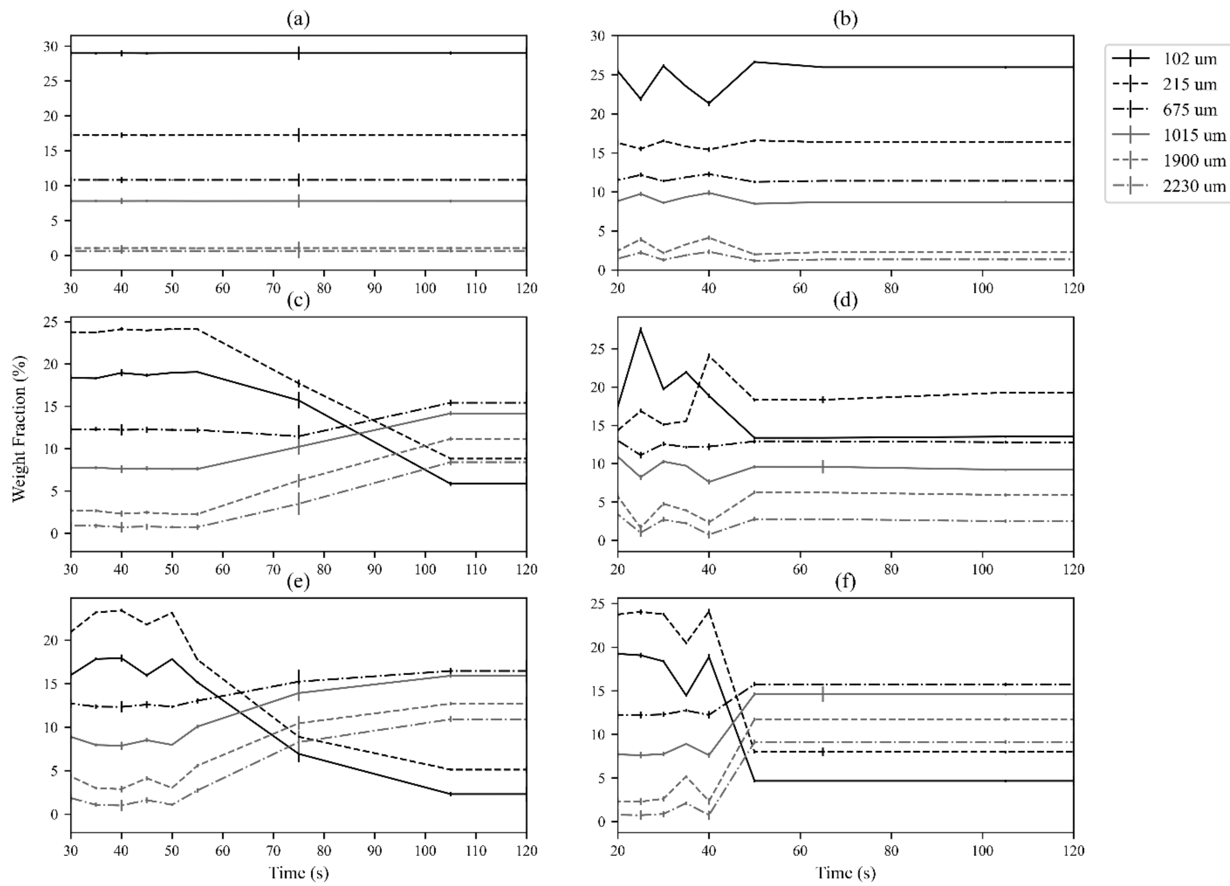

Figure 5-7. Change in particle size over time using the AE PAT from 1xMRT up to 120 s at 12% DF at (a) 18, (c) 27, (e) 39% L/S ratio. Subplots (b), (d), and (f) at 30% DF correspond to the same L/S ratios (18, 27, and 39%, respectively).

5.5.4. Granulation Mechanism

The transient behavior discussed is based on results in Section 5.5.3 and observations after material began to exit the extruder (i.e. ~1xMRT). Fines being the fed solids to the machine, were dominant (~40 wt%) in the earliest stages of startup (1-2xMRT) for both DF, with no significant granulation evident; with little binder built up on the barrel wall in the kneading zone to cause viscous drag, most of the powder will pass through the influential zone without the local decrease in velocity necessary to cause bed compaction. Beyond this period, differences in granule development were noted in the exiting PSD based on degree of fill, except at 18% L/S ratio which was too dry to consider in this analysis of the granulation mechanism.

At 12% DF, after a period corresponding to an additional MRT had passed, the binder wetted particles showed evidence of coalescing into larger granules according to the AE PAT. With so little available volume occupied at this condition, the powder is only being dragged forward by the flight, free to roll, jostle about, and stick with other particles in the conveying zone. It was actually difficult to see the influence of the kneading zone at this low DF with only gradual granule growth seen from ~2-4.2xMRT since compaction should bring about the rapid development of large, even coarse, particles. The poor compaction may be caused by insufficient liquid being squeezed out to coat the barrel in the kneading zone (for viscous drag) and/or insufficient volume to cause pressurization in that zone to create strong enough granules to not breakup in the subsequent conveying zone. At both moderate and high binder concentrations (27 and 39% L/S ratio in this case) the AE PAT showed granule growth at this DF was a gradual process, since granules up to

1015 and 1900 μm were formed. Gradual growth seemed to be characteristic of this low DF while the binder content added determined whether the PSD favored larger sizes.

At 30% DF, increasing the mass flowrate at a fixed screw speed increases the volume occupied by the powder in the screws. Interestingly, the collected particles starting after 1xMRT showed less change in weight fraction over time than seen at the lower DF, especially for a binder concentration below 39% L/S ratio. In the conveying zone, the powder will continue to be dragged by the flights of the screws but collisions arising from such jostling would be reduced (though still expectedly possible due to shear dilatancy) while some portion of the powder bed may now be thrown over the screw root, moving solids with greater frequency from one screw to the other. The increased bed density at this higher DF is thought to promote growth by allowing more compressive forces to build across the kneading zone and in the upstream conveying elements, causing consolidation of the wetted particles exhibiting higher inter-particle forces [37,38]. At the moderate binder concentration (27% L/S), particle growth was only seen at 275 μm from ~1-4xMRT whereas all other sizes seem to be produced to their steady state weight fraction prior to 1xMRT. At the highest binder content of this study (39% L/S ratio), there was a larger degree of change for the fines, desired granulates, and coarse size fraction but after some delay. At ~3-4xMRT, a very sharp growth in granules was seen while fines were correspondingly reduced, unlike the gradual nature seen at 12% DF. This wetting condition was the first definitive instance where the kneading zone was felt to be significantly contributing to the size and strength of granules produced; the zone does not produce a compacted mass until sufficient liquid slows particle movement through the zone and sufficient powder tried to pass through the zone. The kneading zone has been reported in other studies as where intense compaction occurs over a very short distance, once densification begins[38]. The rapid rise in larger granules at ~3-4xMRT can not be explained by conveying, which would have been occurring since startup. A similar effect was seen by Vercruysse et al.[9] where they varied the number of kneading elements in the screw design at multiple fill levels and found that increasing the number of kneading elements increased the time to grow coarse granules (above 1400 μm).

Finally, in consideration of the transition boundary (~20% DF), where the growth mechanism changes based on its dependency on screw speed [14-16], we note the major difference in PSD development on either side is the rate at which larger particles grow. Despite the blackbox nature of the process, we believe the transient period is showing a stronger influence of the kneading zone on granule growth above 20% DF, where screw speed has little effect on particle size; below 20% DF, we believe the conveying zone has a stronger influence on granule growth, consistent with the slower growth along the length of the screws and for which the influence of screw speed is most obvious, undampened by the downstream kneading zone.

5.6. Conclusion

A study was conducted to observe the transient evolution of the particle size distribution produced by twin screw wet granulation from process startup until steady state, using offline mechanical sieving and a newly-developed inline acoustic-based PAT. Observing the PSD over time at low and high degrees of fill by both techniques, it was determined that steady state corresponded to roughly five times the mean residence time of the process. Due to measurement variability, there was less certainty that other granules properties such as moisture content and fracture strength had become steady in the same period of time. Through detailed evaluations of both particle size characterization techniques, the PAT method was ultimately chosen to study the transient period of process startup to learn more about the wet granulation mechanism in a TSG because it could estimate PSD over a shorter period of sampling. At a low degree of fill it was found that the conveying zone seemed to have a stronger impact on granule size on account of the gradual growth witnessed at moderate to high binder contents. Comparatively, at a high degree of fill, it was found that the kneading zone became a stronger contributor to granule development due to the rapid increase in the weight fraction of large granules after a hold up period for the fines over 1-2xMRT. From this work it is believed that liquid distribution can influence growth behaviour so future studies will focus on exploring different wetting methods (2nd injection port, foam granulation) along with their impact on the granulation mechanism.

5.7. Acknowledgements

The authors would like to thank Kevin O’Donnell and International Flavors and Fragrances Inc. (formerly Dow Chemical) for donating the lactose monohydrate, and Shaukat Ali and BASF for donating the Kollidon SR used in this study. We would like to thank the Natural Sciences and Engineering Research Council (NSERC) for its funding of this work. Additionally, our thanks goes to Dr. Prashant Mhaskar for consulting extensively on how the AI model handles its large datasets.

5.8. References

1. Pauli V, Kleinebudde P, Krumme M. From powder to tablets: Investigation of residence time distributions in a continuous manufacturing process train as basis for continuous process verification. *European Journal of Pharmaceutics and Biopharmaceutics.* 2020;153:200-210.

2. Kotamarthy L, Sampat C, Ramachandran R. Development of a Granule Growth Regime Map for Twin Screw Wet Granulation Process via Data Imputation Techniques. *Pharmaceutics.* 2022;14(10).

3. Lee KT, Ingram A, Rowson NA. Twin screw wet granulation: The study of a continuous twin screw granulator using Positron Emission Particle Tracking (PEPT) technique. *European Journal of Pharmaceutics and Biopharmaceutics.* 2012;81(3):666-673.

4. Dhenge RM, Cartwright JJ, Hounslow MJ, Salman AD. Twin screw granulation: Steps in granule growth. *International Journal of Pharmaceutics.* 2012;438(1):20-32.

5. Verstraeten M, Van Hauwermeiren D, Lee K, et al. In-depth experimental analysis of pharmaceutical twin-screw wet granulation in view of detailed process understanding. *International Journal of Pharmaceutics.* 2017;529(1):678-693.

6. Dhenge RM, Washino K, Cartwright JJ, Hounslow MJ, Salman AD. Twin screw granulation using conveying screws: Effects of viscosity of granulation liquids and flow of powders. *Powder Technology.* 2013;238:77-90.

7. Vandevivere L, Van Wijmeersch E, Häusler O, De Beer T, Vervaet C, Vanhoorne V. The effect of screw configuration and formulation variables on liquid requirements and granule quality in a continuous twin screw wet granulation process. *Journal of Drug Delivery Science and Technology.* 2022;68:103042.

8. Thompson MR, Sun J. Wet Granulation in a Twin-Screw Extruder: Implications of Screw Design. *Journal of Pharmaceutical Sciences.* 2010;99(4):2090-2103.

9. Vercruysse J, Córdoba Díaz D, Peeters E, et al. Continuous twin screw granulation: Influence of process variables on granule and tablet quality. *European Journal of Pharmaceutics and Biopharmaceutics.* 2012;82(1):205-211.

10. Thompson MR. Twin screw granulation – review of current progress. *Drug Development and Industrial Pharmacy.* 2015;41(8):1223-1231.

11. Kumar A, Dhondt J, Vercruysse J, et al. Development of a process map: A step towards a regime map for steady-state high shear wet twin screw granulation. *Powder Technology.* 2016;300:73-82.

12. Kumar A, Vercruysse J, Toiviainen M, et al. Mixing and transport during pharmaceutical twin-screw wet granulation: Experimental analysis via chemical imaging. *European Journal of Pharmaceutics and Biopharmaceutics.* 2014;87(2):279-289.

13. Djuric D, Kleinebudde P. Continuous granulation with a twin-screw extruder: Impact of material throughput. *Pharmaceutical Development and Technology.* 2010;15(5):518-525.

14. Seem TC, Rowson NA, Ingram A, et al. Twin screw granulation — A literature review. *Powder Technology.* 2015;276:89-102.

15. Tu W-D, Ingram A, Seville J. Regime map development for continuous twin screw granulation. *Chemical Engineering Science.* 2013;87:315-326.

16. Shi Z. *Understanding Scalability In A Twin Screw Wet Granulation* [Master's Thesis]. http://hdl.handle.net/11375/27950: Chemical Engineering, McMaster University; 2022.

17. Vercruysse J, Delaet U, Van Assche I, et al. Stability and repeatability of a continuous twin screw granulation and drying system. *European Journal of Pharmaceutics and Biopharmaceutics.* 2013;85(3, Part B):1031-1038.

18. Ryckaert A, Stauffer F, Funke A, et al. Evaluation of torque as an in-process control for granule size during twin-screw wet granulation. *International Journal of Pharmaceutics.* 2021;602:120642.

19. Abdulhussain HA, Thompson MR. Considering inelasticity in the real-time monitoring of particle size for twin-screw granulation via acoustic emissions. *International Journal of Pharmaceutics.* 2023;639:122949.

20. Wang W-J, Yan D, Zhu S, Hamielec AE. Kinetics of Long Chain Branching in Continuous Solution Polymerization of Ethylene Using Constrained Geometry Metallocene. *Macromolecules.* 1998;31(25):8677-8683.

21. Zhang M, Karjala TW, Kolthammer BWS. Delayed Dynamics of Polymer Properties in Continuous Stirred Tank Polymerization Reactors. *Industrial & Engineering Chemistry Research.* 2007;46(18):5922-5935.

22. Alvarez AJ, Myerson AS. Continuous Plug Flow Crystallization of Pharmaceutical Compounds. *Crystal Growth & Design.* 2010;10(5):2219-2228.

23. Brown CJ, Adelakun JA, Ni X-w. Characterization and modelling of antisolvent crystallization of salicylic acid in a continuous oscillatory baffled crystallizer. *Chemical Engineering and Processing: Process Intensification.* 2015;97:180-186.

24. BASF. Kollidon® SR | Coprocessed Excipients | BASF Pharma. 2023. Accessed 19-02-2024, 2024.

25. Mozumder S. *Scale-Up Of Pharmaceutical Twin-Screw Wet Granulation Based On The Process Simulation Using Genetic Programming* [Master's Thesis]. http://hdl.handle.net/11375/28417: Chemical Engineering, McMaster University; 2023.

26. Lute SV, Dhenge RM, Salman AD. Twin Screw Granulation: An Investigation of the Effect of Barrel Fill Level. *Pharmaceutics.* 2018;10(2).

27. Adams MJ, Mullier MA, Seville JPK. Agglomerate strength measurement using a uniaxial confined compression test. *Powder Technology.* 1994;78(1):5-13.

28. Abdulhussain HA, Thompson MR. Predicting the particle size distribution in twin screw granulation through acoustic emissions. *Powder Technology.* 2021;394:757-766.

29. Hickey AJ, Crowder, T.M., Louey, M.D., Orr, N. *A Guide to Pharmaceutical Particulate Science*. 1st ed. https://doi.org/10.1201/9780203009673: CRC Press; 2003.

30. Merkus HG. *Particle size measurements: fundamentals, practice, quality.* Vol 17. 1st ed. https://doi.org/10.1007/978-1-4020-9016-5: Springer Science & Business Media; 2009.

31. Franceschinis E, Bressan V, Fontanel E, Realdon N, Volpato S, Santomaso AC. Effect of the drying type on the properties of granules and tablets produced by high shear wet granulation. *Powder Technology.* 2024;434:119316.

32. Oka S, Emady H, Kašpar O, et al. The effects of improper mixing and preferential wetting of active and excipient ingredients on content uniformity in high shear wet granulation. *Powder Technology.* 2015;278:266-277.

33. Ryckaert A, Ghijs M, Portier C, et al. The Influence of Equipment Design and Process Parameters on Granule Breakage in a Semi-Continuous Fluid Bed Dryer after Continuous Twin-Screw Wet Granulation. *Pharmaceutics.* 2021;13(2).

34. Monteyne T, Vancoillie J, Remon J-P, Vervaet C, De Beer T. Continuous melt granulation: Influence of process and formulation parameters upon granule and tablet properties. *European Journal of Pharmaceutics and Biopharmaceutics.* 2016;107:249-262.

35. Pradhan A, Costello M, Yang F, Bi V, Durig T, Zhang F. Using twin-screw melt granulation to co-process mannitol and hydroxypropylcellulose. *Journal of Drug Delivery Science and Technology.* 2022;77:103880.

36. Haser A, Kittikunakorn N, Dippold E, DiNunzio JC, Blincoe W. Continuous Twin-Screw wet granulation process with In-Barrel drying and NIR setup for

Real-Time Moisture Monitoring. *International Journal of Pharmaceutics.* 2023;630:122377.

37. Djuric D, Van Melkebeke B, Kleinebudde P, Remon JP, Vervaet C. Comparison of two twin-screw extruders for continuous granulation. *European Journal of Pharmaceutics and Biopharmaceutics.* 2009;71(1):155-160.

38. Li H, Thompson MR, O'Donnell KP. Understanding wet granulation in the kneading block of twin screw extruders. *Chemical Engineering Science.* 2014;113:11-21.

Chapter 6: Conclusions and Future Recommendations

6.1. Significant Conclusions

In this thesis, a process analytical technology (PAT) based on acoustic emissions (AE) was developed through the use of a newly created particle mechanics-based digital filter coupled with an artificial neural network model, to provide inline monitoring of the particle size distribution (PSD) for the Twin Screw Granulation process. This PAT was originally developed based on Hertz Theory of Impact which showed great promise as the proof-of-concept version for a continuous monitoring system of near-elastic formulations, give an acceptable level of accuracy with a maximum root mean squared error (RMSE) was ~1 wt% based on all particle size fractions. To make this PAT viable for formulations commonly used by the pharmaceutical industry, the original elastic-based digital filter was modified to incorporate micromechanical impact models to account for the difference in a formulation's viscoelastic and elastoplastic nature – with the main parameters of interest being contact force and time. A Hertzian spring-and-dashpot model and the Walton-and-Braun model, representing viscoelastic and elastoplastic mechanics respectively, were tested as alternative micromechanical models to the elastic mechanics (impact force & contact time) present in the original auditory masking filter. It was found that the Walton-and-Braun model showed more repeatable trends across multiple formulations and better stability in comparison to the spring-and-dashpot model, which made it better suited for the purpose of training the underlying neural network model used to estimate the PSD. After retraining, the maximum RMSE for all formulations tested decreased substantially from 8 wt% with the elastic filter to 2.75 wt% with the elastoplastic filter.

The utility of the AE PAT was then tested by examining granule evolution during startup until steady state was reached with regards to the PSD, through variation of liquid-to-solids ratio and degree of fill (DF) as test parameters; the chosen DF conditions lay on either side of a known transition boundary. It was determined that the time to steady state for this process (ie. screw design, machine size and formulation), at the two DF tested, occurred at approximately 5 times the mean residence time by both inline (PAT) and offline (sieving) analyses. Subsequently, the series of PSD were estimated by AE PAT below 120 seconds at the two DF, since the method offered a higher repeatability and lowest sampling time. It was found that the conveying zone had a stronger impact on granule growth at the lower degree of fill due to the gradual growth of particles seen through the AE PAT. Comparatively, at the higher degree of fill it was likely that the kneading zone had a stronger impact on granule growth due to delays seen once the binder content became relatively high which ultimately caused sharper granule growth over time.

6.2. Future Directions for Research

First consideration is modifying the digital filter to account for non-spherical particle shapes. It was found during some TSG trials with 20% Kollidon ® SR that as the L/S ratio increases the more the granules become more “noodle like”. So it is recommended that aspect ratio be incorporated to the filter and ideally that a relationship between signal amplitude and aspect ratio is established to avoid introducing an extra tuneable parameter.

Exploring the effects of introducing a coating to the metal plate and its impact on the AE spectra is recommended. It was observed that if the moisture content is very high or if the particle size is too fine, granules will stick to the metal plate which causes the signal to be dampened affecting the predictions. It is recommended that data is recorded over time at varying L/S ratios for different plate coatings (metallic/ceramic) to observe the maximum amplitude over time along with visual observations of the plate to understand the impact of introducing a coating. Depending on the outcome of the study this PAT may turn into an online technique rather than an in-line if uses of compressed air are continuously needed for operation;

Expanding the outputs of the PAT beyond just a PSD and incorporate more downstream variables such as moisture content and fracture strength, would help develop the tool. As quality by design (and ultimately control) is something both academics and the industry are working towards, the utility of this PAT can be further enhanced by introducing moisture content and fracture strength data to the artificial intelligence model as impact properties are the basis of this technology.